

# **“DENSE-SAMPLING” INVERSE MODELING FOR ENVIRONMENTAL AND COASTAL SYSTEMS**

**Yongyan Wang**

**M.S. Environmental Chemistry, Nankai University, P. R. China, 1989**

**B.S. Chemistry, Nankai University, P. R. China, 1986**

A dissertation submitted to the faculty of the  
Oregon Graduate Institute of Science & Technology  
in partial fulfillment of the  
requirements for the degree of Doctor of Philosophy  
in  
Environmental Science and Engineering  
October, 1996

The dissertation “‘Dense-sampling’ Inverse Modeling for Environmental and Coastal Systems” by Yongyan Wang has been examined and approved by the following examination committee:

---

António M. Baptista, Ph.D., Thesis Advisor

---

William Fish, Ph.D., Associate Professor

---

Paul G. Tratnyek, Ph.D., Assistant Professor

---

J. Fred Holmes, Ph.D., Professor

*To*  
*My Parents*

# ACKNOWLEDGEMENTS

I wish to express my sincere thanks to my advisor, Dr. António M. Baptista, for his guidance, instruction, and encouragement during this research. I am very grateful to my thesis examination committee members, Dr. William Fish, Dr. Paul G. Tratnyek, and Dr. J. Fred Holmes. My thanks also go to my fellow students for their cooperation in the research and friendship during my stay at OGI. I would like to thank the students, staff, and faculty members of the ESE department for making OGI such a wonderful research environment. Finally, I would like to thank my parents for their love and encouragement and my wife, Chunyan Zhou, for her enormous help in my research.

# TABLES OF CONTENTS

ACKNOWLEDGEMENTS .....	iv
ABSTRACT .....	xi
CHAPTER 1: Introduction and Overview .....	1
1.1 Context and Scope.....	1
1.2 Background .....	2
1.2.1 Inverse modeling theory.....	2
1.2.2 Concepts and their definitions.....	3
1.2.3 Sensitivity of different inversion methods .....	5
1.2.3.1 The overdetermined inversion problem .....	5
1.2.3.2 The underdetermined inversion problem .....	7
1.2.3.3 Quasi-determined inversion problem.....	8
1.2.4 Special topics in inversion methods.....	10
1.2.4.1 Noise reduction and prior-knowledge representation .....	10
1.2.4.2 Non-linear inversion.....	12
1.3 “Dense-sampling” inversion formulation .....	13
1.3.1 “Dense-sampling” inversion method .....	14
1.3.2 Comparison of the proposed method with previous methods .....	15
1.4 Reader’s guide to the thesis.....	17
1.5 References .....	22
CHAPTER 2: Identifying the time history of contaminant sources in surface waters: a linear time-domain inversion method .....	25
2.1 Abstract .....	25
2.2 Introduction .....	25
2.3 Background and overview.....	28
2.4 Problem description and formulation.....	29
2.4.1 Formulation of the “dense-sampling” inverse method.....	30
2.4.2 Source identifiability .....	32
2.5 Numerical experiments .....	32
2.5.1 Synthetic St. John’s Landfill surface water environment .....	33
2.5.2 Integrity test .....	33
2.5.3 Error reduction by the “dense-sampling” method.....	35
2.5.3.1 Random error reduction .....	35
2.5.3.2 Systematic error reduction .....	37
2.5.4 Sampling network design.....	38
2.6 Summary and conclusions.....	41
2.7 References .....	52
CHAPTER 3: A sampling network design method for monitoring pollutant sources using inverse modeling.....	54
3.1 Abstract .....	54
3.2 Introduction .....	55

3.3	Sampling network design and the inverse modeling .....	57
3.3.1	Source identifiability .....	57
3.3.2	Sampling network design .....	59
3.4	Numerical experiments and results .....	60
3.4.1	Synthetic St. John's Landfill surface water system.....	60
3.4.2	Condition number spatial variation .....	60
3.4.3	Condition number and the number of sampling data .....	61
3.4.4	Condition number variation with the "dense-sampling" parameter .....	62
3.4.5	Condition number as the identifiability index .....	63
3.4.6	Sampling network design and validation .....	64
3.5	Conclusions and final remarks .....	65
3.6	References .....	76
CHAPTER 4: A method of estimating oceanic and riverine boundary conditions for hydrodynamic models using inverse modeling .....		77
4.1	Abstract.....	77
4.2	Introduction .....	77
4.3	Statement of the problem.....	79
4.4	Non-linear "dense-sampling" method .....	81
4.5	Numerical experiments.....	82
4.5.1	Non-linear, noise-free, elevation-flux boundary inversion .....	82
4.5.2	Random and systematic error reduction .....	86
4.5.3	Comparison between the proposed time-domain method and the frequency-domain (ITM) method .....	87
4.6	Oceanic boundary inversion of the Tejo estuary .....	88
4.7	Summary and Conclusions .....	89
4.8	References .....	107
CHAPTER 5: Summary and conclusions.....		108
5.1	Scientific Contributions.....	108
5.2	Theoretical and practical limitations .....	109
5.3	Directions for future research.....	110
5.4	References .....	111
CHAPTER 6: VITA.....		112

# LIST OF TABLES

Table 2.1	Relationship between the inversion parameter and the “dense-sampling” parameter $N_D$ with different sampling error levels .....36
Table 2.2	Source identifiability table for the eight source and eight station case, with “dense-sampling” parameter, $N_D$ , of 20.....39
Table 3.1	Condition number table of the synthetic St. John’s Landfill surface water environment. Note that the table has 8 sources and 18 stations and the condition number is in log scale. It indicates that the 8 sources can be identified by stations 4, 9, 13, and 16. ....75
Table 4.1	The condition numbers (log scale) of the transfer functions .....84

# LIST OF FIGURES

Figure 1.1	The concept of inverse modeling .....	19
Figure 1.2	Diagram showing the groundwater flow simulation .....	19
Figure 1.3	Locations of Atlantes 215 stations used to invert the reference velocity around a closed path from Wunsch and Minster, 1982).....	20
Figure 1.4	Diagram showing simple mixing and water mass analysis.....	20
Figure 1.5	The diagram showing the concept of non-linear inversion.....	21
Figure 2.1	Conceptual diagram of the transfer function ( $w$ ) of a generic surface water environment. In the figure, represents a unit source; $i$ and $j$ are the station index and the source index; $t$ and $t_0$ represent the sampling time and source release time respectively.....	43
Figure 2.2	Synthetic St. John's Landfill surface water environment. Its water circulation is modeled by the shallow-water equation. Its hydraulic transport is simulated by the advection-diffusion equation. It has 8 spatially distributed sources and 8 sampling stations. ....	44
Figure 2.3	The method integrity test case, which has 4 stations and 4 sources .....	45
Figure 2.4	The transfer function between station 1 and source 1, where $X$ is the sampling time, $Y$ is the release time, and $Z$ is the magnitude of the transfer function. ....	46
Figure 2.5	Measured tracer concentrations at the four sampling stations. Note that when the sampling error is zero, the inversion corresponds to tests of the basic integrity of the method. When the concentrations has 10% sampling error, the corresponding inversion illustrates the ability of the method to reduce random-sampling error.....	47
Figure 2.6	Inverted 4 source time series from the method's integrity test. Note that when $N_D=2$ , while round-off errors are amplified eventually leading for unstable inversion (source 4) when $N_D=10$ , round-off errors are suppressed (source 4).....	48
Figure 2.7	The comparison of the estimated time-history of the sources with varying sampling random errors. The dense-sampling parameter $N_D$ is 20 in all cases.....	49
Figure 2.8	Estimated source histories by four stations, when systematic errors exist. The systematic errors include 6.4 hours sampling time-shift errors and 100% diffusion coefficient error. $\epsilon$ is the time-shift error and $\Delta t$ is the sampling time interval (1.24 hours). ....	50
Figure 2.9	Estimated source histories based on the designed sampling network. Note that the number of stations (2) is less than the number of sources (5).....	51
Figure 3.1	Conceptual diagram of the transfer function ( $w$ ) of a generic surface water environment. In the figure, represents a unit source;	

	$i$ and $j$ are the station index and the source index; $t$ and $t_0$ represent the sampling time and source release time, respectively.....	67
Figure 3.2	Synthetic St. John's Landfill surface water environment. The tidal-driven system has 8 sources and 18 stations.....	68
Figure 3.3	Condition number spatial distribution of source 3 and station 8. Note that the figure utilizes the station index to represent the spatial index.....	69
Figure 3.4	Relationship between the condition number and the number of the sampling data. Note that the condition number of the transfer function is calculated from the constant transfer functions.....	70
Figure 3.5	Relationship between the condition number and the "dense-sampling" parameter. Note that the condition numbers are calculated for source 3 and stations 1-11.....	71
Figure 3.6	Source 6 is identified by different stations with different condition numbers. Clearly, when condition numbers $< 10^5$ , the station can precisely invert the source. When condition numbers $> 10^7$ , the station can't obtain a stable inversion.....	72
Figure 3.7	Transfer function between source 6 and station 13. Note that the transfer function has a periodical pattern due to the moon-tide-advection and a decrease in time as a result of diffusion. ....	73
Figure 3.8	The validation of the designed sampling network. The 8 sources are identified based on the designed sampling network. ....	74
Figure 4.1	General steps for the non-linear estimation of water sources.....	91
Figure 4.2	The finite element grid of the channel case. Notice that the problem includes one elevation boundary, one flux boundary, and three sampling stations. ....	92
Figure 4.3	The transfer functions of the channel, with two open boundaries and three sampling stations. ....	93
Figure 4.4	Measured water elevations at three stations (original and with 10% relative error).....	94
Figure 4.5	Nonlinear noise-free inversion of both water elevation and flow boundary conditions from sampled elevation at three stations (channel case).....	95
Figure 4.6	The root mean square errors of noise-free nonlinear inversion, where there are one water elevation boundary, one flux boundary, and three sampling stations ....	96
Figure 4.7	The root mean square error of the estimated water elevation and flux boundary conditions of each iteration. Note that non-linear inversions demonstrate both the sampling error reduction and simultaneous elevation and flux boundary inversion. ....	97

Figure 4.8	Comparison between the inverted boundary elevation and the imposed boundary elevation by the frequency-domain method. ....	98
Figure 4.9	Comparison between the inverted elevation boundary and the imposed boundary elevation by the time-domain inversion. ....	99
Figure 4.10	Comparison between inverted water elevations and the measured water elevations for the frequency domain inversion .....	100
Figure 4.11	Comparison between the inverted water elevation and the sampled water elevation for the time domain inversion .....	101
Figure 4.12	Comparison of the converging speed between the frequency-domain inversion and the time-domain inversion.....	102
Figure 4.13	Diagram of the Tejo's finite element grid and the tidal station locations. Note that the Tejo application utilizes the 5 stations (Cascais, Pedroucos, Lisboa, Cacilhas, and Trafaria) to invert the oceanic boundary condition. ....	103
Figure 4.14	Estimated Tejo oceanic boundary condition based on the measured water elevations at Cascais, Pedroucos, Lisboa, Cacilhas, and Trafaria stations using the developed "dense-sampling" inversion method. ....	104
Figure 4.15	Comparisons of the measured water elevations of Tejo estuary with the simulated elevations based on the inverted boundary conditions. ....	105
Figure 4.16	Comparisons of the measured water elevation with the inverted water elevation by the root-mean-square errors.....	106

# ABSTRACT

“Dense-sampling” Inverse Modeling for Environmental and Coastal Systems

Yongyan Wang

Oregon Graduate Institute of Science & Technology, 1996

Supervising Professor: António M. Baptista

Inverse modeling has been used sporadically in the analysis of environmental systems, in particular when inputs (e.g. contaminant sources) or model parameters (e.g. dispersion coefficients) are difficult to quantify directly. The concept is deceptively straightforward: use selected measurements as fingerprints of system behavior, and use physically-based models to determine expected responses (“transfer functions”) of the system to generic “unit forcings”; then, match fingerprints to transfer functions through optimization techniques, and use the same relationships to map the generic “unit forcings” into the actual forcing of interest.

The first contribution of our research relates to the identification and overcoming of some of the fundamental difficulties that have plagued the actual implementation of the inverse modeling concept. One key difficulty is that inversion amplifies errors in the measurement of system fingerprints, often resulting in unstable or misleading results. We show that sensitivity to error amplification is characterizable by the condition number of the matrix that formulates the inversion. To reduce condition numbers and therefore sensitivity to error amplification, we propose a “dense-sampling” inversion. This entails sampling the system fingerprints in time more frequently than the desired time interval for input characterization. As shown for the problem of sources of linearly transported tracers, the extra data makes the inversion dramatically more robust at a cost that should be marginal for most “tracers” that can be measured “continuously”.

The second contribution of our research relates to the application of the understanding of the relationship between condition number and invertibility, to the design of efficient sampling networks. This is a question of huge practical importance. Millions of dollars are spent annually on environmental monitoring, but rarely is monitoring optimized in objective ways. We suggest, based on a specific example, that inversion modeling theory can be applied prior to any instrument deployment, to guide the choice of the

minimum number and location of sampling stations required to identify contaminated sources. This remarkable fundamental capability could and should be incorporated, in practice, in an iterative loop that does not initially require but takes advantage of monitoring results as they become available.

The third and final contribution of this research pertains to the extension of our inversion modeling concepts and techniques to non-linear systems. We show, in particular, that dense-sampling is also effective for time-domain inversion of boundary conditions (tides and river discharges) for circulation models in coasts and estuaries, based on modest tidal gauge networks. Implementation is, in this case, based on an iterative loop consisting of linear inversion and non-linear forward modeling steps. A parallel effort of our research group, still in progress, suggests that the generation mechanisms of tsunamis can also be effectively inverted with extended dense sampling techniques, based on a combination of time explicit waveform data and instantaneous run-up data.

Overall, we consider that the contributions of this research bring us within reach of the practical use of inversion modeling to characterize time-explicit environmental forcings that are difficult to measure directly, as long as a reasonable mechanistic model is available to describe the impact of such forcing. This still leaves open the need to address inversion modeling of a variety of important environmental problems, in particular those related to the fate and transport of critical non-conservative, non-linear tracers.

# CHAPTER 1

## Introduction and Overview

### 1.1 Context and Scope

Inverse modeling has been used sporadically in the analysis of environmental systems, particularly when quantities that we usually think of as “known” (e.g., contaminant sources, hydrodynamic boundaries, and model parameters) are difficult to characterize directly.

The general concept of inverse modeling is sound and attractive: use selected measurements as fingerprints of system behavior, and use physically-based models to determine expected responses (“transfer functions”) of the system to generic “unit forcings”; then, match fingerprints to transfer functions through optimization techniques; and use the same relationships to map the generic unit forcings into the actual forcing of interest.

Unfortunately, there are substantial practical difficulties in the implementation of the inverse modeling concept. For instance, no current technique appears to have been successful in producing well resolved time-explicit inversion of contaminant sources. Most of the practical difficulties appear to be related to the high-sensitivity of inversion to observed errors of the system fingerprints. These errors are strongly amplified by most inversion formulations, resulting either in instability or in unreliable results.

Practical difficulties in the application of inverse modeling concepts have motivated us to re-examine the available inverse modeling theories and to extend them. Consistently, the objectives of this research are (a) to identify areas of uncertainty in existing inverse modeling theories; (b) to expand the current understanding of inversion modeling theory by overcoming key restrictions; and (c) to develop a framework and criteria for practical inversion modeling of linear and non-linear environmental systems.

## 1.2 Background

### 1.2.1 Inverse modeling theory<sup>1</sup>

Inverse modeling theory can be described based on three concepts, model ( $S$ ), model space ( $\hat{p}$ ) and data space ( $\hat{d}$ ) (Menke, 1989), as illustrated in Figure 1.1. The relationship is expressed as  $\hat{d} = S(\hat{p})$ , where the linear or non-linear operator  $S$  represents the physics of the system. The model space  $\hat{p}$  denotes model inputs, such as model parameters, initial conditions, boundary conditions, and source/sink terms. The data space ( $\hat{d}$ ) denotes the measurable variables, such as water elevation and contaminant tracer concentration.

The establishment of the model ( $S$ ), called model identification, includes defining the system boundaries, system input ( $\hat{p}$ ), and system output ( $\hat{d}$ ). Based on the defined model, we can analyze the system in different ways. When the model space is known and the data space is unknown, *forward modeling* calculates the data space based on the model and model inputs. Alternately, if the data space is known and the model space is unknown, *inverse modeling* infers the model inputs  $\hat{p}$  from the model ( $S$ ) and data space ( $\hat{d}$ ). Because inverse modeling matches the way we measure environmental and coastal systems, it is arguable that inverse modeling is more physically-based than the forward modeling. However, because the solution of inverse modeling problems involves many unsolved theoretical issues, inverse modeling is typically more difficult than forward modeling.

Inverse modeling has been applied to different disciplines to solve different problems. The model space ( $S$ ) determines the application fields, which include seismology (Chen, 1987), oceanography (Bennett, 1992), geophysics (Parker, 1994, Hero and Taylor, 1988, Copty et al., 1993, Dimri, 1992), and environmental science (Yeh, 1986). Additionally, different model spaces can illustrate the applications of inversion methods in solving different problems. For instance, if  $\hat{p}$  is a model parameter, the inversion is referred to as parameter estimation (Cheng and Yeh, 1992); if  $\hat{p}$  is a model boundary condition, the

---

1. Inversion methods fall into two categories (Tarantola, 1988): finite-dimensions and infinite-dimensions. This thesis addresses only finite-dimensions inversion, where, by definition, a finite number of parameters is required to define the system of interest.

inversion is denoted as boundary inversion (Nuñez, 1990); and if  $\hat{p}$  is a contaminant source, the inversion is called source estimation (Gorelick et al., 1983, Wagner, 1992). It is easy to see that inversion theory has a broad field of application and can solve a wide variety of problems.

The variety of the inversion problems determine the variety of inversion formulas. This is exemplified by the fact that linear and non-linear inversion formulations can be either overdetermined, determined, or underdetermined numerical systems. This chapter introduces important concepts of inverse modeling theory and analyzes different inversion formulations based on the ratio of the number of knowns and unknowns.

### 1.2.2 Concepts and their definitions

As introduced by Courant and Hilbert (1962), mathematical **well-posedness** of a model describing a physical reality requires that three conditions be met. First, the solution must exist. Second, the solution must be uniquely determined. Finally, the solution must be continuous. The first condition expresses the importance of correctly formulating the problem. If the inversion cannot properly formulate the physical reality, the inversion is not meaningful. In most cases, even if the model correctly formulates the reality, its solution still relies on powerful numerical techniques. For instance, the contaminant source estimation method developed in this research correctly formulates the relationships between the measured contaminant concentration and contaminant source. However, its inversion is not possible, because the formula can amplify round-off error and sampling error to create numerical instability. Obviously, even though the formulation is physically correct, it is not numerically solvable. In order to numerically solve the formulation, we developed the “dense-sampling” concept to reduce the sampling error amplification so that the inversion is solvable. Therefore, the developed inverse method meets the first criterion. It is worthwhile to point out that the inversion solvability is equivalent to the unknown’s **identifiability**. When the inversion does not have a stable solution, the inverted unknown is defined as *unidentifiable*. Otherwise, the inverted items are *identifiable*. The second criterion excludes the possibility of multiple solutions, which is posed as the inversion’s non-uniqueness. The last criterion excludes the discontinuity between the model space and data space. If an inversion method does not satisfy the three criteria, it is defined as having **ill-posedness**. Obviously, an inversion is either well-posed or ill-posed, depending on its ability to represent a reality and the availability of numerical solutions.

For an inverse problem  $\hat{d} = s(\hat{p})$ , **sensitivity** is defined as the variation of  $\hat{p}$  in response to a perturbation of  $\hat{d}$ . The perturbation can be represented by the relative errors  $\|\Delta p\|/\|p\|$  and  $\|\Delta d\|/\|d\|$ . For a linear system  $\hat{d} = S\hat{p}$ , the sensitivity is measured by the condition number  $S$ , as illustrated by the equation (Golub and Loan, 1983).

$$\frac{\|\Delta p\|}{\|p\|} \leq \text{cond}(S) \frac{\|\Delta d\|}{\|d\|} \quad (1.1)$$

Equation (1.1) shows that for a given “relative error” in  $\hat{d}$ , the “relative error” in  $\hat{p}$  is large if the condition number is large. Hence, the condition number scales the sensitivity of a linear inversion. When the  $\text{cond}(S)$  is close to unity, the system is called **well conditioned**; on the contrary, when the  $\text{cond}(S)$  is very large, the system is called **ill conditioned**.

Unfortunately, most inversion methods are highly sensitive, which hinders the development of time-domain inversion. This is because time-domain inversion has a large number of inverted unknowns which results in high inversion sensitivity. Sensitivity-reduction techniques, such as digital filtering, cannot effectively decrease the inversion sensitivity. Consequently, time-domain inversion is still in its infancy. Another example of high inversion sensitivity is that the application of the inversion methods in estimating model parameters has been widely accepted, even though they are still confronted with high inversion sensitivity. However, because the number of inverted parameters are relatively small compared to the amount of the sampled data, the inversion sensitivity can be controlled by techniques such as digital filtering. It is very difficult to balance the sampling error reduction and the sampling information loss. The above examples illustrate that sensitivity reduction limits both the inverse-method’s development and its application.

**Non-uniqueness** refers to an inversion where multiple model spaces correspond to one data space. That is to say, one inversion has multiple inversion results. The non-uniqueness involves both numerical non-uniqueness and conceptual non-uniqueness. Numerically, the uniqueness of *linear* inversion is related to the ratio of the number of unknowns and the number of equations. When the number of equations is less than, equal to, or greater than the number of unknowns, the system is defined as an underdetermined, determined, or overdetermined system respectively. An underdetermined system has an infinite number of solutions hence its solution is non-unique. Numerically, its inversion

result is the model space with the minimum Euclidean length (Press et al., 1992, Wunsch and Minster, 1982). Similarly, the inversion result of the overdetermined system is the least-square model space. In contrast, the inversion of a determined system has a unique result. It is obvious to see that the non-uniqueness of a linear inversion results from the different known-to-unknown ratios.

The uniqueness of a *non-linear* inversion is based on the fact that non-linear inversion minimizes the objective function that measures the difference between the inverted data space and the measured data space. When the objective function has one global minimum and several local minima, the optimization can have several “solutions”, corresponding to several inversion results. Because it is difficult to determine which solution corresponds to the global minimum, it is not easy to find the inversion result among several “inversion results”. That is to say the non-uniqueness of nonlinear inversion does not have an easy solution.

*Conceptual non-uniqueness* is derived from model conceptualization. Because one problem can be simulated by different models, its inversion can employ different models. Consequently, inversions with different models generate different inversion results. That is to say, the inversion is conceptually non-unique. It is important to point out that the model selection used in the inversion is mostly based on the modeler’s conceptual understanding of the inverted problem so that the conceptual uniqueness contributes to the majority of the inversion uniqueness (Mackas et al., 1987).

In summary, well-posedness implies that the inversion can be inverted, and has a unique continuous result. Sensitivity is the necessary and sufficient condition of identifiability. Non-uniqueness, dominated by conceptual non-uniqueness, makes inversion modeling more difficult than predictive modeling. Our limited ability to detect and solve ill-posedness suggests the need for theoretical development.

### **1.2.3 Sensitivity of different inversion methods**

#### **1.2.3.1 The overdetermined inversion problem**

The overdetermined inversion problem has a larger number of knowns than unknowns. Its standard solution is the least square method (Press et al., 1992). The over-

determined problem is often exemplified by parameter estimation, in which the number of model parameters is generally smaller than the number of measurable data.

In subsurface hydrology, inversion is commonly used to estimate model parameters (Xiang and Elsworth, 1992). Consider, for example, the system illustrated in Figure 1.2 and assume that the groundwater flow is described by equation (1.2).

$$\frac{\partial}{\partial x_i} \left( T \frac{\partial h}{\partial x_i} \right) = \sum_{w=1}^{N_{well}} (Q_w(t)) \prod_{i=1}^{N_{Dimension}} (\delta(x_i - x_w) + S \frac{\partial h}{\partial t}) \quad (1.2)$$

where  $x_i$  is the coordinate index,  $x_w$  is the coordinates of sampling wells,  $h$  is the head,  $Q_w(t)$  is the pumping flux time history at the wells,  $\delta$  is the delta function, and  $S$  and  $T$  are the storage and the transmissivity coefficients. By assuming  $H$  as a vector of nodal head magnitudes, the discretization of this equation and leads to

$$(H^{i+1} + H^i) T = Q^{i+1} + Q^i + 2S \frac{(H^{i+1} - H^i)}{\Delta t} \quad (1.3)$$

Equation (1.3) can be arranged in the form  $ET=b$ , where  $E$  is an  $(m+n)*k$  matrix,  $T$  is a  $k$  vector, and  $b$  is an  $(m+n)$  vector. Note that  $m$ ,  $n$ , and  $k$  are the number of data sets, the number of nodes, and the number of parameters respectively. Because the number of equations is greater than the number of unknowns, equation (1.3) represents an overdetermined inversion problem, which has a least-square solution. Note that the model space of the inversion is the storage coefficient ( $S$ ) and transmissivity ( $T$ ). The data space is the measured water head ( $h$ ).

Overdetermined inversion has controllable sensitivity. Xiang and Elsworth (1992) explicitly mentioned the method's high sensitivity by stating that "the noise in head distribution will largely affect the accuracy of the estimated parameters.", and suggests that "using a digital filter to reduce the noise level is an acceptable procedure. The comparison shows that the least-square method combined with a digital filter gives stable results." This stable inversion of the overdetermined problem can be explained by the fact that the overdetermined system has limited power to reduce sampling noise, so that the overdetermined parameter inversion, after the sampling noise is digitally filtered, can generate a stable inversion result. This is why parameter estimation generally leads to stable inversions.

### 1.2.3.2 The underdetermined inversion problem

The underdetermined inversion problem occurs when the number of knowns is smaller than the number of unknowns. Because their inversions are generally numerical unstable, underdetermined inversion must use different optimization algorithms in order to reach stable results. Some of the algorithms are the Conjugate Gradient method (Neuman et al., 1980), the Gauss-Newton method with Rosen's gradient projection (Yeh and Yoon, 1981), the maximum likelihood method (Carrera and Neuman, 1986), and the Kriging method (Kitanidis and Vomvoris, 1983). In this review, we discuss the underdetermined inversion by velocity inversion using linear and quadratic Lagrange multiplier optimization.

In oceanography, velocity inversion estimates the simultaneous reference velocity around a closed path in the ocean (Wunsch and Minster, 1982), as illustrated in Figure 1.3. The idea is that the total water influx equals the total water outflux, as formulated by equation (1.4). In the equation,  $\Delta z_{mn}$  is the thickness of the  $m$ -th water layer at the  $n$ -th station;  $\Delta x_n$  is the distance between the  $n$ th station pair;  $\bar{v}_{mn}$  and  $b_n$  denote the inverted velocity;  $M$  is the number of layers; and  $N$  is the number of stations.

$$\sum_{n=1}^N (\bar{v}_{mn} + b_n) \Delta z_{mn} \Delta x_n = 0 \quad (1 \leq m \leq M) \quad (1.4)$$

By assuming

$$A_{mn} = \Delta z_{mn} \Delta x_n \quad (1.5)$$

and

$$C = - \sum_{n=1}^N \bar{v}_{mn} A_{mn} \quad (1.6)$$

equation (1.4) is a linear equation  $Ab=C$ , where matrix  $A$  represents the model ( $S$ ), vector  $b$  the model space, and vector  $C$  the data space. The application of the method to the analysis of the velocities of the Atlantic ocean yields an underdetermined inversion. The number of equations ( $M=5$ ) is less than the number of unknowns ( $N=43$ ). In order to stabilize the inversion, the method adds the additional constraint that the inversion results have the

smallest Euclidean length  $(b \bullet b)^{1/2}$ . This constraint can be formulated by either a strong constraint, equation (1.7),

$$J_1 = b \bullet b + 2\lambda \bullet (Ab - c) \quad (1.7)$$

or a weak quadratic constraint, equation (1.8):

$$J_2 = W_1 b \bullet b + W_2 (Ab - c) \bullet (Ab - c) \quad (1.8)$$

where  $\lambda, W_1, W_2$  are Lagrange multipliers. As a result, the underdetermined inversion is formulated by  $Ab=C$  and equations (1.7) or (1.8).

The underdetermined inversion has a small known-to-unknown ratio ( $\ll 1$ ). Therefore, under-determined inversion results are more sensitive to the sampling error than overdetermined inversion. This is why this inversion method applies the  $(b \bullet b)^{1/2}$  constraint to increase the known-to-unknown ratio so as to decrease the inversion sensitivity. However, even though  $(b \bullet b)^{1/2}$  prevents instability, it has more numerical meaning than physical meaning.

### 1.2.3.3 Quasi-determined inversion problem

Quasi-determined inversions have a known-to-unknown ratio approximately equal to unity. Because their inversions' known-to-unknown ratios are similar, they share similar theoretical limitations. These limitations are exemplified by an example of water mass analysis.

The water analysis for a binary mixture is shown in Figure 1.4, where  $X_a$  and  $X_b$  are concentrations of tracers  $a$  and  $b$  in the water container  $O, P$ , and  $Q$ .  $O$  and  $P$  denote water sources and  $Q$  represents the mixed water. By assuming the mixture is a simple mixture ( $V_O + V_P = V_Q$ ) and considering the concentrations are positive values, the inversion is formulated by equations (1.9) and (1.10). By solving the two equations, the inversion estimates model space  $\{X^O, X^P\}$  from the model (equation (1.9)) and data space  $\{X_a^Q, X_b^Q\}$ .

$$\begin{bmatrix} X_a^O & X_a^P \\ X_b^O & X_b^P \end{bmatrix} \times \begin{bmatrix} X^O \\ X^P \end{bmatrix} = \begin{bmatrix} X_a^Q \\ X_b^Q \end{bmatrix} \quad (1.9)$$

$$\begin{bmatrix} 1 & 0 \\ 0 & 1 \end{bmatrix} \times \begin{bmatrix} X^O \\ X^P \end{bmatrix} \geq \begin{bmatrix} 0 \\ 0 \end{bmatrix} \quad (1.10)$$

Generally, a water mass analysis estimates  $M$  water sources from the measured  $N$  tracers. The general formulations is:

Minimization of

$$(Ax - b) \bullet (Ax - b) \quad (1.11)$$

subject to

$$Fx \geq h \quad (1.12)$$

where  $A$ ,  $x$ ,  $b$ ,  $F$ , and  $h$  have dimensions of  $L \times M$ ,  $M \times 1$ ,  $L \times 1$ ,  $K \times M$ , and  $K \times 1$ , respectively ( $L=N+1$ ,  $K=M$ ). The solution method is the Karush-Kuhn-Tucker theorem (Peressini et al., 1988).

Mackas et al. (1987) applied the method to the analysis of the water sources of the British Columbia coast. The five water sources ( $M=5$ ) are Juan de Fuca, the California Undercurrent, Coastal Deep, Offshore, and Subarctic water sources. The six tracers ( $N=6$ ) are temperature, salinity, nitrate, phosphate, silicate, and oxygen. Obviously, the known-to-unknown ratio (6/5) is very close to 1. Therefore, the inversion is quasi-determined. Its solution involves the least square objective function and predefined inversion limits ( $x \geq 0$ ). Similar to the underdetermined inversion, the quasi-determined inversion uses additional information ( $x \geq 0$ ) to increase the inversion's know-to-unknown ratio, so as to reduce the inversion sensitivity.

In summary, the inversion of overdetermined, quasi-determined, and underdetermined problems illustrates the different approaches to reduce inversion sensitivity. Overdetermined inversion minimizes the least-square distance between the measurable values and the inverted values. Because the least square method has only limited capability in sensitivity reduction, it cannot guarantee a stable solution. Quasi-determined and underdetermined inversions impose limit constraints on inversion to reduce the inversion sensitivity. However, because the inversion is numerically stable, the solution sometimes remains meaningless (Carrera and Neuman, 1986). Obviously the inversion method still has no general guidelines for sensitivity reduction.

## 1.2.4 Special topics in inversion methods

### 1.2.4.1 Noise reduction and prior-knowledge representation

The inverse methods discussed in section 1.2.3, solve for the model space based on model space and data space (Figure 1.1). However, in reality, we frequently have additional information about model space and data space. This information is referred to as prior knowledge. For example, in some cases, we know that different sampling data have different levels of sampling errors, and we want this prior knowledge to be represented in the optimization so that the data with small sampling error contribute more to the objective function than those with large sampling errors. Another example is that the field measurement and other publications provide many pieces of “prior-knowledge”, such as the inverted variable range. This “prior-knowledge” should enhance the inversion performance. The methods of utilizing “prior-knowledge” to enhance the inversion are discussed below.

Different from the sensitivity reduction by increasing the known-to-unknown ratio (discussed in section 1.2.3), another noise reduction approach is to modify the objective function through prior knowledge. The method is called the weighted least square inversion. Generally, the objective function of linear inversion  $Ax = b$  is  $(Ax - b)^T(Ax - b)$ . However, when data have different error magnitudes, the objective function should have large weighting factors for the most accurate data. This idea leads to the weighted least square method, in which the objective function  $(Ax - b)^TW^{-1}(Ax - b)$  is scaled by the weighting factor matrix  $W$ .

The use of “prior-knowledge” is able to eliminate the inversion's non-uniqueness problem. This is because the prior-knowledge represents the expected model space. When the objective function has several local minimums, this “prior-knowledge” assists the optimization to select the local minima that is close to the prior-knowledge. As a result, prior-knowledge eliminates the numerical non-uniqueness.

As an example, Bentley (1993) formulated the problem of parameter estimation for a groundwater flow model as a weighted least square inversion. He stated the problem as:

Minimize J:

$$J = (\hat{h} - h^*)^T C_M^{-1} (\hat{h} - h^*) + \lambda \times (\hat{p} - p^*) C_P^{-1} (\hat{p} - p^*) \quad (1.13)$$

Subject to the equation:

$$-\frac{\partial}{\partial x} \left( T \frac{\partial h}{\partial x} \right) - \frac{\partial}{\partial y} \left( T \frac{\partial h}{\partial y} \right) + B (h - h_r) - I - \sum_{p=1}^{N_Q} Q_p \delta(\bar{x} - \bar{x}_p) = 0 \quad (1.14)$$

and to the boundary condition

$$h = H_B \quad \text{or} \quad q \bullet \hat{n} = q_B \quad (1.15)$$

In the above equations,  $\hat{h}, h$  are vectors of calculated and measured heads;  $\hat{p}, p$  are vectors of the inverted parameter values and prior-known values;  $C_M$  and  $C_P$  are the covariance matrix, representing the “prior-knowledge”;  $\lambda$  is a weighting parameter representing the relative importance of governing equation and prior knowledge of parameters;  $h$  is the hydraulic head;  $T$  is the transmissivity;  $B$  and  $h_r$  are leakage parameters;  $I$  is infiltration;  $Q_p$  is pumping rate for well  $p$ ;  $H_B$  is the value of the specified head;  $q_B$  is the value of the specified flux. The equation shows that the major difference between the weighted least square method and the least square inversion methods is that the weight lease-square inversion introduces the weighted objective function to represent prior knowledge. For example, the first term of equation (1.13) indicates that the solution keeps the minimum weighted distance to the sampled head. Similarly, the second term of equation (1.13) states that inversion results also minimize the weighted distance to the prior-known parameter.

By taking into account the prior knowledge about unknowns, the method provides a solution for both the sampling noise reduction and the non-uniqueness problems. However, this approach has several drawbacks. First of all, it is not a systematic approach to improve the inversion. In fact, the calculation of the covariance matrix is a serious practical issue that can introduce artificial effects. Secondly, the selection of weighting factor  $\lambda$  is a trade off between the enforcement of the governing equations against stability of the iterative solution. Its selection is still a open topic. Finally, the method is an optimization method, which can easily lose physical meaning in the optimization process. All in all, this approach is one of the most effective sampling noise reduction methods based on prior-knowledge representation.

### 1.2.4.2 Non-linear inversion

Non-linear inversion is another interesting topic. In the terminology of *model*, *model space*, and *data space*, the non-linear problem represents the situation where model space is not linearly related with the data space. The corresponding nonlinear inversion is illustrated by the boundary inversion of a hydrodynamic model (Nuñez, 1990). The non-linear model is the shallow water equation, the *model space* is the measured water elevation, and the *data space* is the water elevation boundary. The non-linear inversion estimates the water boundary conditions based on the hydrodynamic model and the measured water elevation. Its solution involves two steps. The first phase establishes the linear inversion; and the second phase solves the non-linear inversion by iterations between linear inversions and nonlinear simulations.

The non-linear *model* is represented by the shallow water equation (1.15).

$$\begin{aligned} \eta_{,t} + (uh)_{,x} + (vh)_{,y} &= - (u\eta)_{,x} - (v\eta)_{,y} \\ u_{,t} + g\eta_{,x} - fv &= \left[ c_f \frac{(u^2 + v^2)^{1/2}}{(h + \eta)} \right] u - (uu_{,x} + vu_{,y}) \\ v_{,t} + g\eta_{,y} - fu &= \left[ c_f \frac{(u^2 + v^2)^{1/2}}{(h + \eta)} \right] v - (uv_{,x} + vv_{,y}) \end{aligned} \quad (1.16)$$

t: time

x, y cartesian coordinates

u, v: depth averaged components of velocity

$\eta$ : surface elevation relative to mean sea level

h: depth to mean sea level

g: acceleration due to gravity

f: Coriolis factor

$c_f$ : bottom friction coefficient

$\lambda$ : linearized friction factor

The *model space* is the boundary condition ( $y_i$ ), which is the weighted ( $c_i$ ) summation of the unit forcing  $\phi_i(t)$ .

$$y_i = \sum_1^n c_i \phi_i(t) \quad (1.17)$$

The *data space* is the measured water elevation ( $\hat{\eta}_i$ ), which is the weighted summation of the unit-forcing response  $\hat{\eta}_i(t)$ .

$$\hat{\eta} = \sum_1^n c_i \eta_i(t) \quad (1.18)$$

The linear inversion solves the weighting factor ( $c_i$ ) by minimizing the  $(\eta - \hat{\eta})^2$ , where  $\eta$  is the inverted water elevation. Then, inverted boundary condition  $y_i$  can be calculated by equation (1.17).

The non-linear inversion is conceptualized in Figure 1.5, where  $Y$  represents the model space,  $X$  denotes the data space, and the curve describes the non-linear model. The figure suggests that the first linear inversion (step (1)) has a large inversion error. The second inversion (steps (3) (4)) has a smaller inversion error. After several iterations (step (5)), the inversion converges to the true boundary condition. Clearly, nonlinear inversion can be accomplished by the iterated linear inversions.

Figure 1.5 conceptually shows how non-linear inversion is solved by iterations of linear inversions. First of all, the non-linear inversion requires a solid linear-inversion methodology. Secondly, it requires a well behaved non-linear model to represent the non-linear system. Finally, the non-linear inversion solves the problem in an iteration fashion. Undoubtedly, the conceptual diagram can be applied to solve other non-linear inversions.

### 1.3 “Dense-sampling” inversion formulation

The “dense-sampling” inversion modeling method developed in this thesis can invert general time-variant linear/nonlinear systems, such as those represented by hydraulic transport and hydrodynamic models. The following two sections overview the “dense-sampling” inversion method and its application. They also compare the “dense-sampling” method with the available inversion methods.

### 1.3.1 “Dense-sampling” inversion method

The concept of the “dense-sampling” described in Chapter 2 reduces the high inversion sensitivity. The idea of the “dense-sampling” is to use more measured data to invert one unknown by selecting an inversion time resolution coarser than the sampling time resolution. In the context of the know-to-unknown ratio, the “dense-sampling” concept is capable of converting under/quasi determined inversion problems to overdetermined inversion problems. Additionally, it can increase the know-to-unknown ratio of an overdetermined inversion problem. Consequently, the “dense-sampling” concept successfully suppresses the inversion's high sensitivity. This solution is demonstrated in the context of both linear (Chapter 2) and nonlinear (Chapter 4) inversion problems.

The linear inversion solved by the “dense-sampling” method is described in Chapter 2, where the “dense-sampling” method linearly inverts a contaminant source. The model is represented by the advection-diffusion equation; the model space is spatial-temporal variation of the contaminant source; and the data space is the concentration of the measured tracer concentration. The “dense-sampling” method converts a quasi-determined inversion into an overdetermined inversion to suppress the sampling errors, thus allowing a successful estimation of the contaminant source.

Non-linear inversion using the “dense-sampling” method is illustrated in Chapter 4, through the deformation of boundary conditions for the circulation in a confined surface water environment. The model is represented by the shallow water equations; the model space corresponds to the water elevation/flux boundaries; and the data space is the measured water elevation. One important point is that the “dense-sampling” method effectively reduces the inversion sensitivity so that the non-linear inversion is possible. Another important point is that the “dense-sampling” method is capable of non-linearly converging to the result by iteration between linear inversions and nonlinear simulations. This method is the first time-domain water source estimation method.

The concept of “dense-sampling” also solves the inversion's invertibility (identifiability) issue. This is because the identifiability is determined by the inversion sensitivity. Indeed, when the inversion sensitivity is high, the inverted unknown is not identifiable. Therefore, by reducing the sensitivity of the inversion, we also inherently solve the inversion “identifiability” problem. The solution of the “identifiability” has two parts. First of

all, the “dense-sampling” concept converts high sensitive inversions to low sensitive inversions, so that non-identifiable problems become identifiable. Secondly, the method discovers that the unknown's identifiability is equivalent to the inversion-equation's solvability. The solution of the identifiability leads to a method for design of sampling networks for both water elevation and pollutant tracer measurements. The idea is that the source identifiability is equivalent to the inversion's solvability. And the equation's solvability is scaled by its condition number. Therefore, the inversion's identifiability can be scaled by the condition number. Consequently, the “dense-sampling” concept creates the sampling network design method based on the condition number. Detail discussion of the method is in Chapter 3.

### 1.3.2 Comparison of the proposed method with previous methods

The diagnostic analysis of the “dense-sampling” method suggests that this method is more sound than the existing inverse methods, because it systematically reduces the inversion sensitivity, expresses the source identifiability, and accomplishes the non-linear inversion.

Reducing inversion sensitivity has been the major challenge in developing and applying inversion methods. The problem is that the inversion result is so sensitive to the sampling error that even round-off error in the sample data can generate numerical instability. Consequently, the inversion has no solution. Generally, the inversion sensitivity is positively correlated with the ratio of available information in  $\vec{d}$  to the unknown information in  $\vec{p}$ . This relationship can be expressed as the ratio of the number of equations and constraints to the number of unknowns (*RECU*), expressed as follow:

$$Sensitivity \propto RECU = \frac{Dimension\_of\_ \vec{p}}{Dimension\_of\_ \vec{d}} \quad (1.19)$$

Equation (1.19) shows that increasing the number of knowns or decreasing the number of unknowns can reduce the inversion sensitivity. That is to say in order to reduce the inversion sensitivity, more information is required to generate equations and constraints. For instance, the example of the underdetermined inversion (section 1.2.3.2) adds the minimum norm constraint to increase the *RECU*. Similarly, the example of the quasi-determined inversion (section 1.2.3.3) applies physical constraints (water fractions are

non-negative values) to increase the *RECU*. Intentionally, these methods are trying to suppress the inversion sensitivity by increasing the *RECU*.

Superior to the above sensitivity reduction efforts, the “dense-sampling” inverse modeling formulation develops the “dense-sampling” concept to reduce the inversion sensitivity. The method increases *RECU* dramatically so that the underdetermined and quasi-determined inversions are converted to overdetermined inversions. Along the way, “dense-sampling” can also effectively increase the *RECU* of the overdetermined inversion. Consequently, the “dense-sampling” inverse modeling formulation successfully reduces the inversion's sensitivity. In other words, we will show in this thesis that the long-existing problem of error reduction, universally encountered in inversion can be solved by the “dense-sampling” concept, at least in the context of our applications.

The solution of the inversion sensitivity also implies the solution of the source identifiability. In fact, the “dense-sampling” concept provides a new approach to defining the inversion's identifiability. The approach is based on the fact that the inversion's identifiability is equivalent to the inversion's stability, which can be scaled by its condition number. Therefore, the method discovers that the condition number of the inversion equation can represent the source identifiability. When the condition number closes to unity, the inversion has low inversion sensitivity and the inverted model space is defined as identifiable. Otherwise, a large condition number indicates high inversion sensitivity, which defines the inverted data space as non-identifiable. Clearly, the theory is able to predict the unknown's identifiability by investigating the condition number of the inversion matrix.

In contrast to the proposed theory, available inversion methods (e.g. Kool and Parker, 1988, Yeh and Sun, 1984) have neither the essential and sufficient condition for identifiability nor the effective ways to increase the identifiability. For example, some inversion methods reduce the inversion sensitivity by digitally filtering the sampled data (Thiébaux and Pedder, 1987, Xiang and Elsworth, 1992). As a result, they can not control the balance between information loss and error elimination. Also, they can neither predict the invertibility prior to inversion, nor provide suggestions for improving the identifiability. In summary, we conclude that the developed method defines the inversion's identifiability as the solvability of inversion equation and provides a numerical variable (condition number) to express the unknown's identifiability.

The uniqueness problem exists in the proposed method as well as in the available inversion methods. The existing inversion method uses optimization techniques to solve the inverse problem. Therefore, they have numerical non-uniqueness when the objective function has several local minimums. Nevertheless, because the developed method solves the equation by the least square method, which does not have numerical non-uniqueness, the “dense-sampling” approach eliminates the numerical non-uniqueness. This means the developed method does not have mathematical non-uniqueness. By this comparison, it is easy to conclude that the developed method has a better chance to correctly approach the solution of conceptual non-uniqueness.

## **1.4 Reader’s guide to the thesis**

Chapter 1 both reviews the previous inverse modeling methods and compares them with the proposed “dense-sampling” method. First, the chapter discusses the concept of the inverse modeling. Second, it summarizes important concepts describing inverse modeling methods. Third, it groups the inverse modeling methods in three categories according to the known-to-unknown ratio. Finally, the chapter compares the available inversion methods with the “dense-sampling” inverse theory, in regard to the method's sensitivity to sampling error, identifiability index, the conceptual non-uniqueness and mathematical non-uniqueness, and the non-linear inversion.

Chapter 2 discusses the linear formulation of the “dense-sampling” inverse modeling formulation and its application in identifying contaminant source. The chapter concentrates on describing the “dense-sampling” formulations and diagnostically analyzing its effectiveness in reducing both random error and systematic error. Readers should pay special attention to the system inputs, system outputs and the system characterization. Once you have understood the concept of “dense-sampling,” you are able to explain why the method can reduce both random error and systematic errors.

A sampling-network design method is pursued in Chapter 3, which extensively discusses the source identifiable index - the condition number of the transfer function. Since the condition number expresses the inversion's invertibility, it is a universal index for different inversion methods, such as contaminant source identifiability and water source identifiability. This chapter investigates the factors affecting the condition number magnitude. Moreover, the chapter demonstrates the designed sampling network for moni-

torial the contaminant source of St. John's landfill environment. Finally, the chapter validates the designed sampling network by the contaminant source characterization method. Readers are advised to go through Chapters 1 and 2, before reading Chapter 3. In addition, a sound knowledge about linear system theory (Golub and Loan, 1983) and singular value decomposition (Press et al., 1992) is helpful in understanding the content.

Chapter 4 highlights non-linear inversion of the “dense-sampling” inverse theory. In the nonlinear inversion, the system is the shallow water equation, which is solved by the time domain model ADCIRC (Luettich et al., 1991). The system inputs are the oceanic/riverine boundary conditions (time series), and the system outputs are the measured water elevation (time series). The non-linear relationships of advection, bottom friction and finite amplitude are inverted through an iterative process involving linear inversions and non-linear flow simulations.

Chapter 5 summarizes our conclusions and suggests directions for future research.

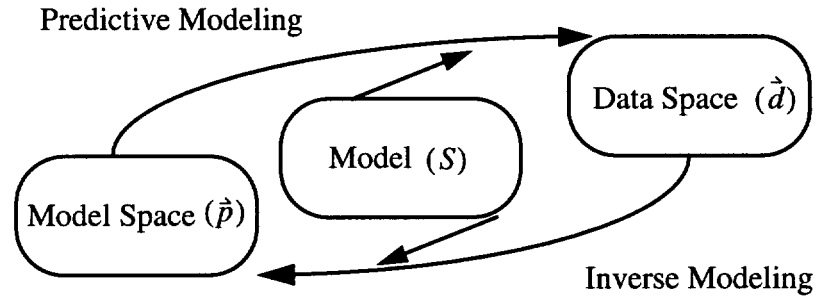


**Figure 1.1 The concept of inverse modeling**

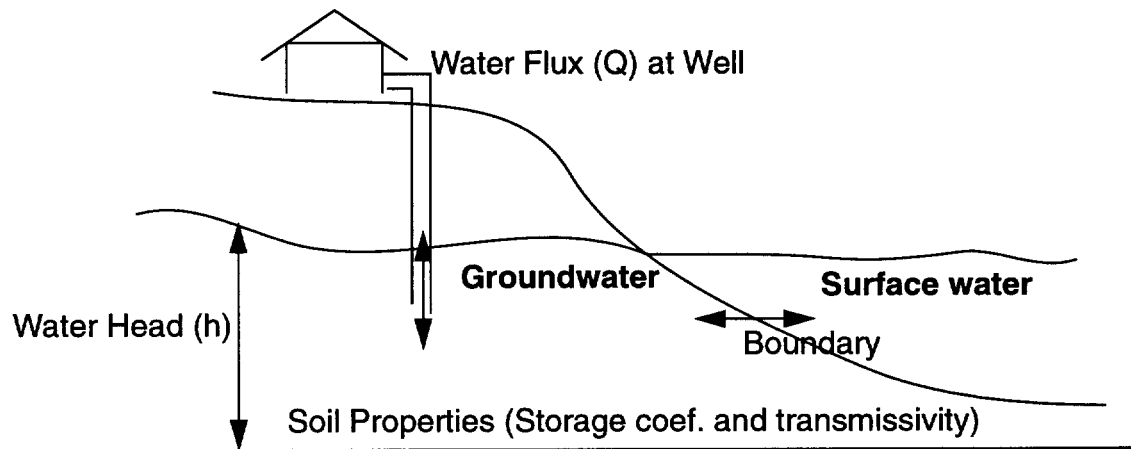


**Figure 1.2 Diagram showing the groundwater flow simulation**

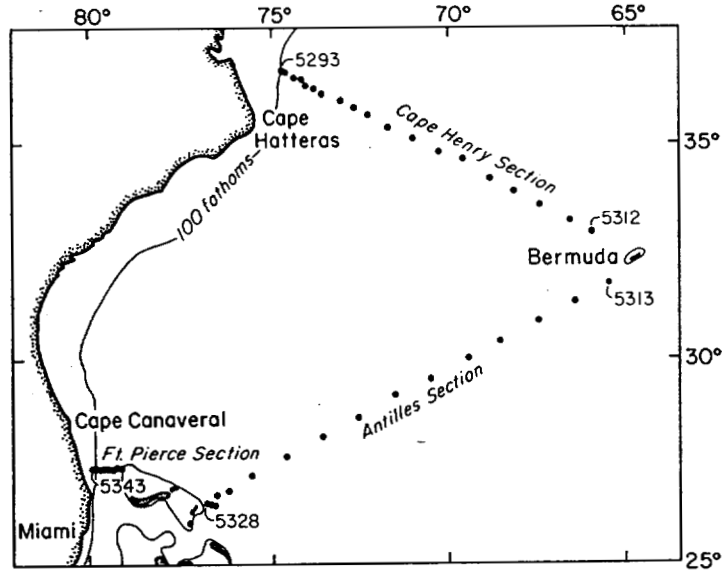


Figure 1.3 Locations of Atlantis 215 stations used to invert the reference velocity around a closed path from Wunsch and Minster, 1982)

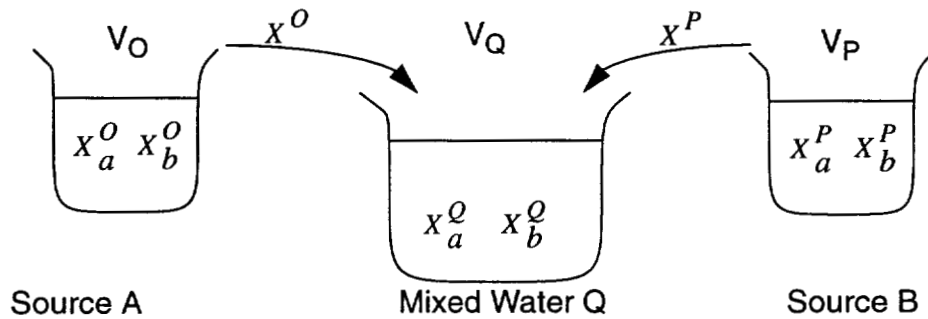
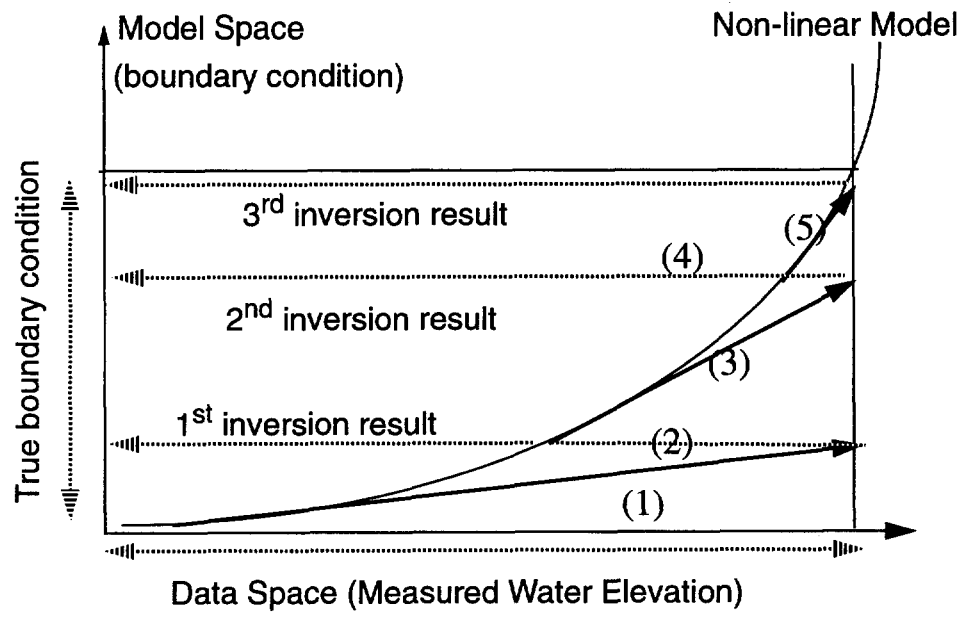


Figure 1.4 Diagram showing simple mixing and water mass analysis



**Figure 1.5** The diagram showing the concept of non-linear inversion

## 1.5 References

- Bennett, F. A., *Inverse Methods in Physical Oceanography*, Cambridge University Press, New York, 1992.
- Bentley, L. R., Least squares solution and calibration of steady state groundwater flow systems, *Advances in Water Resour. Res.*, 16, 137-148, 1993.
- Carrera, J. and S. P. Neuman, Estimation of aquifer parameters under transient and steady state conditions: 1. maximum likelihood method incorporating prior information, *Water Resour. Res.*, 22(2), 199-210, 1986.
- Chen, C. H., *Computer-aided Seismic Analysis and Discrimination*, Elsevier North-Holland, 1987.
- Cheng, J. M. and W. W.-G. Yeh, A proposed quasi-Newton method for parameter identification in a flow and transport system, *Advances in Water Resources*, 15, 239-249, 1992.
- Copt, N., Y. Rubin, and G. Mavko, Geophysical-Hydrological Identification of Field Permeability Through Bayesian Updating, *Water Resour. Res.*, 29(8), 2813-2825, 1993
- Courant, R., and D. Hilbert, *Methods of Mathematical Physics*, Interscience Publishers, New York, 1962.
- Dimri, V., *Deconvolution and Inverse Theory: Application to Geophysical Problem*, New York, Elsevier, New York, 1992.
- Gorelick, S. M., B. Evans, and I. Remson, Identifying sources of groundwater pollution: An optimization approach, *Water Resour. Res.*, 19(3), 779-790, 1983.
- Golub, H. G., and C. F. Loan, *Matrix Computation*, The John's Hopkins University Press, 1983.
- Hero, C. J. and R.W. Taylor, *Geophysical Determination of Lakebed Sediment Hydraulic Properties, The Great Lakes: Living with North America's Inland Waters. Proceedings of a Symposium*, American Water Resources Association, Bethesda, Maryland, 163-171, 1988.
- Kitanidis, P. K., and E. G. Vomvoris, A geostatistical approach to the inverse problem in groundwater modeling (steady state) and one-dimensional simulations, *Water Resour. Res.*, 19(3), 677-690, 1983.
- Kool, J.B. and J. X. Parker, Analysis of the inverse problem for transient unsaturated flow, *Water Resour. Res.*, 24, 817-30, 1988.

- Luetlich, R. A., J. J. Westerink, and N. W. Scheffner, *ADCIRC: An Advanced Three-dimensional Circulation Model for Shelves, Coasts and Estuaries*, Coast. Engr. Res. Ctr., U.S. Army Engrs. Wtrways. Experiment Station, Vicksburg, Miss, 1991.
- Mackas, L. David, K. L. Denman, and A. F. Bennett, Least squares multiple tracer analysis of water mass composition, *J. of Geophysical Research*, 92(C3), 2907-2918, 1987.
- Menke, W., *Geophysical Data Analysis: Discrete Inverse Theory*, Academic Press, San Diego, 1989.
- Neuman, S. P., G. E. Fogg, and E. A. Jacobson, A statistical approach to the inverse problem of aquifer hydrology, *Water Resour. Res.*, 16(1), 33-58, 1980.
- Núñez, R. H., *Prediction of tidal propagation and circulation in Chilean inland seas using a frequency domain model*, M. Sc. dissertation, Oregon State University, Corvallis, OR, 1990.
- Parker, R. L. *Geophysical Inverse Theory*, Princeton University Press, 1994.
- Peressini, A. L., F. E. Sullivan, and J. Jr. Uhl, *The Mathematics of Nonlinear Programming*, Springer Verlag, New York, 1988.
- Press, H. W, S. A. Teukolsky, W. T. Vetterling, and B. P. Flannery, *Numerical Recipes in C*, Cambridge University Press, New York, 1992.
- Tarantola, A., *Inverse Problem Theory - Methods for Data Fitting and Model Parameter Estimation*, Elsevier Science Publishing Company, New York, 1988.
- Thiébaux, H. J. and M. A. Pedder, *Spatial Objective Analysis: With Applications in Atmospheric Science*, Academic Press, London, 1987.
- Wagner, B. J., Simultaneous parameter estimation and contaminant source characterization for coupled groundwater flow and contaminant transport modelling, *J. of Hydrology*, 135, 275-303, 1992.
- Wunsch, C. and J. F. Minster, Methods for box models and ocean circulation tracers: Mathematical programming and nonlinear inverse theory, *J. of Geophysical Research*, 87, 5647-5662, 1982.
- Xiang, J. and D. Elsworth, Parameter identification of nonsteady groundwater flow systems, *Advances in Water Resources*, 15, 259-269, 1992.
- Yeh, W. W.-G., and N. Z. Sun, An extended identifiability in aquifer parameter identification and optimal pumping test design, *Water Resour. Res.*, 20(12), 1837-1847, 1984.

Yeh, W. W.-G., Review of parameter identification procedures in groundwater hydrology: The inverse problem, *Water Resour. Res.*, 22(2), 95-108, 1986.

Yeh, W. W.-G., and Y. S. Yoon, Parameter identification with optimum dimension in parameterization, *Water Resour. Res.*, 17(3), 664-672, 1981.

## CHAPTER 2

# Identifying the time history of contaminant sources in surface waters: a linear time-domain inversion method

### 2.1 Abstract

This chapter describes a new method to estimate time series of spatially-distributed tracer sources in surface water environments. In our method, the measured tracer concentrations are formulated as the convolution of the source time series with the system transfer functions. To obtain source time histories, the method relies on the observation of tracer concentrations at selected stations and numerical simulations of flow and transport processes. By having a sampling resolution higher than the inversion resolution, with which we want to characterize sources (“dense-sampling”), results are stable and meaningful. Through diagnostic modeling, we demonstrate the capability of the method with regard to the identification of source time history and reduction of random and systematic errors. We also explore the sensitivity of the method to the number and the location of sampling stations. The study suggests that (a) source scenarios can be recovered perfectly if the synthetic observations are not contaminated by errors, (b) the inversion method is robust enough to “filter” out random error and selected system errors, and (c) the inversion method is capable of identifying more sources than the number of existing stations.

Key words: inversion, singular value decomposition, source identification, source estimation, sampling network design

### 2.2 Introduction

Source characterization is a limiting factor in regional-scale analysis of water quality issues. A common use of environmental modeling is to estimate pollutant sources in an environmental system from the measurable information. In this context, the source characterization needs to discover the source location, source spatial distribution and source temporal variations. Despite its obvious importance and the intensive investigations in both

surface and ground water environments, there are few successful source estimation methods. Although mathematical models are reasonably well developed to simulate the measurable variables according to initial conditions, boundary conditions, model parameters, and source variations, the question of how to quantify the source variations with respect to model inputs has not been completely resolved. In this research, we address the problem in the context of inverse modelling and provide a suitable solution.

The theoretical challenges of the source temporal inversion can be exemplified by the model parameter inversion. This is because the inverse modeling conceptually inverts “model input” from “model output”. The model output refers to the measured pollutant tracer concentration. The model input includes pollutant source and model parameters. Consequently, the source identification inversion and parameter inversion share the same theoretical limitations. Because, unlike the parameter estimation, the source characterization methods are scarce, a good understanding of their common theoretical limitations is helpful in developing the source estimation method.

One difficulty associated with parameter estimation and source identification stems from the fact that the inverse results, such as model parameters and source magnitudes, are highly sensitive to the sampling error. Even round-off error in the measured variables can result in unstable inversions. To achieve a stable inversion, we must either minimize the sampling error or reduce the sensitivity of the inversion. Since there is always round-off error in the measured variables, we can not totally eliminate the sampling errors by increasing the accuracy of the measurements. Consequently, the only solution is to decrease the inversion sensitivity. It is quite clear that the reduction of the inverse sensitivity critically determines the success of the inversion.

A second difficulty related with the parameter estimation and source estimation is non-uniqueness. Non-uniqueness represents the cases where the inversion of model parameters and pollutant sources has multiple results. The non-uniqueness problem is closely related to the invertibility of parameter estimations and pollutant sources. “Identifiability” has been defined in several different ways (Yeh, 1986), but the term is used in all cases to describe the degree to which the input parameters of a specific model can be identified by the sampled information. Based on this definition, it is intuitively obvious that there should be a numerical variable to represent identifiability. Based on statistical con-

cepts, Yeh and Sun (1984) developed the parameter identifiability index. However, scientists have not found a numerical index that can indicate the source identifiability.

The third difficulty of the inversion is its inability to estimate source spatial and temporal variations. The reason is that the number of unknowns required to represent the spatial and temporal variation of a source is so large that the inversion's high sensitivity makes a stable inversion impossible. That is why parameter estimation and constant source estimation have had some success, whereas identification of spatial and temporal variation of sources has not been achieved.

All three difficulties are associated with high inversion sensitivity. The first problem states that when the inversion has high sensitivity, a solution is not possible. The second problem is equivalent to saying that when the inversion sensitivity of one station and one source is high, the station can not identify the source. The third challenge is due to the fact that inversion sensitivity increases dramatically with the number of unknowns. Consequently, the large number of inversion unknowns, representing the source's spatial-temporal variation, results in high inversion sensitivity and unstable results. In summary, the high inversion sensitivity makes both parameter estimation and source identification difficult to achieve.

In this research, we propose a "dense-sampling" inverse method to address the above three difficulties. The approach applies the "transfer function" concept to formulate the relationships between the source-spatial-temporal distribution and the measured pollutant concentrations. Additionally, the research develops the "dense-sampling" concept to decrease the inversion sensitivity by increasing the inversion's equation-to-unknown ratio. In fact, the "dense-sampling" concept converts under-determined quasi-determined inversions to the overdetermined inversions. By applying the concepts of "transfer function" and "dense-sampling", the method develops systematic solutions for the three inversion's difficulties. First of all, the method decreases the inversion sensitivity to overcome the first difficulty. Second, the method discovers the inversion sensitivity index--condition number which can determine the source invertibility before the inversion. As a result, the method solves the second difficulty. Finally, the method can successfully achieve temporal inversion of the unknowns. The solution of the three difficulties are demonstrated in this chapter.

## 2.3 Background and overview

The source identification method has not been well established to estimate pollutant sources in either surface water or groundwater environments. In spite of this, several conventional approaches have been proposed. These approaches can be grouped into four broad categories: conceptual-argument approach, statistical methods, trial-and-error simulations, and inversion methods.

The purely conceptual argument finds the source locations and their magnitudes based on the prior-knowledge of sources, measured pollutant concentration (Wechsler et al., 1982), and remote-sensing image (Ishaq and Huff, 1979). One problem with this approach is that source identification is very inaccurate when pollutant transport is very active. Another problem is that the approach can not estimate source temporal variation. Thus, conceptual argument approaches only answer the source location and magnitude, leaving the source spatial and temporal variation unsolved. Different from the purely conceptual argument approach, the statistical methods use techniques such as regression analysis and factor analysis to estimate the source locations and source types. Even though the statistical methods can estimate the source location and source magnitude, they also fail to deal with source temporal variability (Grimshaw and Lewin, 1980; Ginn and Cushman, 1990). Another method for source identification is the trial-and-error simulation approach, in which the system's sources and model parameters are manually adjusted until an acceptable agreement between the measured pollutant concentration and the modeled concentration is obtained. However, the trial-and-error approach relies heavily on the modeler's experience and his or her understanding of the modeled processes. Due to the subjective nature of the approach, the results are not optimized.

The inverse modeling approach is very attractive in estimating pollutant sources. In this approach, the inversion estimates the source from the measurable variables (like water head, pollutant concentration) and model simulations (like water flow equation and advection-diffusion equation). Consequently, the inverse approach shows the most promising results in achieving source identification.

One study about source identification in the groundwater environment is that of Gorelick et al. (1983). As an optimization approach, the method generates a series of constraints by the flow and transport model. Then, the method applies least-square regression,

integer programming and linear programming methods to determine source locations and source magnitudes. Since the method assumes that the source magnitude is constant, it can only select the source's location and magnitude. The method can not address the source identifiability issue or describe source temporal variability.

Wagner (1992) presented a methodology for simultaneously estimating model parameter and pollutant sources. The method combines ground water flow and contaminant transport simulations with non-linear maximum likelihood method (Carrera, 1984, Carrera and Neumann, 1986) to determine the source scenario and model parameters. Similar to the previous case, the method can only estimate constant source magnitudes. Even though the method uses the 1st-order uncertainty analysis to assess identifiability, the statistical analysis can not provide a solid-mechanism to design a sampling network. Again, the method does not numerically approach the identifiability issue and can not accomplish the source temporal inversion.

This research develops a source temporal-inversion method, which systematically address the theoretical issues of inversion. This chapter diagnostically analyzes the method's capability in addressing the sensitivity reduction and the source identifiability by demonstrating the source-temporal inversion and sampling network design.

## **2.4 Problem description and formulation**

Source time series cannot be estimated easily and accurately. Generally, their temporal variations are estimated by measuring pollutant concentrations near pollutant sources. However, without considering hydraulic transport, and the source-station location, the measurements cannot accurately estimate pollutant source. This research formulates the relationships between the source magnitudes and the measured concentration magnitudes by considering the pollutant transport and source-station location. Consequently, the research solves the source temporal inversion problem. Mathematically, the research characterizes the pollutant transport through the "transfer functions". Accordingly, the measured tracer concentrations are the convolution of the source time series and the transfer functions. Along the way, the source time series are the deconvolution of the measured concentration and the transfer function.

### 2.4.1 Formulation of the “dense-sampling” inverse method

The “dense-sampling” inversion method is based on the concept of the transfer function. The “transfer function” of station  $i$  and source  $j$  is defined as the measured concentration ( $\omega$ ) at station  $i$  in response to a unit forcing at source  $j$  (Figure 2.1). In the surface water environment, the transfer function is a function of source location  $j$ , station location  $i$ , release time  $t_0$  and sampling time  $t$ . Therefore, it is represented as  $\omega_{i,j,t_0}(t)$ . For a conservative tracer, the measured concentration time series ( $C$ ) is represented as the convolution of the source strength ( $S$ ) and transfer function ( $\omega$ ), as shown in equation (2.1).

$$C_i(t) = \sum_{j=1}^{N_s} \left\{ \sum_{t_r=0}^{N_r} \omega_{i,j,t_0}(t_r) S_j(t-t_r) \right\} \quad (2.1)$$

In the equation,  $t_r$  is a variable for linear interpolation of the transfer function, and station index  $i$  changes from 1 to the number of stations,  $N_a$ . The equation shows that the measured tracer concentration at station  $i$  and time  $t$ ,  $C_i(t)$  is the summation of  $N_s$  sources over  $N_r$  release times. Equation (2.1) represents a system with  $N_a \times N_r$  equations and  $N_s \times N_r$  unknowns. When  $N_a/N_s = 1$ , the system yields a unique solution. When  $N_a/N_s > 1$ , the system is overdetermined and has a unique least square solution. When  $N_a/N_s < 1$ , the system is underdetermined and has an infinite number of solutions. Clearly, one of the limitations of the method is that it requires  $N_a/N_s \geq 1$ . That is to say the number of stations must be equal to or larger than the number of sources. Additionally, in most cases, equation (2.1) is close to singular. That means that any sampling error in  $C$  can generate large inversion errors in  $S$ .

In order to eliminate both the singularity and station/source ratio constraints, we propose the “dense-sampling” concept, which is represented by the “dense-sampling” parameter  $N_D$ ,

$$N_D = \frac{\Delta t_{source}}{\Delta t_{sampling}} \quad (2.2)$$

where  $\Delta t_{source}$  is the inversion time resolution and  $\Delta t_{sampling}$  is the sampling time resolution.

The idea of dense sampling is that the sensitivity of the inversion can be reduced at the expense of the temporal resolution of the inverted source. The sampling rate at the monitoring stations, and the value of  $N_D$ , effectively control the achievable temporal resolution for  $S$ . While the Nyquist frequency for the sampling instrument may impose a limit on the temporal resolution of  $S$ , this limit will for many environmental applications be quite acceptable.

By introducing  $N_D$ , equation (2.1) becomes the “dense-sampling” formulation.

$$C_i(t) = \sum_{j=1}^{N_s} \left\{ \sum_{j_1=1}^{N_D} \left\{ \sum_{j_2=-N_D}^{N_D} \frac{N_D - |j_2|}{N_D} \times \omega_{i,j} (j_1 \times N_D + j_2) \times S' (j_1 \times N_D) \right\} \right\} \quad (2.3)$$

In the equation,  $j_1$  is the time index ( $t = (j_1 \times N_D) \times \Delta t$ ),  $j_2$  is a variable for the linear interpolation of the transfer function, and  $S$  is the inverted source. It is important to point out that the number of unknowns of the “dense-sampling” equation decreases to

$$\left( \frac{N_r - 1}{N_D} + 1 \right) \times N_s \quad (2.4)$$

and the number of equations is the same  $N_a \times N_r$ . Therefore, by selecting the “dense-sampling” parameter  $N_D$  to satisfy equation (2.5),

$$\left( \frac{N_r - 1}{N_D} + 1 \right) N_s \leq N_a \times N_r \quad \text{or} \quad \frac{(N_r - 1)}{\left( \frac{N_a N_r}{N_s} - 1 \right)} \leq N_D \quad (2.5)$$

there is always one unique least-square solution. Obviously, equation (2.5) shows that  $N_D$  determines the ability of station in identifying contaminant source.

“Dense sampling” has both theoretical and practical advantages. First, equation (2.3) correctly formulates the relationship between the source strength and the sampled concentration magnitude. Additionally, equation (2.5) suggests the idea of sampling network design by the fact that  $N_a$  can be less than  $N_s$ . Furthermore, the inversion sensitivity of equation (2.3) can be effectively reduced by increasing  $N_D$ . Consequently, the method can accomplish the time-domain contaminant source estimation.

### 2.4.2 Source identifiability

Based on the “dense-sampling” formulation (2.3), this research shows that the inversion’s solvability determines the source identifiability. That is to say, the high inversion sensitivity indicates the low source identifiability and vice versa. Additionally, because the inversion sensitivity can be measured by the condition number of equation (2.3) and the condition number decreases dramatically as  $N_D$  increases, the “dense-sampling” inverse method is able to increase the source identifiability by increasing the “dense-sampling” parameter  $N_D$ . Clearly, the dense-sampling scheme converts non-identifiable source to identifiable source and provides the condition number to measure the source identifiability. Detailed discussion about the condition number and its ability to improve the inversion efficiency is presented in Chapter 3.

The method application includes the system characterization, system measurement, and system inversion. The system characterization calculates the transfer functions among every source-station pair and assembles the transfer function matrix  $A$ . At this stage, we assume that source locations, source spatial distributions, and station locations are known. The second step samples the tracer concentration time series and forms vector  $B$ . Note that station locations for tracer measurement must be the same as the station locations used to calculate the transfer functions. The third step estimates the source  $\vec{X}$  by solving the deconvolution equation  $A\vec{X}=\vec{B}$ , where matrix  $A$  includes the transfer function and vector  $\vec{B}$  consists of the measured tracer concentrations. In this step, the “dense-sampling” parameter  $N_D$  determines the known-to-unknown ratio.

## 2.5 Numerical experiments

This section numerically analyzes the method by inverting pollutant sources of a synthetic surface water environment. The advantages of analyzing the method in a synthetic reality are that the method can be tested for a variety of hypotheses and the inversion results can be evaluated by comparing with the imposed sources. Accordingly, the designed synthetic reality is simple enough for method testing while it is sufficiently complex to include different factors for diagnostic analysis.

### 2.5.1 Synthetic St. John's Landfill surface water environment

The proposed method is diagnostically analyzed in the synthetic St. John's Landfill surface water environment, which has fully controlled water circulation, hydraulic transport, sampling scheme, and source scenarios (Figure 2.2). The finite element grid of the synthetic St. John's Landfill surface water system includes 1957 nodes and 713 elements. The water circulation is simulated by solving the 2-D depth averaged shallow water equations in the frequency domain (*Westerink et al., 1987*). To make the test simpler, we used the  $M_2$  tide only. The hydraulic transport is modeled by the advection-diffusion equation (*Baptista, 1987*). The diffusion coefficient is  $1 \text{ m}^2/\text{s}$ . For the purpose of computation efficiency, the simulated time interval is 1.24 hours, i.e. one tenth of the  $M_2$  period, so that the model can read the foot of the characteristic lines of one tidal cycle instead of backward tracking the entire simulation time. The total simulation time is 200 time steps, which has many integer factors for dense-sampling. The eight sources and eight stations are spatially equally distributed along the slough. This source-station configuration is able to represent the spatial pattern of source-station response for the entire slough. Clearly, the synthetic St. John's Landfill environment is sophisticated enough to evaluate the source temporal inversion method regarding the sampling network design and the sampling error reduction.

### 2.5.2 Integrity test

The integrity test recovers time history of four sources by sampling concentrations at four stations (Figure 2.3). Because the sampling error is zero, the test can investigate method ability in reducing the effect of the round-off errors. Also, the four source time series vary dramatically during the sampling period. Therefore, the test can show the effects of source variations on the inversion results. Furthermore, the four sources are spatially overlapped so that the test is able to show the method's robustness to invert spatially overlapped sources. Clearly, the integrity test evaluates the method's performance without introducing sampling error.

The integrity test follows the inversion's three steps: system characterization, system measurement, and system inversion. The first step evaluates the transfer functions to characterize the system's hydraulic transport. This is exemplified by the transfer function between source 1 and station 1 (Figure 2.4). Firstly, the transfer function corresponding to

each release time shows a periodic variation, as a result of tidal advection. In addition to the periodic variation, transfer function decreases due to the diffusion process. This is shown by the fact that the transfer function magnitude, after a short diffusion period, is higher than the transfer function magnitude after a long diffusion period. Finally, the transfer function matrix is a triangular matrix, which indicates the inverted source time-step equals the sampling time step. Obviously, the transfer function characterizes the hydraulic transport.

The second step simulates the situation with four pollutant sources and four sampling stations (Figure 2.5). The concentrations at the four sampled stations share both a long term trend and a short term trend. In the long trend, the sampled concentration begins from a zero initial condition and increases to a specific value. In the short trend, the sampled concentrations demonstrate a 12.4-hour variation in response to the tidal signal. It is clear that the measured tracer concentration illustrates the hydraulic transport of the synthetic reality.

The third step uses inversion to recover the four source time-series. The inversion results (Figure 2.6) provide insight into the proposed method. First of all, the inverted source 4 has large inversion errors when  $N_D=2$ . This is because the round-off errors in the measured concentration are amplified by the high inversion sensitivity to create inversion errors. However, when  $N_D=10$ , the sources are recovered without inversion errors. The reason is that the “denser inversion ( $N_D=10$ )” can reduce the inversion sensitivity more efficiently than the “less-dense inversion ( $N_D=2$ )”. The comparison shows the ability of the “dense-sampling” concept to effectively reduce the impact of round-off error, and to achieve temporal inversion of the source. Most notably, the method can recover sources with large temporal variations, like source 3, suggesting that the content of temporal variability does not affect the inversion performance. Also of significance, the proposed method is capable of distinguishing between sources that are spatial overlap (Figure 2.3), a characteristic of interested to environmental systems (e.g. point sources overlapping on non-point sources). Finally, we stress that the effective sampling error reduction achieved by “dense-sampling” has a price, that of losing time resolution. As illustrated in Figure 2.6, a larger  $N_D$  (10 versus 2) is more effective in reducing inversion sensitivity. However, time resolution in the inverted time series is 5 times lower for  $N_D=10$  than for  $N_D=2$ .

### 2.5.3 Error reduction by the “dense-sampling” method

The ability to average different kinds of errors determines the success of the inverse methods (Xiang and Elsworth,1992). This section demonstrates the method capability in reducing both the random error and systematic error.

#### 2.5.3.1 Random error reduction

The ability of the method to reduce random error is demonstrated by estimating the four sources with different sampling error levels. Again, the developed method effectively inverts the four sources (Figure 2.7). Because 10% random sampling error is higher than round-off error, a larger  $N_D$  is required ( $N_D=20$ ) than in the case discussed earlier. Also the figure clearly shows that the method can carry out stable inversion when the random sampling error is as high as 10%.

The inversion parameter<sup>1</sup> can also efficiently measure the inversion sensitivity, because it eliminates the effects of error magnitude and sampling number on the inversion sensitivity. indicates that the “dense-sampling” method is very effective in averaging sampling errors to stabilize inversion results. For example, when  $N_D=2$ , the sensitivity parameter of 96.07 reveals that the sampling error can be amplified as much as 96 times. However, when  $N_D$  increases from 2 to 40, the inversion sensitivity decreases dramatically. Moreover, the table shows that the “dense-sampling” technique is able to average as large as 10% relative sampling error, which is higher than a common instrumental error. Therefore, it shows that the method is capable of real-world inversion. In summary, the graphical comparisons and sensitivity analyses indicate that the “dense-sampling” technique is robust enough to filter out the random sampling error.

---

1. The inversion parameter is defined as  $InverseSensitivity = \frac{Norm(L_2)}{|rel-Error|}$ .

Because it minimizes the effects of the error magnitude and the sampling number on the error amplification, it can precisely measure the inversion sensitivity. As illustrated in , when the sampling error changes from 1% to 10%, the inversion parameter doesn't change. This confirms that the inversion parameter is not a function of sampling errors.

**Table 2.1 Relationship between the inversion parameter and the “dense-sampling” parameter  $N_D$  with different sampling error levels**

**Table 2.1a: No Sampling Error**

$N_D$	source 1	source 2	source 3	source 4
2	017796	0.018957	0.027099	11.25980
4	0.017897	0.019161	0.025813	2.007610
10	0.018373	0.021197	0.023073	0.018132
20	0.022653	0.025173	0.025163	0.025984
25	0.022822	0.034347	0.029184	0.028398
40	0.028347	0.041784	0.053586	0.066180

**Table 2.1b: Relative Sampling Error = 1%**

$N_D$	source 1	source 2	source 3	source 4
2	0.021811	0.026717	0.079328	96.07190
4	0.019257	0.020806	0.034600	3.783030
10	0.018877	0.021441	0.024510	0.027518
20	0.022491	0.026222	0.023668	0.027353
25	0.022730	0.035177	0.029632	0.030075
40	0.028060	0.043445	0.055865	0.067946

**Table 2.1c: Relative Sampling Error = 5%**

$N_D$	source 1	source 2	source 3	source 4
2	0.063574	0.081795	0.349123	438.0770
4	0.036763	0.036713	0.102649	10.88590
10	0.024130	0.025812	0.043862	0.101509
20	0.023891	0.030945	0.026942	0.039845

**Table 2.1c: Relative Sampling Error = 5%**

$N_D$	source 1	source 2	source 3	source 4
25	0.023889	0.039256	0.040496	0.045710
40	0.026970	0.050445	0.066101	0.078047

**Table 2.1d: Relative Sampling Error = 10%**

$N_D$	source 1	source 2	source 3	source 4
2	0.122847	0.156267	0.690246	865.6630
4	0.065795	0.062916	0.196080	19.76480
10	0.034700	0.035994	0.077066	0.199655
20	0.029394	0.037649	0.044301	0.062198
25	0.028237	0.045654	0.063794	0.073173
40	0.025747	0.059763	0.080590	0.095500

### 2.5.3.2 Systematic error reduction

Systematic error reduction is more difficult than random error reduction. This is because systematic sampling error induces both amplitude-related inversion error and phase-related inversion error, while random sampling error only introduces amplitude-related inversion errors (Figure 2.8).

This experiment evaluates the method's capability in reducing both types of systematic errors. The phase-related systematic error is induced by phasing out a 6.2 hours the sampling "clock". Intuitively, phase errors in sampling data should lead to phase errors in the identified results (square symbol in Figure 2.8). The result suggests that the method successfully averages the 6.2-hours tidal clock error. The reason is that the inversion time interval ( $\Delta t \times N_D = 24.8$  hours) is larger than the tidal clock error (6.2 hours). Therefore, "dense-sampling" can effectively average, in this case, the phase-related systematic sampling errors. However, when the phase error becomes very large, equal or larger than the inversion time interval, the inversion's capability of reducing the phase error becomes less effective. Larger phase-related errors can destabilize inversion results. Therefore, the

experiment shows that the method can effectively reduce the phase-related systematic error when the inversion time interval is larger than the phase-related systematic error.

The amplitude-related systematic sampling error are produced by an incorrect diffusion coefficient ( $D_x=2.0 \text{ m}^2/\text{s}$ , instead of the value  $D_x=1.0 \text{ m}^2/\text{s}$  used in the definition of the synthetic reality). The larger diffusion coefficient introduces the amplitude-related inversion errors (Figure 2.8). It is interesting to note that amplitude-related inversion errors are quite different for different sources. Sources 1 and 4 have negative errors, while sources 2 and 3 have positive errors. The reason is that, when the synthetic reality has a large diffusion coefficient ( $D_x=2.0 \text{ m}^2/\text{s}$ ), its hydraulic transport changes. With the same source spatio-temporal scenario, the sampled tracer concentration becomes higher at some stations and lower at other stations than their true values. Therefore, based on the wrong sampling information, some of the inverted sources (1 and 4) have negative errors and some of the inverted sources (2 and 3) have positive errors.

The relative locations of sampling stations, land boundaries, and flow boundaries also play an important role in transforming the sampling error into the inversion error. For instance, the inverted source 1 generally has a larger phase error than other sources. This is due to the fact that source 1 is located in the dead end slough, where diffusion becomes more dominant than advection compared with other parts of the slough. Additionally, station 1 is placed at the edge of dead-end slough and main channel where advection is more dominant than diffusion. Therefore, when the tracer of source 1 leaves the dead-end slough, it seldom moves back. As a result, station 1 can not respond to the tracer lost to the main channel.

#### **2.5.4 Sampling network design**

The sampling error reduction tests require that the number of stations must equals the number of sources. Releasing this limitation is important, and leads to the following questions:

- What is the minimum number of stations that can monitor all the pollutant sources?
- Where should these stations be located?
- What is the sampling frequency and sampling time?

The following experiment answers the three questions by designing a sampling network for monitoring the eight sources of the synthetic St. John's landfill environment.

The tested environment includes eight pollutant sources and eight sampling stations (Figure 2.2). The condition numbers between the 8 sources and the 8 stations are tabulated in Table 2.2. One point of interest is that small condition numbers are diagonal elements, indicating that station  $i$  can efficiently identify source  $i$ , which is closely located. In addition, when the difference between source index  $i$  and station index  $j$  is big, their condition number is also big. This is due to the fact that when  $i$  and  $j$  are different, the source  $i$  is located away from station  $j$ . Therefore, station  $i$  can not identify source  $j$ . Clearly, the condition number table signifies the source identification of the synthetic St. John's Landfill surface water environment. This statement can be further validated by investigating each row and column of the table.

In Table 2.2, each column demonstrates the response of one source at different stations. For example, the small condition numbers in the third column are 110 for station 2, 95 for station 3 and 410 for station 4. This suggests that source 3 can be identified by stations 2, 3 and 4.

**Table 2.2 Source identifiability table for the eight source and eight station case, with "dense-sampling" parameter,  $N_D$ , of 20**

	Source 1	Source 2	Source 3	Source 4	Source 5	Source 6	Source 7	Source 8
Station 1	INF	INF	INF	INF	INF	INF	6.6E+14	9.5E+3
Station 2	INF	INF	INF	INF	INF	4.5E+13	4.2E+5	5.3E+3
Station 3	INF	INF	INF	2.7E+14	4.9E+8	8.1E+4	1.0E+3	2.6E+13
Station 4	2.0E+13	2.6E+7	1.3E+6	1.6E+5	5.2E+2	1.3E+3	3.5E+9	INF
Station 5	8.6E+7	2.2E+3	4.1E+2	3.1E+2	1.2E+3	2.1E+4	3.5E+14	INF
Station 6	2.1E+7	3.2E+2	9.5E+1	8.3E+1	4.2E+3	2.8E+9	INF	INF
Station 7	2.2E+6	7.7E+1	1.1E+2	3.9E+2	7.6E+6	2.0E+12	INF	INF
Station 8	4.7E+3	3.5E+2	1.6E+4	1.8E+5	6.2E+9	5.2E+15	INF	INF

For this synthetic case, we empirically choose 5000 as the identifiability criterion. Any condition number smaller than 5000 indicates identifiability between the source and station. By applying this criterion to every column of Table 2.2, we conclude that source 1 can be identified by station 1; source 2 can be identified by stations 1, 2, 3 and 4; source 3 can be identified by stations 2, 3 and 4; source 4 can be identified by station 2, 3 and 4; source 5 can be identified by station 3, 4 and 5; source 6 can be identified by station 5; source 7 can be identified by station 6; source 8 can be identified by station 7. On the other hand, applying the criterion to every row, we find that station 1 can identify sources 1 and 2; station 2 can identify sources 2, 3 and 4 and so on. Therefore, in order to identify the eight sources we need at least 5 stations (stations 1, 4, 5, 6 and 7). Obviously, the condition number table optimally selects the station numbers and station locations. The sampling frequency and sampling time are  $1/4464$  s and 248 hours, according to the transfer function.

In Table 2.2, each row shows the response of one station to different sources. For instance, the fourth row has four small condition numbers<sup>1</sup>, illustrating that station 4 can identify sources 2 through 5. Similarly, station 1 can identify sources 1 and 2. The different number of sources that are identifiable by stations 2 and 4 shows that the condition number table represents the effects of the hydraulic transport on the source identification. For instance, the 4<sup>th</sup> station can identify more sources than any other station. One reason is that the tidal boundary expands the source response area for station 4. The other reason is that the dead-end land boundary is located far away from station 4, so that it does not restrict the source response area of station 4. These two reasons explain why station 4 can identify more sources than other stations. In contrast, station 1 can identify fewer sources than all other stations. This is because the station 1 is located inside the dead-end slough and the dead-end land boundary restricts the station response area. It is quite clear that the effects of land and tidal boundaries on source identifiability is expressed by the condition number of the transfer function.

As an extreme design, the table indicates that we can use 2 stations (stations 1 and 4) to identify 5 sources (sources 1, 2, 3, 4 and 5), when the sampling resolution=4464 sec-

---

1. We empirically define "small" condition number as numbers below 5,000 in this chapter. Further numerical investigations are discussed in Chapter 3.

onds, number of sampling steps=200 and  $N_D=20$ . According to the designed sampling network, we successfully estimate the five sources time series (Figure 2.9). That is to say, the designed sampling network is validated. With this simplified test, we demonstrate the ability of the developed method to optimally select the station number, station location, sampling frequency and sampling time for an environmental field survey.

## 2.6 Summary and conclusions

This research develops a time-explicit inverse method for estimating time history of pollutant sources. In the method, we apply the transfer function concept to formulate the relationship among the source strength, hydraulic transport, and the measured concentration. In addition, we developed the “dense-sampling” concept to reduce the inversion sensitivity. Consequently, the method can suppress both random errors and systematic errors to achieve a stable and meaningful inversion. Moreover, the research shows that the source identifiability can be determined by the condition number, so that it can guide a field survey, an issue that is further explained in the next chapter. In summary, the research successfully addresses three important inversion challenges: inversion sensitivity reduction, source identifiability, and source-temporal inversion.

The diagnostic analysis of the method illustrates that (a) the pollutant source scenarios can be recovered perfectly if the synthetic observations are not contaminated by errors and if the number of observation stations equals the number of sources to identify; (b) the inversion method is robust enough to “filter” out both random error and systematic errors, if the time interval of sampling is appropriately (often, an order of magnitude) denser than the time-interval at which we want to recover the time-history of the sources; (c) the inversion method is capable of identifying more sources than the number of sampling stations; however, the larger the ratio between the number of sources and sampling stations, the less time-resolution should be expected from the inversion; (d) the inversion method inherently provides a mechanism (condition number) to guide the choice of the sampling location and sampling schemes.

There are several avenues for extension of the method. For instance, when bio-geo chemical processes are involved, we need to combine parameter estimation with the source identification. Also, the inclusion of more than one pollutant would be a natural extension. Moreover, we do not have a universal criterion for the source identifiability.

Searching for this general criterion will be accomplished by the theoretical analysis of the method. Furthermore, the method still requires the prior knowledge of source locations and their spatial distributions. It is obvious that their solutions can definitely enhance the proposed source estimation method.

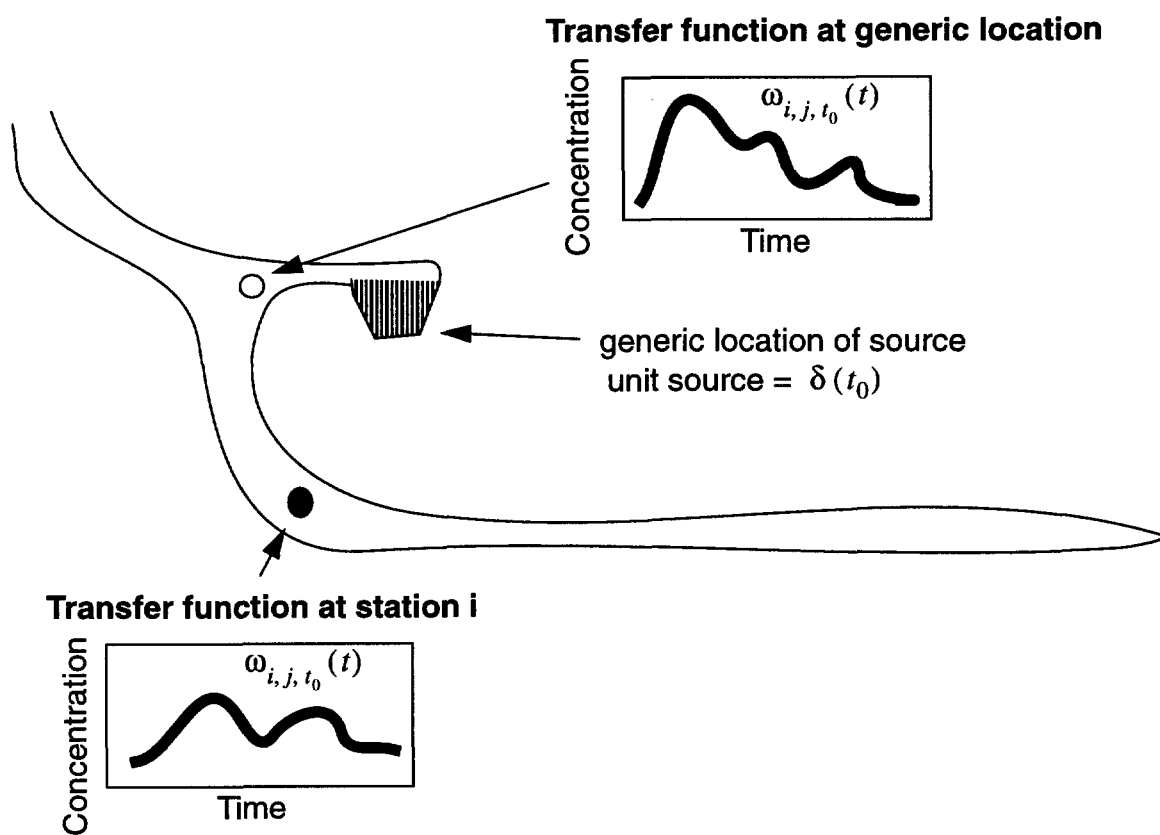


**Figure 2.1** Conceptual diagram of the transfer function ( $\omega$ ) of a generic surface water environment. In the figure,  $\delta(t_0)$  represents a unit source;  $i$  and  $j$  are the station index and the source index;  $t$  and  $t_0$  represent the sampling time and source release time respectively.

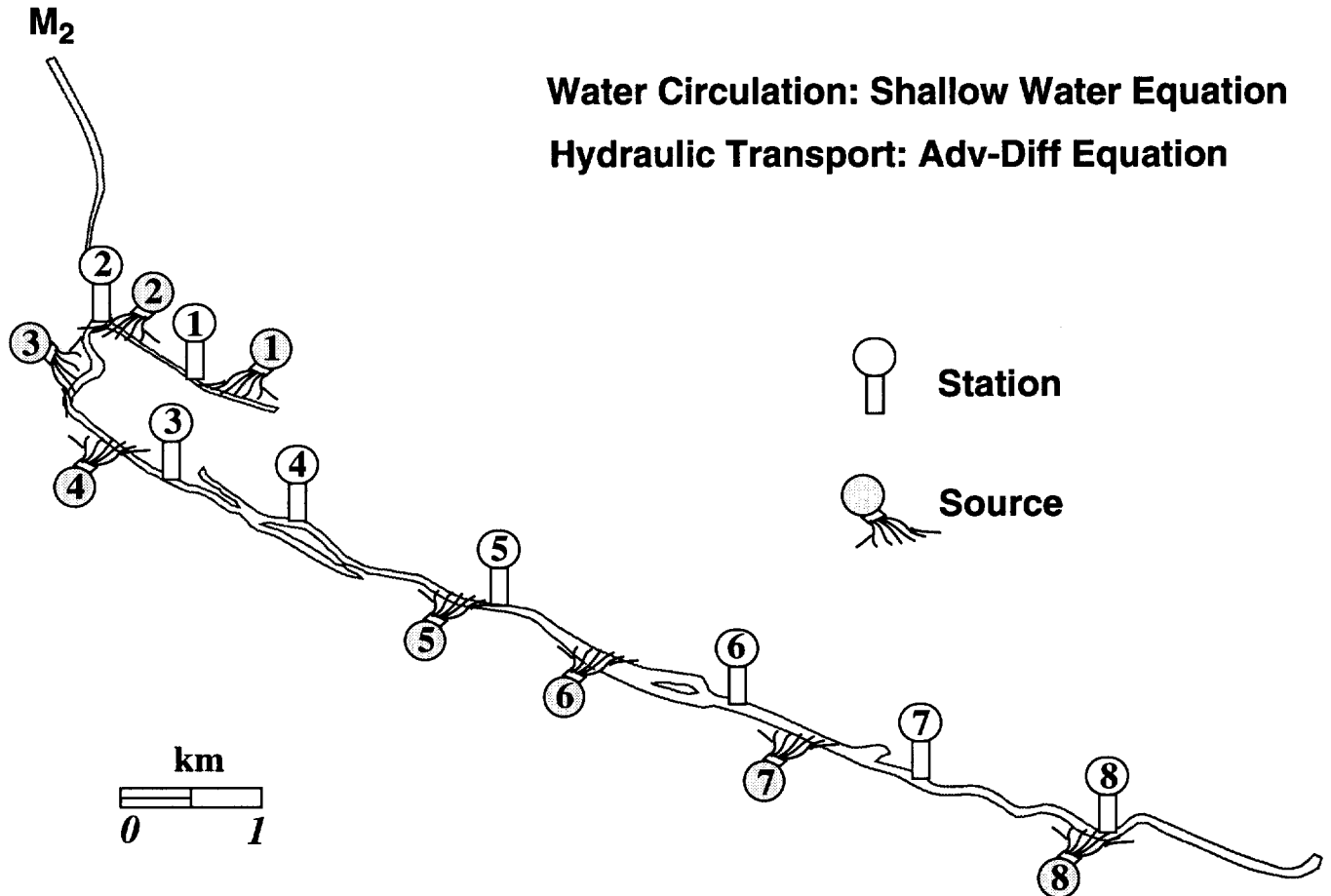


**Figure 2.2 Synthetic St. John's Landfill surface water environment. Its water circulation is modeled by the shallow-water equation. Its hydraulic transport is simulated by the advection-diffusion equation. It has 8 spatially distributed sources and 8 sampling stations.**

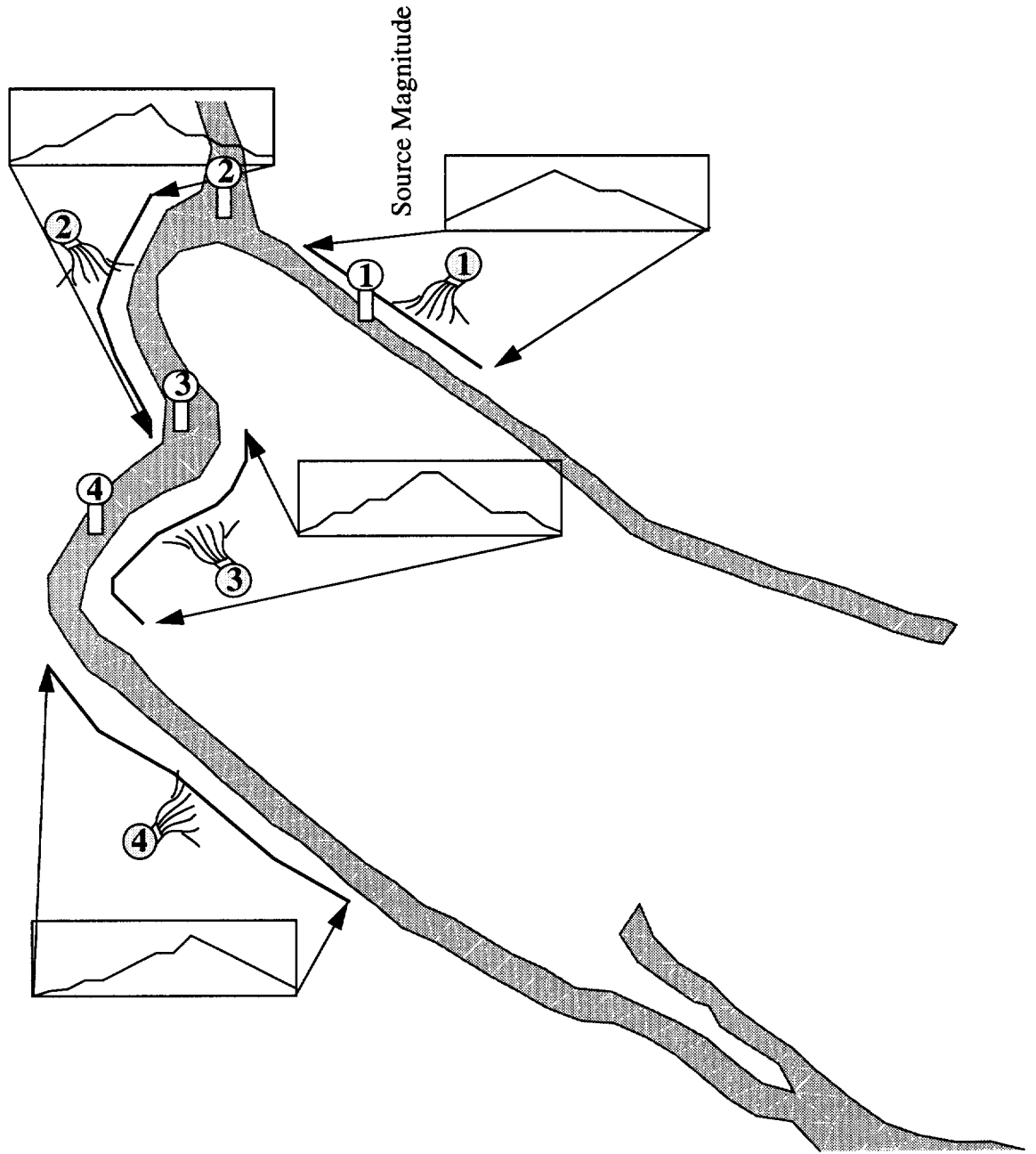


**Figure 2.3** The method integrity test case, which has 4 stations and 4 sources

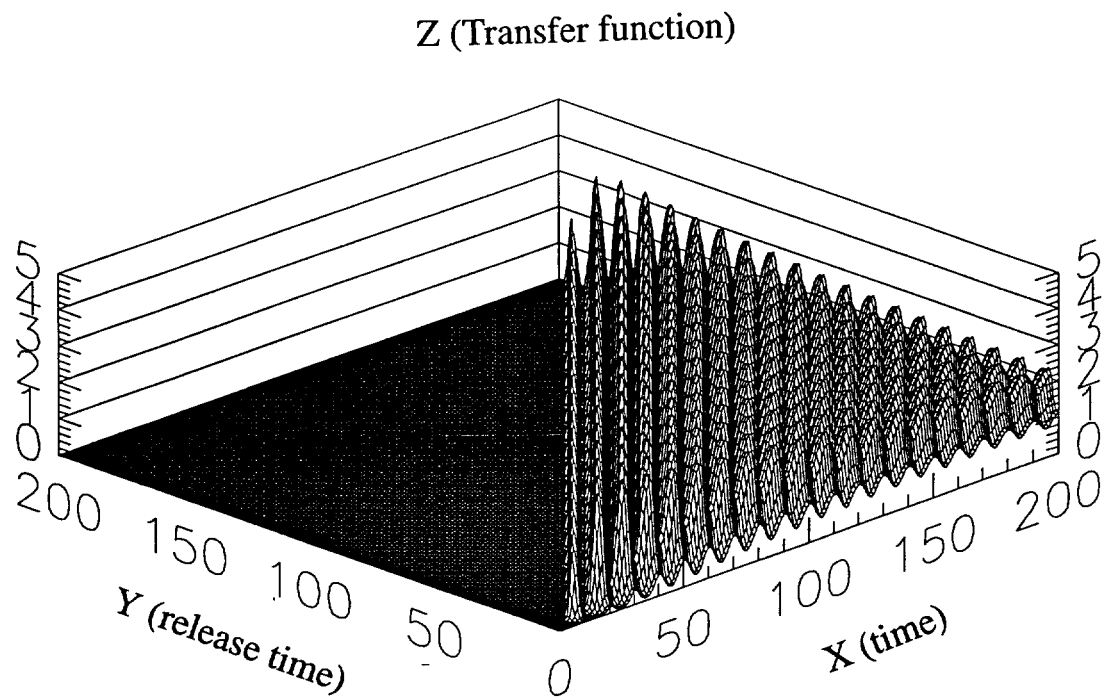


**Figure 2.4** The transfer function between station 1 and source 1, where X is the sampling time, Y is the release time, and Z is the magnitude of the transfer function.

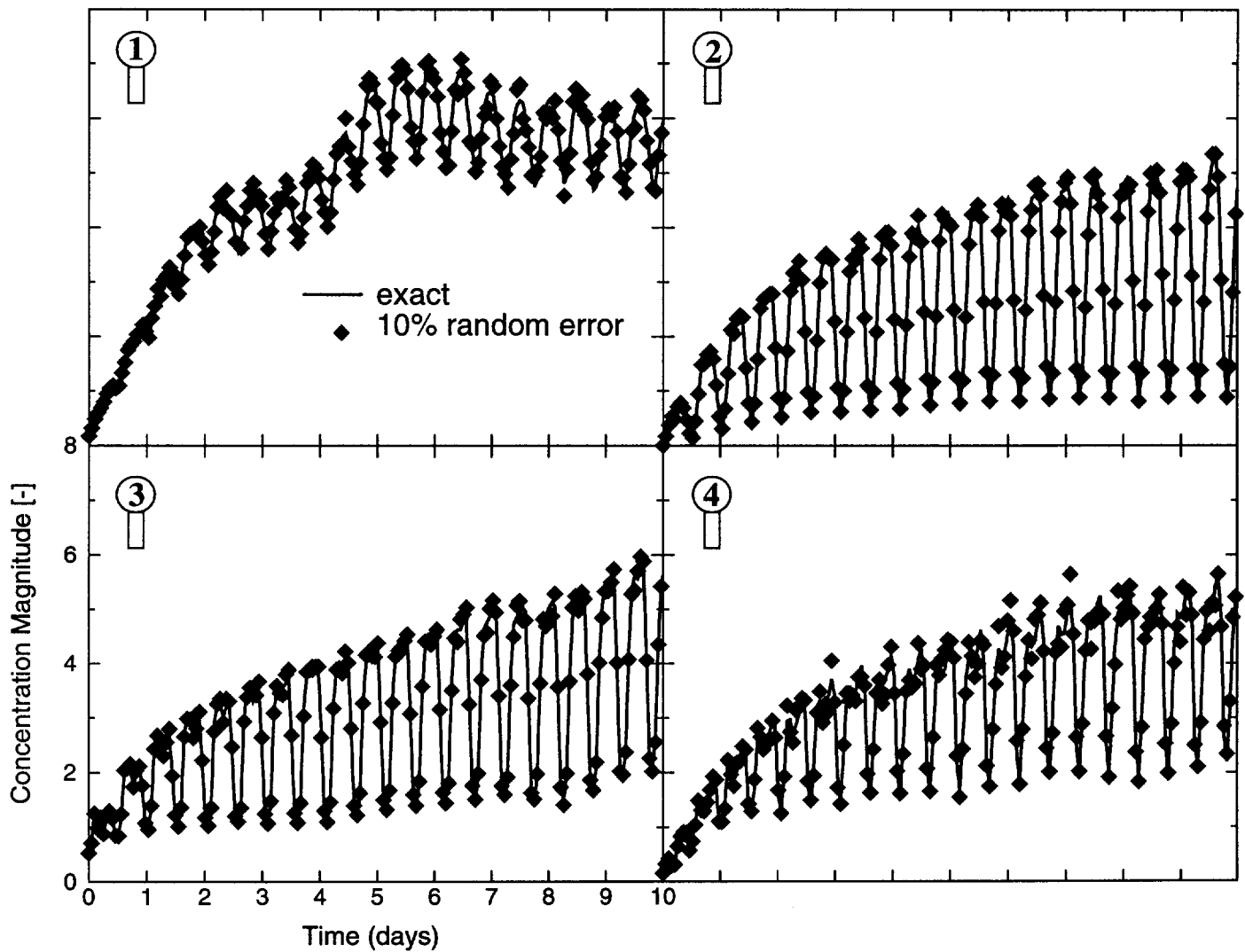


**Figure 2.5** Measured tracer concentrations at the four sampling stations. Note that when the sampling error is zero, the inversion corresponds to tests of the basic integrity of the method. When the concentrations has 10% sampling error, the corresponding inversion illustrates the ability of the method to reduce random-sampling error.

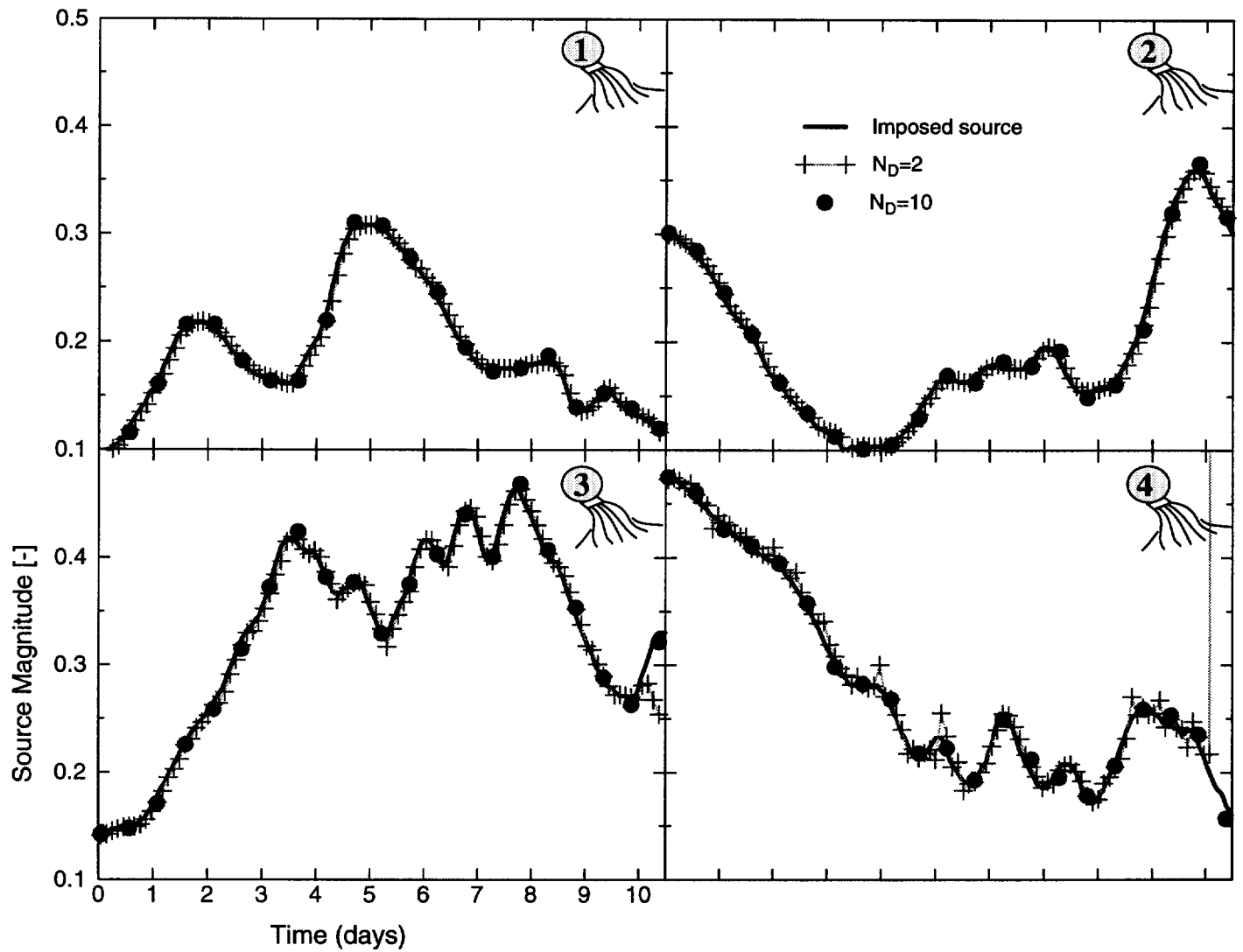


**Figure 2.6** Inverted 4 source time series from the method's integrity test. Note that when  $N_D=2$ , while round-off errors are amplified eventually leading for unstable inversion (source 4) when  $N_D=10$ , round-off errors are suppressed (source 4).

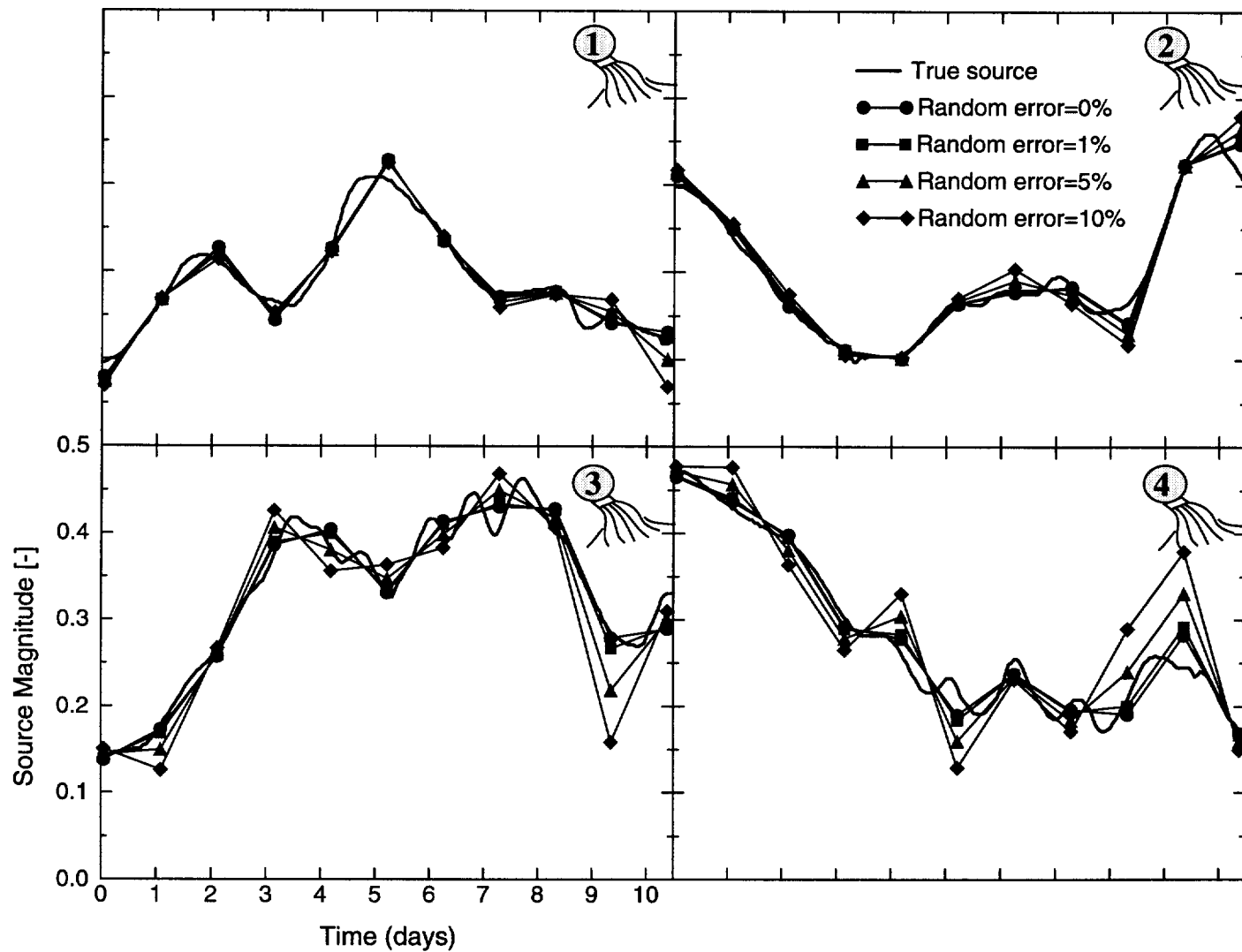


**Figure 2.7** The comparison of the estimated time-history of the sources with varying sampling random errors. The dense-sampling parameter  $N_D$  is 20 in all cases.

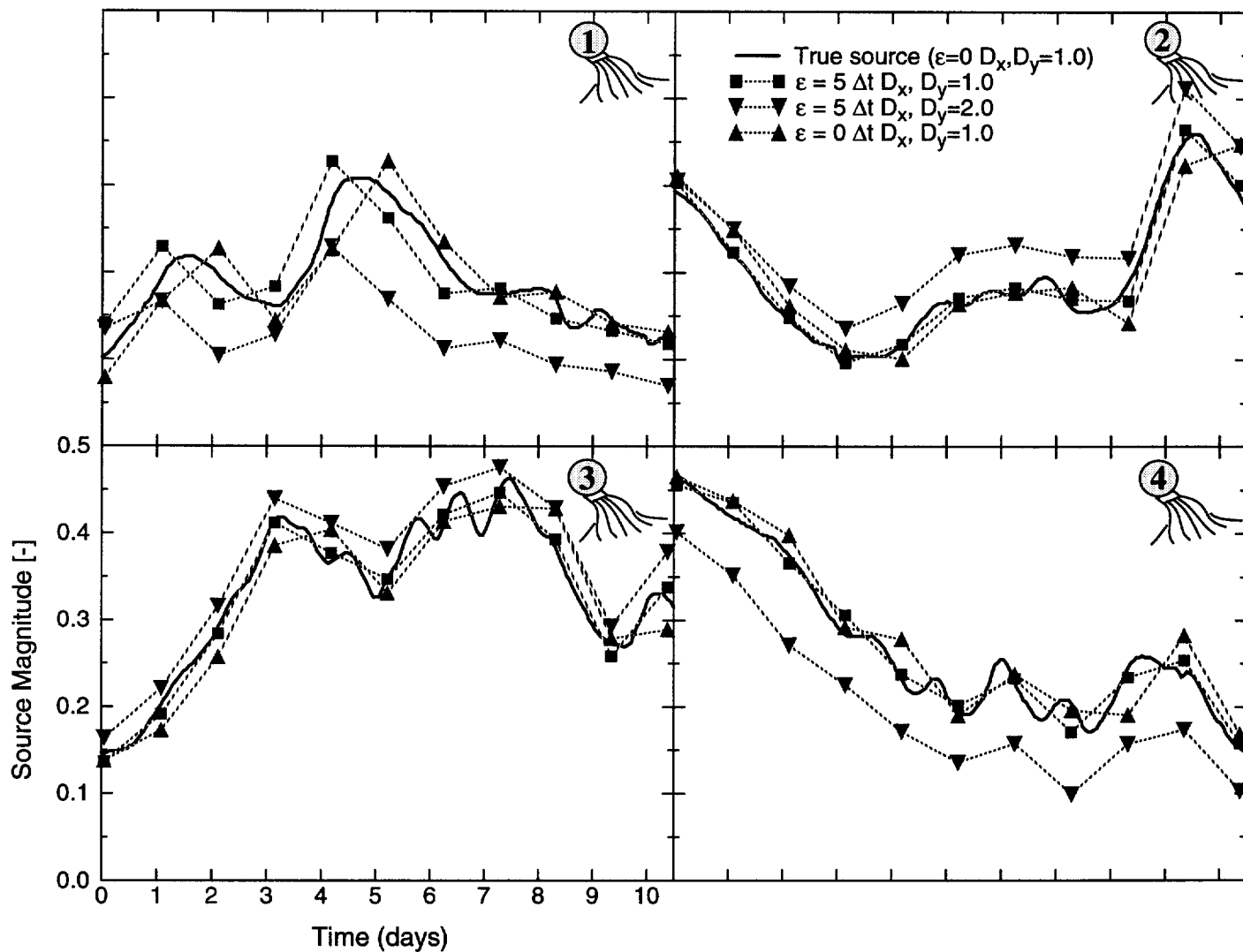


**Figure 2.8** Estimated source histories by four stations, when systematic errors exist. The systematic errors include 6.4 hours sampling time-shift errors and 100% diffusion coefficient error.  $\epsilon$  is the time-shift error and  $\Delta t$  is the sampling time interval (1.24 hours).

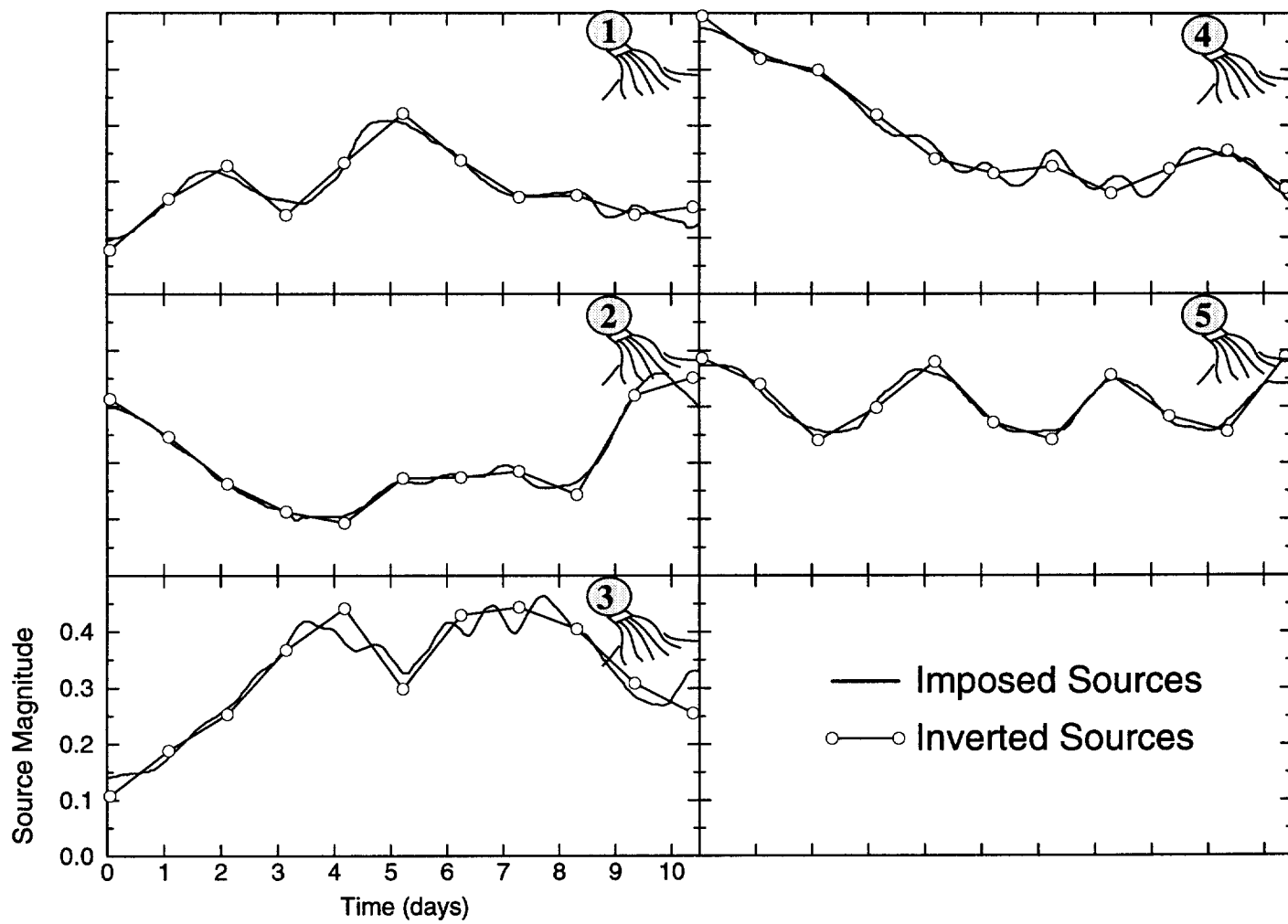


**Figure 2.9** Estimated source histories based on the designed sampling network. Note that the number of stations (2) is less than the number of sources (5).

## 2.7 References

- Baptista, A.M., *Solution of Advection Dominated Transport with Eulerian Lagrangian Methods Using the Backwards Method of Characteristics*, Ph.D. Thesis, MIT, Cambridge, Mass., 1987.
- Carrera, J. and S.P. Neumann, Estimation of aquifer parameters under transient and steady state conditions: 1. Maximum likelihood method incorporating prior information. *Water Resour. Res.*, 22, 199-210, 1986.
- Carrera, J., *Estimation of aquifer parameters under transient and steady-state conditions*. Ph.D. Dissertation, Dept. of Hydrology and Water Resources, University of Arizona, Tuscon, AZ, 1984.
- Ginn, T. R. and J. H. Cushman, Inverse methods for subsurface flow: A critical review of stochastic techniques. *Stochastic Hydrol. Hydraul.*, 4, 1-26, 1990.
- Gorelick, S. M., B. Evans and I. Remson, Identifying sources of groundwater: An optimization approach. *Water Resour. Res.*, 19(3), 779-790, 1983.
- Grimshaw, D. L. and J. Lewin, Source identification for suspended sediments, *Journal of Hydrology*, 47, 151-162, 1980.
- Ishaq A.M. and D. D. Huff, *Hydrologic Source Area - A technique for identifying, in Modeling Hydrologic Processes*. ed. Hubert J. Morel-Seytoux et al, Water Resources Publications P.O.Box 303, Fort Collins, Colorado 80522, USA, 1979.
- Wagner, B. J., Simultaneous parameter estimation and contaminant source characterization for coupled groundwater flow and contaminant transport, *Journal of Hydrology*, 135, 275-303, 1992.
- Wechsler, E.A., A. Q. Eschenroeder, D. Gilbert, K. Loos, P. Poston, and J. M. Stevens, *Feasibility of developing a comprehensive methodology for source identification and environmental loading* (materials balance), EPA Report EPA 600/3-82-047, 1982.
- Westerink, J.J., J. J. Connor, and K. D. Stolzenbach, A Primitive Pseudo Wave Equation Formulation for Solving the Harmonic Shallow Water Equations, *Advances in Water Resources*, 10, 188-199, 1987.
- Xiang, J., and D. Elsworth, Parameter identification of nonsteady groundwater flow systems, *Advances in Water Resources*, 15, 259-269, 1992.
- Yeh W. W.-G., Ne-Zheng Sun, An Extended identifiability in Aquifer Parameter Identification and Optimal Pumping Test Design, *Water Resour. Res.*, 20(12), 1837-1847, 1984.

Yeh, W. W.-G., Review of parameter identification procedures in groundwater hydrology:  
The inverse problem, *Water Resour. Res.*, 22, 95-108, 1986.

## CHAPTER 3

# A sampling network design method for monitoring pollutant sources using inverse modeling

### 3.1 Abstract

This chapter presents a sampling network design method for surface water quality, based on the inverse modeling. A sampling network design consists of selecting the number and location of sampling stations as well as deciding the sampling frequency and total sampling time. The inverse modeling technique developed in this research formulates the source-station response as the convolution between sources and their transfer functions. From this formulation, the proposed inverse method measures the source-station response by a numerical index - the condition number of the transfer function. The sampling network design, therefore, utilizes the condition number to select a minimum number of stations to identify all the pollutant sources. The proposed sampling-network design includes the following five steps: (1) simulating the water circulation and the hydraulic transport of the surface environment, (2) activating the system with different pollutant sources, and measuring the response at different sampling stations to evaluate the system's transfer functions, (3) tabulating condition numbers of the transfer function by station and sources, (4) designing the sampling network from the condition number table, and (5) validating the designed sampling network by inverting the imposed source. The proposed method has been successfully tested in the synthetic St. John's Landfill surface water environment by designing its sampling network to recover eight imposed sources. The test illustrates that the condition number can determine the number and location of stations, the sampling frequency, and the total sampling time.

Key words: inversion, singular value decomposition, source identification, source estimation and source network design

## 3.2 Introduction

The extensive use of water resources has increased the need to design a sampling network in order to monitor pollutant sources. Unfortunately, there exists little comparative research on methods for selecting station numbers, station locations, and the sampling frequency that can measure the source spatial and temporal variations.

The sampling network design has been investigated more extensively for groundwater problems than for the surface water problems. There are three approaches for designing a subsurface water-quality monitoring network: (1) optimization methods, (2) simulation approaches, and (3) variance reduction techniques. The optimization approach formulates a sampling network endeavoring to minimize the standard deviation between the measured data and the modeled data in selecting of the best sampling spatial pattern and spatial density. The optimization approach can be further categorized as the analytical optimization method (Hsueh and Rajagopal, 1988 and Loaiciga, 1988), integer programming approach (Carrera et al., 1984), and mixed integer programming approach (Hsu and Yeh, 1989). Because the optimization approaches rely on the comparison between the measured data and the modeled data, the method can not be used to design the sampling network if there is no available sampling data. The simulation methods (Meyer and Brill, 1988; Massann and Freeze, 1987 *a, b*; Andricevic and Georgiou, 1991) choose the sampling locations for water quality monitoring via numerical models. In the Monte Carlo approach, statistical properties (mean and covariance) of the measured tracers are generated by repeated simulations of different synthetic plumes. Then, the method selects sampling locations to best represent the generated statistical behaviors.

The simulation methods are statistical approaches, which can not address the specification of sampling frequency. Therefore, its designed sampling network does not have enough information for practical implementation. Different from the two approaches, the variable reduction method chooses the sampling network in an iterative way (Christakos and Olea, 1992, Christakos and Killam, 1993, and Shakrokh, 1985). With each iteration, the method adds one more sampling site that contributes most to the reduction of the estimated error (mean or covariance). Along the way, additional sampling stations are added, one at a time, until the variance of estimation cannot be further reduced or the addition of further sites is deemed economically impractical. Obviously, the variable reduction method has the same limitations as the optimization and modeling approaches.

The existing sampling network design methods rely on statistical variables, like mean and covariance. Consequently, they do not work in applications where there is no sampling data. For example, because discarded sewage-dumping-sites generally do not have sampling data available, the discussed methods cannot design their sampling network. Moreover, because the available sampling network design methods are not associated with the sampling schemes, they cannot decide the sampling frequency and the total sampling time. As a result, they can locate the sampling stations, but can not guide sampling processes. At worse, their designed sampling network cannot be feasibly calibrated and validated. The above three major shortcomings justify a new approach for designing a sampling network.

The purpose of this chapter is to introduce a new sampling network design methodology that relies on solid mathematical and physical concepts. The idea is based on the fact that when a pollutant enters the environment, it leaves identifiable “fingerprints” in the environment. By proper monitoring of these “fingerprints,” we can revert back to the original spatio-temporal distribution of the source. This idea leads to the development of the time-explicit source characterization method (*Chapter 2*). Equally important, these “fingerprints” characterize the magnitude of the source-station response, such that they can guide the field survey. This idea lead to the development of this sampling network design method. From this prospect, the developed sampling network design method is more theoretically robust than the applications presently available. First, it does not use the sampling information. The method designs the sampling network based on its physical and mathematical description. Therefore, it is not limited by the field data. Secondly, the design can determine the station numbers, station locations, as well as the sampling frequency and the total sampling time. Finally, the designed sampling network can be both calibrated and validated by the source characterization method (*Chapter 2*).

This research investigates the relationships among the source location, source number, station location, station number, sample frequency, and the total sampling time, which are exemplified by the following practical questions: What is the minimum number of stations needed to recover all sources? Where should these stations be located? What is the sampling frequency and the total sampling period? How does one calibrate and validate the designed sampling network? The successful answers to the above questions are demonstrated by the method’s diagnostic analysis in the synthetic St. John’s Landfill surface water environment.

### 3.3 Sampling network design and the inverse modeling

The developed method designs the sampling network based on a numerical variable generated by the time-explicit source identification method (*Chapter 2*). In the source identification method, the “transfer function” expresses the relationship between the pollutant source strength and the measured pollutant magnitude. This relationship can be measured by its condition number. By understanding this relationship, the basic idea of designing a sampling network is to use the condition number of the transfer function to select the station number, station locations, the sampling frequency, and the total sampling period, so that all the pollutant sources can be monitored. This section, following the “dense-sampling” inversion formulation (Section 2.4.1), discusses the source identifiability and the sampling network design method.

#### 3.3.1 Source identifiability

Because equation (2.3) associates a pollutant source term with its response at a sampling station, the formulation numerically defines the source identifiability. As discovered in this research, source identifiability is equivalent to the solvability of the dense-sampling inversion formulation. Consequently, source identifiability is determined by the singularity of the inversion formulation. Also, the singularity of the inversion formulation is measured by its condition number. Therefore, the condition number of the inversion equation can measure the pollutant source identifiability.

The condition number is defined as the error amplification factor<sup>1</sup> of a matrix equation  $AX = B$  (Golub and Loan 1983).

$$\frac{\|\Delta x\|}{\|x\|} = \text{cond}(A) \frac{\|\Delta b\|}{\|b\|} \quad (3.1)$$

In equation (3.1),  $\|x\|$  corresponds to the norm of an identified source, and  $\|b\|$  corresponds to the norm of a measured concentration. Equation (3.1) shows that a large  $\text{cond}(A)$ , signifying the sampling error, can generate large errors in the identified source. In the extreme case, the round-off error in vector  $B$  can be amplified to infinity in vector  $x$ . The criterion of source identifiability can be defined such that the amplified inversion error doesn't exceed the acceptable error, as shown in equation (3.2).

$$\frac{\|\Delta x\|}{\|x\|_{\text{acceptable}}} \geq \text{cond}(A) \times \frac{\|\Delta b\|}{\|b\|_{\text{measured}}} \quad (3.2)$$

The identifiable criterion of the condition number is determined by the following factors: sampling error in vector  $b$ , acceptable inversion error in vector  $x$ , and machine accuracy. For instance, if we assume the sampling error is zero, there exists only the round-off error. The relative error of a single precision variable in FORTRAN is  $10^{-7}$ . So, if the acceptable error in the identified source is  $10^{-3}$ , the condition number should not be larger than  $10^4$ . For the double precision variable, the criterion is  $10^{12}$ . However, the sampling error is always larger than the round-off error. Therefore,  $\|\Delta b\|/\|b\|$  is generally determined by the relative sampling error. It should also be noted that the condition number evaluated in equation (3.10) is the error amplification factor for equation (3.9), not for the original  $Ax = b$ . The relationship of error amplification by equation  $\Sigma z = d$  and equation  $Ax = b$  varies from system to system. For the synthetic St. John's landfill surface water system, their relationship is evaluated in the diagnostic analysis.

---

1. The condition number is evaluated by the Singular Value Decomposition (SVD) technique. In the SVD technique, any m-by-n matrix A can be decomposed in the following form

$$A = U \Sigma V^T \quad (3.8)$$

where U is an m-by-m orthogonal matrix, V is an n-by-n orthogonal matrix, and  $\Sigma$  is an m-by-n diagonal matrix with  $\sigma_{ij} = 0$  if  $i \neq j$  and  $\sigma_{ii} = \sigma_i \geq 0$ .  $\sigma_i$  is the singular value of A. With simple matrix manipulation, the original equation  $AX = B$  becomes

$$\Sigma z = d \quad (3.9)$$

where  $z = V^T x$  and  $d = U^T b$ . The condition number of matrix A can be evaluated from the singular number according to equation (3.10)

$$\text{cond}(A) = \frac{\sigma_{\max}}{\sigma_{\min}} \quad (3.10)$$

where  $\sigma_{\max}$  and  $\sigma_{\min}$  are the largest and smallest singular values of A.

### 3.3.2 Sampling network design

The proposed sampling network design method is based on the source identifiability index - the condition number of the transfer function. The above discussion concludes that the transfer function formulates the relationship of the measured concentration (time series), the hydraulic-transport characteristics (transfer function), and the pollutant source (time series). The condition number of the transfer-function determines the identifiability of a source by a station. The idea of the sampling network design is illustrated by the following application steps.

The first step calculates the transfer functions, which represent the source-station response. Secondly, we evaluate the condition number of the transfer function to measure the source-station response magnitude. The condition number of each source by each station is tabulated to form the condition number table. Third, the condition number table determines the station locations and station number such that each source can be identifiable by one station. Consequently, all source temporal and spatial variations can be recovered by the least number of stations. Finally, the designed sampling network is validated by the source estimation method (*Chapter 2*). Obviously, the above steps demonstrate that the developed design method selects the station number and station locations by the condition number table, determines the sampling frequency and total sampling time from the those of the transfer function, and validates the designed sampling network by the source characterization method.

In order to understand the sampling network method, we design the following numerical experiments to investigate factors affecting the magnitude of the condition number. The next section first describes the testing environment, then analyzes the condition number magnitude regarding the transport characteristics (condition number spatial variation), sampling scheme (number of sampling data), and inverse method (dense-sampling parameter). Later, the experiment numerically suggests that the condition number is the source identifiability index. Finally, it designs a sampling network for the synthetic reality and validates the design by the source estimation method.

## 3.4 Numerical experiments and results

### 3.4.1 Synthetic St. John's Landfill surface water system

The proposed method is diagnostically analyzed in the synthetic St. John's Landfill surface water environment, which has fully controllable water circulation, hydraulic transport, sampling scheme, and source scenarios (Figure 3.2). The finite element grid of the synthetic St. John's Landfill surface water system includes 1,957 nodes and 713 elements. The water circulation is simulated by solving a 2-D depth averaged wave equation (Westrink et al., 1987). To make the test simpler, we use the moon tide to represent the boundary condition. The hydraulic transport is modeled by the advection-diffusion equation. The diffusion coefficient in  $x$  and  $y$  is  $1 \text{ m/s}^2$ . For the purpose of computational efficiency, the simulated time interval (1.24 hr) is one tenth of the  $M_2$  period, so that the model can read the foot of the characteristic lines of one tidal cycle instead of backward tracking the entire simulation time. The total simulation time is 200 time steps, which has many integer factors for dense-sampling. The eight sources and eighteen stations are spatially equally distributed along the slough. This source-station configuration is able to represent the spatial pattern of source-station response for the entire slough.

### 3.4.2 Condition number spatial variation

The spatial variation of the condition number is determined by natural processes. In the synthetic reality, these natural processes include advection and diffusion. Advection affects the source identifiability by changing the tracer moving path. For example, when the pollutant tracer moves into the dead-end slough, the advection determines that the tracer must move along the land boundary. Thus tracer concentration in the dead-end-slough is higher than that in the main slough. Consequently, the stations inside the dead-end slough have higher source response than those in the main slough. Similarly, the diffusion influences the source identifiability by changing the tracer concentration. Diffusion decreases the tracer concentration. As a result, diffusion generally decreases the source identifiability. The relationship between the natural processes and the source identifiability can be demonstrated by the condition number's spatial variation.

Figure 3.3 plots the condition number spatial variation of source 3. It is obvious that condition number is inversely proportional to the distance from the source. For

instance, station 5, the station staying closest to source 3, has a low condition number. This means that station 5 is one of the stations that can identify source 3. Additionally, the magnitude of the condition number is also governed by the land boundary. For example, the condition number of station 4 is less than that of station 5, even though station 5 is closer to source 3 than station 4. The reason is that station 4 is located in the dead-end slough so that it has a better chance to identify source 3 than stations in the main slough. This is why station 4 has a better response to source 3 than station 5. As such, Figure 3.3 illustrates the effects of natural processes and the land boundary on the condition number.

Figure 3.3 can also determine the spatial density of the sampling stations. The synthetic reality is a quasi 1-D environment. The spatial variation of condition number is almost linear within a certain range. This is illustrated by the fact that the condition numbers of stations 6 and 7 can be linearly interpolated from the condition numbers of stations 5 and 8. This linear relationship further implies that the distance between source 3 and its identifiable stations could not be greater than two miles. Otherwise, the station's condition numbers would approach infinity. At this point, the figure can determine that the distance between two stations is two miles. To sum up, the condition number spatial variation is dependent upon the hydraulic transport characteristics.

### 3.4.3 Condition number and the number of sampling data

The relationship between the number of sampling data and the condition number is tested in an ideal case, where the transfer function is a non-zero constant value. This is because the condition number is determined by the hydraulic transport characteristics, number of sampling data, and the "dense-sampling" parameters. In order to investigate the relationship between the condition number and number of sampling data, the system characterization must be independent of the sampling time. This is done by assigning the transfer function a constant value. As a result, the condition number is a function of the number of sampling data and the dense-sampling parameter  $N_D$ .

Figure 3.5 shows the relationship between the condition number and the number of sampling data. First of all, the condition number increases as the number of the sampling data increases. When the sampling steps are greater than 200, this trend approaches a linear pattern. This is quite clear when  $N_D = 10$ , where the plot is almost a straight line when the number of sampling data increases from 200 to 600. Secondly, the condition number

decreases as  $N_D$  increases. This illustrated, when  $N_S=200$ ,  $\log(\text{condition number})$  decreased from about 4.5 to approximately 3.5, as  $N_D$  increases from 5 to 20. Thirdly, the condition number increases as  $N_S$  increases. The figure shows that, when  $N_D=20$ , the  $\log(\text{condition number})$  increases from 3 to 4 when  $N_S$  increases from 180 to 290, which demonstrates that the increment due to the increment of the number of the sampling data can be compensated by a denser inversion ( $N_D$  increases from 20 to 60). This suggests that in order to identify more source data or invert a long period of unknown data, a denser inversion is necessary.

#### 3.4.4 Condition number variation with the “dense-sampling” parameter

When the source responses at a station is small, the condition number of the transfer function approaches infinity. This means that the inversion amplifies the sampling error towards infinity. As a result, the source is unidentifiable. This experiment demonstrates the improvement of the source identifiability by showing how the condition number reduced by dense-sampling.

In Figure 3.5, the dashed line represents the condition number variation for the constant transfer function. The condition number reduction by the dense-sampling concept is explained by the fact that more sampling information is used to invert one unknown. Because the additional sampling information reduces the linearity of the transfer function, its inversion has a smaller condition number. The dashed line also illustrates that the increment of source identifiability is the trade-off of inversion resolution. In this test case, the total sampling data is 600. When the dense-sampling parameter ( $N_D$ ) is 10, the 600 sampling data estimates 60 source data. But when  $N_D=20$ , the 600 sampling data only estimate 30 source data. Indeed, the dense-sampling method converts the unidentifiable source to identifiable source and at the same time increases the identified source temporal resolution.

In Figure 3.5, the lines, other than the dashed line, illustrate the condition number reduction of source 3 and station 1-11. Different from the dashed line, these condition numbers are determined by both  $N_D$  and the hydraulic characteristics. There are three salient items to note in this figure. First, the comparison of the ideal transfer function with the synthetic reality illustrates the effects of  $N_D$  and system characteristics. The decrement of the condition number is obvious when  $N_D=10, 20, 30$ . Secondly, the condition number

shows an obvious increment at  $N_D=40$ . This is because the synthetic system is driven by a tidal period of 12.4 hours. The inversion for  $N_D=40$ , corresponds to the inversion period of 49.6 hours. By comparing the signal period (12.4 hours) and the identified source time interval (49.6 hours), we can see that the “dense-sampling” inversion averages the tidal signal, so that the transfer function matrix becomes more singular than the less dense-sampling inversion. This explains the condition number increment when  $N_D=40$ . When  $N_D>40$ , the decreasing trend is, once again, the effect of dense-sampling. Finally, at the extreme case where  $N_D$  equals the sampling number, the method has the minimum condition number, and the identified source data is the averaged source magnitude for the entire 148.8 hours. From the Figure 3.5, it is obvious that the “dense-sampling” scheme is capable of decreasing the condition number in a natural environment.

### 3.4.5 Condition number as the identifiability index

The application of the condition number as the source identifiability index requires a condition number criterion below which the source is defined as identifiable and above which the source is unidentifiable. The criterion may be different for different environments. Its further understanding depends on a theoretical analysis of the method. In this research, we define this criterion by a numerical experiment in which source 6 is inverted by different stations, corresponding to different condition numbers. By inspecting the relationship between the inversion results and the inversion’s condition number, we define the source identifiability criterion for the synthetic St. John’s Landfill environment.

In Figure 3.6, the “Y-axis” is the identified source 6 history by station8 through 15, with different values of condition numbers. The “X-axis” is the time index. In this experiment, the relative sampling error is 5%, the dense-sampling parameter ( $N_D$ ) is 20, and the sampling number is 200. The figure demonstrates that stations close to the source can better identify source 6. The improvement can be measured by the condition number of the transfer function. For instance, stations 12, 11, and 10 are the three stations that are close to source 6. Their condition numbers ( $10^{2.8}$ ,  $10^{3.1}$ ,  $10^{3.3}$ ) are also smaller than the other sources. It is not surprising to see that station 12, with the smallest condition number, has the most accurate inversion. A similar relationship is true for stations 11 and 10. However, when the condition number increases to  $10^{7.9}$ , station 8 can not produce a stable inversion due to the amplified sampling error. Furthermore, stations with high condition numbers,  $10^8$  (station 14),  $10^{13.6}$  (station 15) produce unstable inversions. Based on these experi-

ments, we can define the low criterion of the condition number, for  $N_D=20$  and the number of steps equal to 200, as  $10^5$ . Any condition number smaller than  $10^5$  indicates an identifiable source. When  $10^5 < \text{condition number} < 10^7$ , the source is defined as quasi-identifiable. This is because a condition number within this range can be decreased below  $10^5$  by a denser inversion (Figure 3.6), so that the source becomes identifiable. When the condition number is larger than  $10^7$ , the source is referred to as non-identifiable. The establishment of the criterion concludes that the condition number can represent the source identifiability.

### 3.4.6 Sampling network design and validation

This section applies the method by designing the sampling network of the synthetic St. John's landfill environment. The synthetic reality includes 8 sources and 18 stations. The sources and stations are spatially distributed so that they can represent the source-station response of the entire system. The first step calculates the transfer functions of the environment. For the case where there are 8 sources and 18 stations, we get  $8 \times 18 = 144$  transfer functions.

The transfer function of source 6 to station 13 is illustrated in Figure 3.7. The "X-axis" corresponds to different release times. The "Y-axis" represents the sampling time. The "Z-axis" displays the transfer function magnitude. Obviously, for a release time, the response-magnitude (Z) shows a 12.4 hour periodic pattern, in response to the moon-tide-generated advection. Additionally, the response magnitude also decreases due to the diffusion. The effects of advection and diffusion on the source identifiability can be measured by the condition number.

The second step tabulates the condition number of every source and station (Table 3.1). In the row, the table illustrates the response of each station to different sources. For instance, the 9th row, representing station 9, has five condition numbers that match the identifiability criterion. This means that station 9 can identify five sources (2 - 6). Because the 9th row has the largest number of condition numbers that are smaller than  $10^5$ , station 9 is able to identify more sources than any other station. Physically, this is because station 9 is located in the most dynamic part of the slough; therefore, it responds to more sources than any other station. For the same reason, stations 14 through 18 cannot identify more

than two sources each. In summary, the table shows the effectiveness of the station in identifying different sources.

In the table, the columns represent the eight sources. Column 5, for example, determines how many stations can identify the corresponding source. For instance, the 5th-column, corresponding to source 5, has seven condition numbers that fall within the identifiable criterion. This means the 5th-source can be identified by seven stations (6-12). The above conclusion is not surprising when we check the map of the synthetic reality and notice that all of the seven stations are within two miles of source 5.

The optimally designed sampling network selects the minimum number of stations necessary to identify all sources. Therefore, each source must be identified by at least one station. That is to say, each column (source) should have at least one condition number that is less than  $10^5$ . Meanwhile, the design must also keep the selected column numbers (the number of stations) at a minimum. Applying the above two rules to Table 3.1, we can design the sampling network for the synthetic reality. The sampling stations are 4, 9, 13 and 16.  $N_D$  equals 20, sampling  $\Delta t$  is 1.24 hours and the number of sampling data is 200. The designed sampling network is validated by successfully inverting the 8 sources from the sampled information at four stations (Figure 3.8).

### **3.5 Conclusions and final remarks**

A sampling network design method is proposed for monitoring contaminant sources. The method systematically provides the spatial and temporal sampling pattern, which is not available from other available methods. Secondly, the method is associated with the source characterization method. On the one hand, the sampling network design can guide the source characterization method. On the other hand, the source characterization method can validate the designed sampling network. Therefore, the integrity of the sampling network design method and the pollutant source characterization method provides a systematic technique for environmental practice. Finally, the developed method is independent from its applications. The pollutant transport models used in this research could have been groundwater or atmospheric models. Therefore, the combination of the sampling network method and the source characterization method has broad application possibilities.

The method however has several limitations. The sampling network design method, for example, is based on the time-explicit source characterization method, which assumed the transport processes only include advection and diffusion. Consequently, the source identification method and the sampling network design method can not be directly applied to non-linear transformation processes to solve problems like bio-geo-chemical transformation. The solutions to this type of problem must rely on the application of the “dense-sampling” formulation to estimate model parameters through an iterative scheme (Chapter 4). A second limitation is that the proposed method still cannot be accomplished via automatic or even semiautomatic means. Even though the method does provide a theoretical basis for the automatic sampling network design, a successful automatic design method depends on spatial interpolation of the condition number and on non-linear programming optimization. The research of the automatic sampling network design will be a very interesting upcoming research.

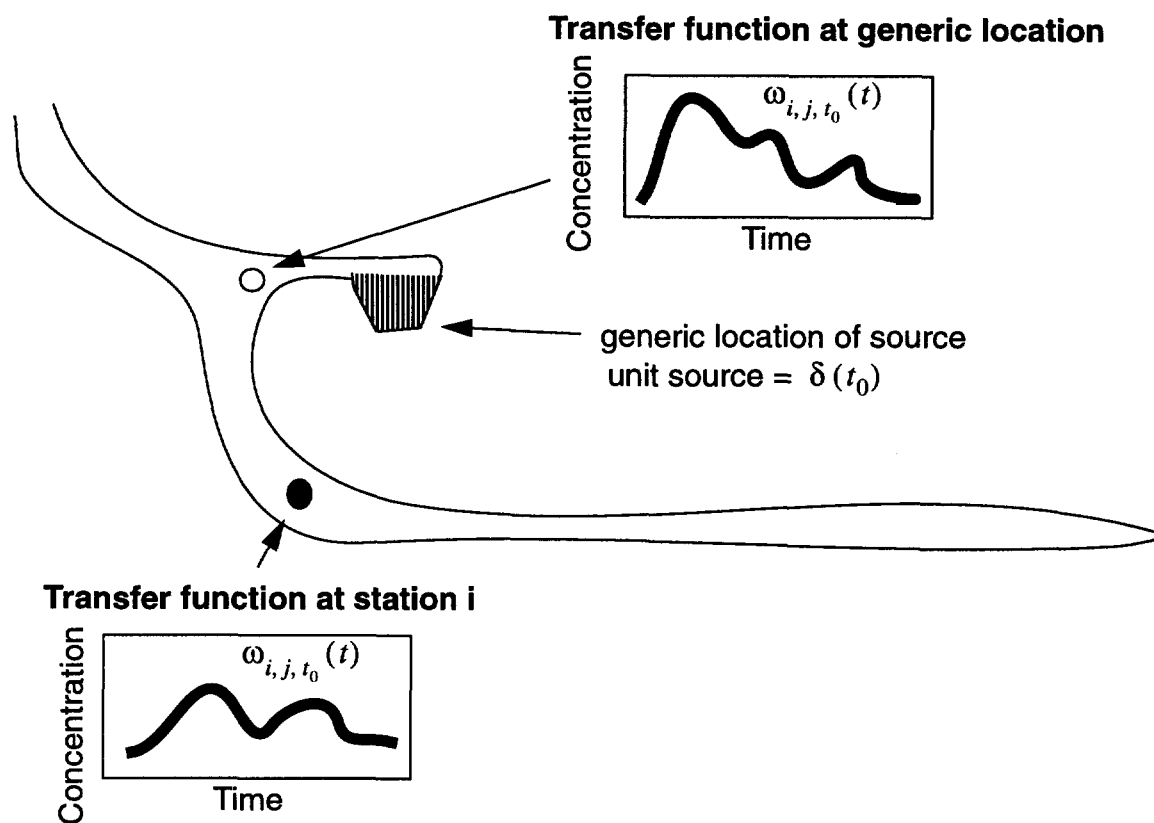


**Figure 3.1 Conceptual diagram of the transfer function ( $\omega$ ) of a generic surface water environment. In the figure,  $\delta(t_0)$  represents a unit source;  $i$  and  $j$  are the station index and the source index;  $t$  and  $t_0$  represent the sampling time and source release time, respectively.**

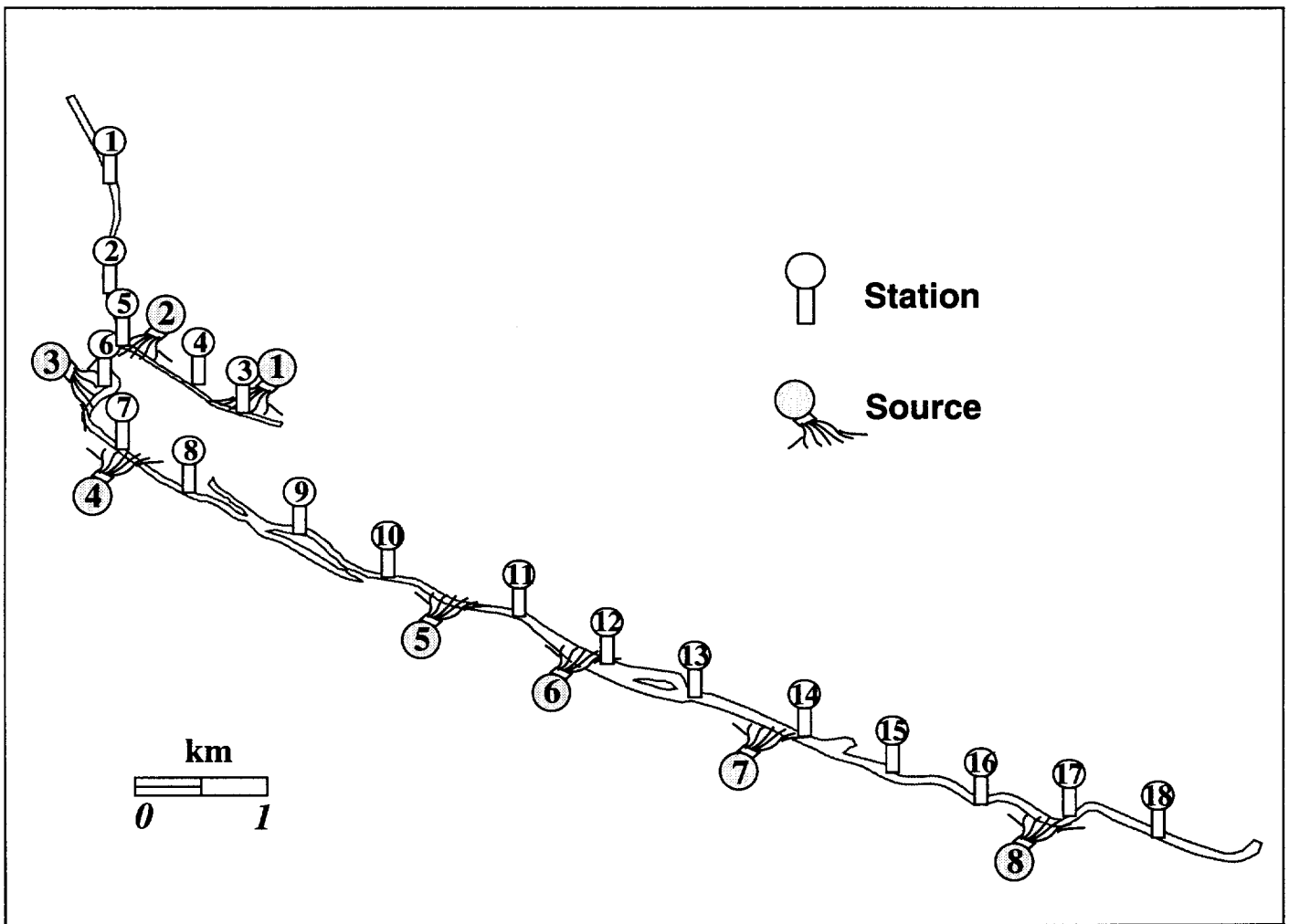


**Figure 3.2 Synthetic St. John's Landfill surface water environment. The tidal-driven system has 8 sources and 18 stations.**

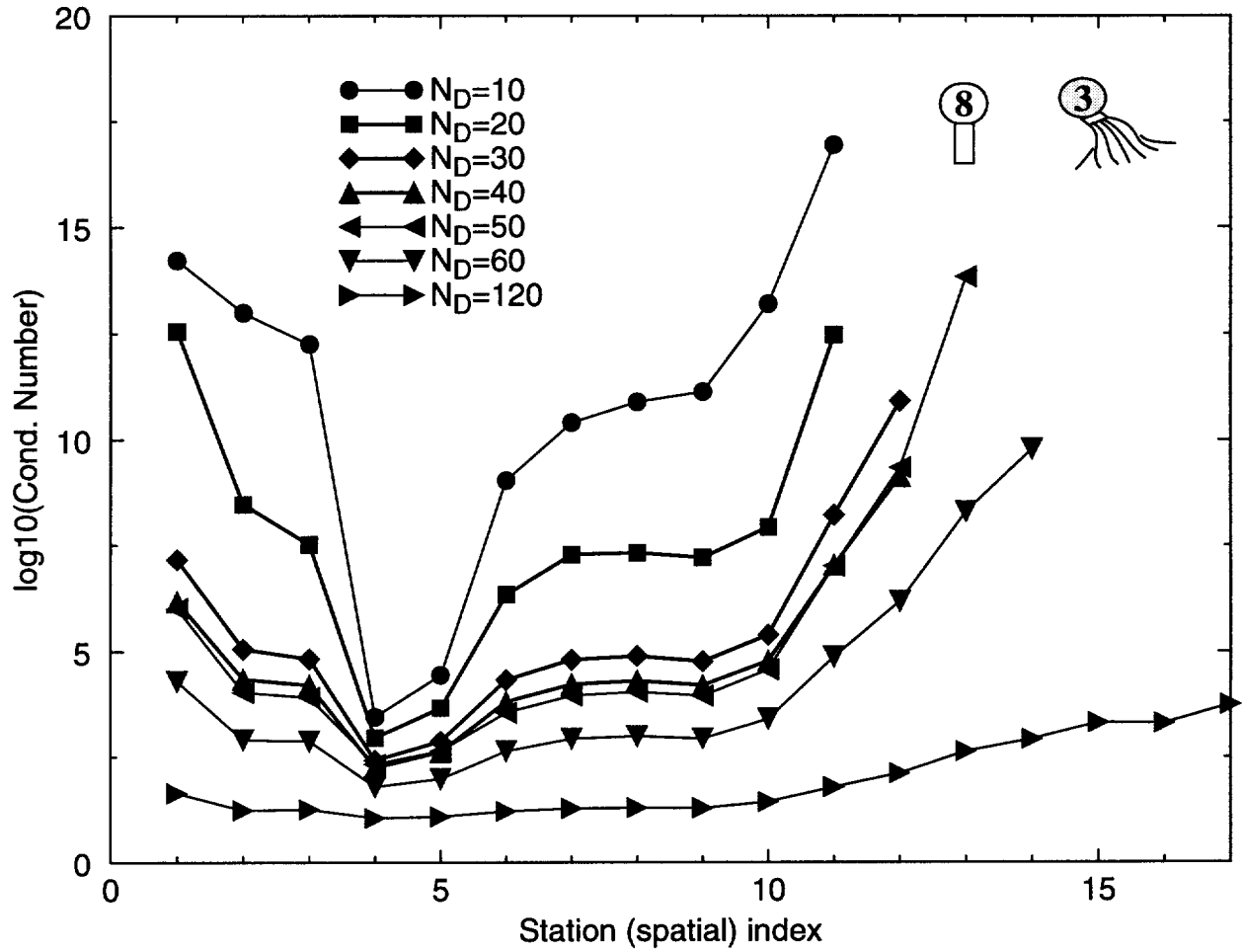


**Figure 3.3 Condition number spatial distribution of source 3 and station 8. Note that the figure utilizes the station index to represent the spatial index.**

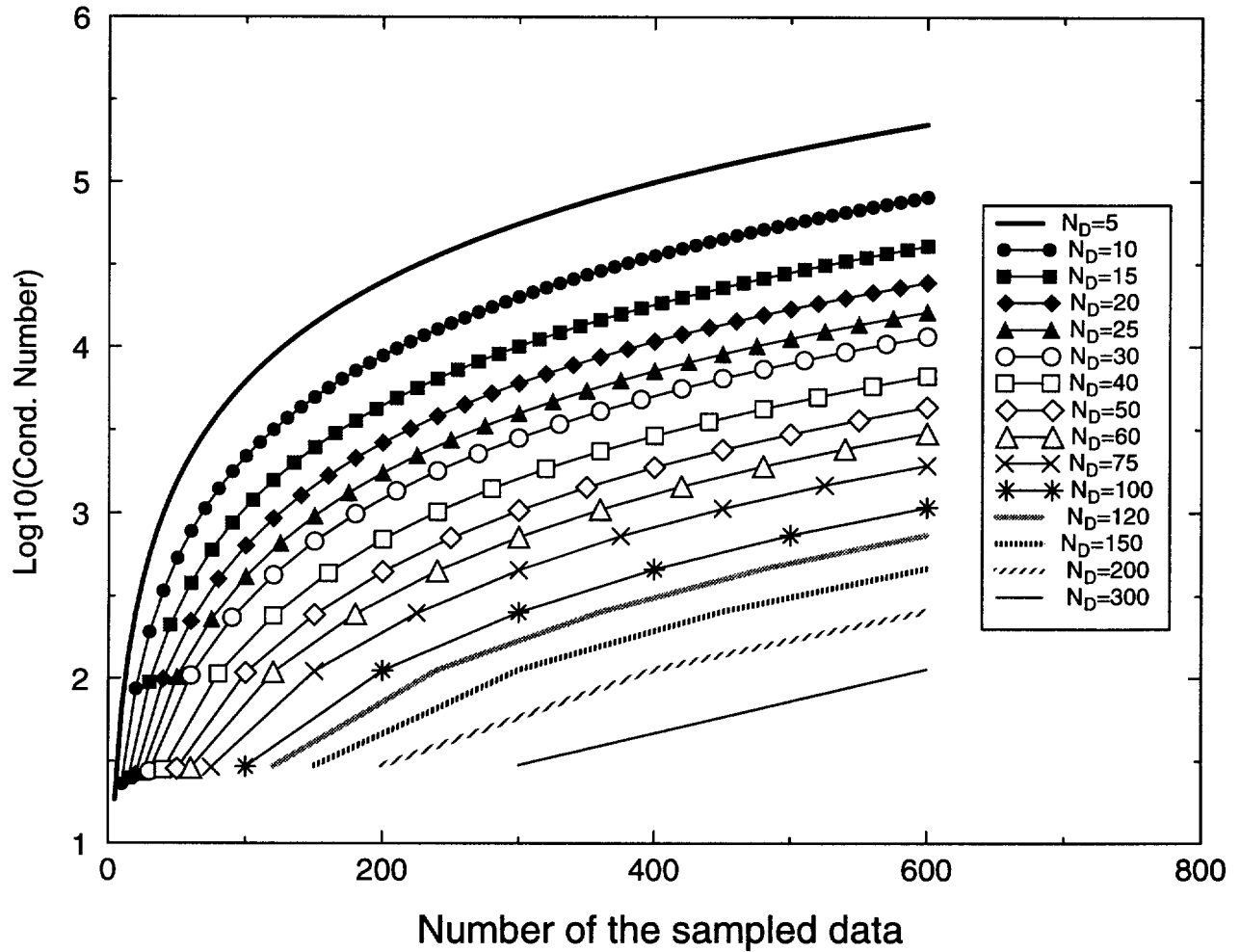


**Figure 3.4 Relationship between the condition number and the number of the sampling data. Note that the condition number of the transfer function is calculated from the constant transfer functions.**

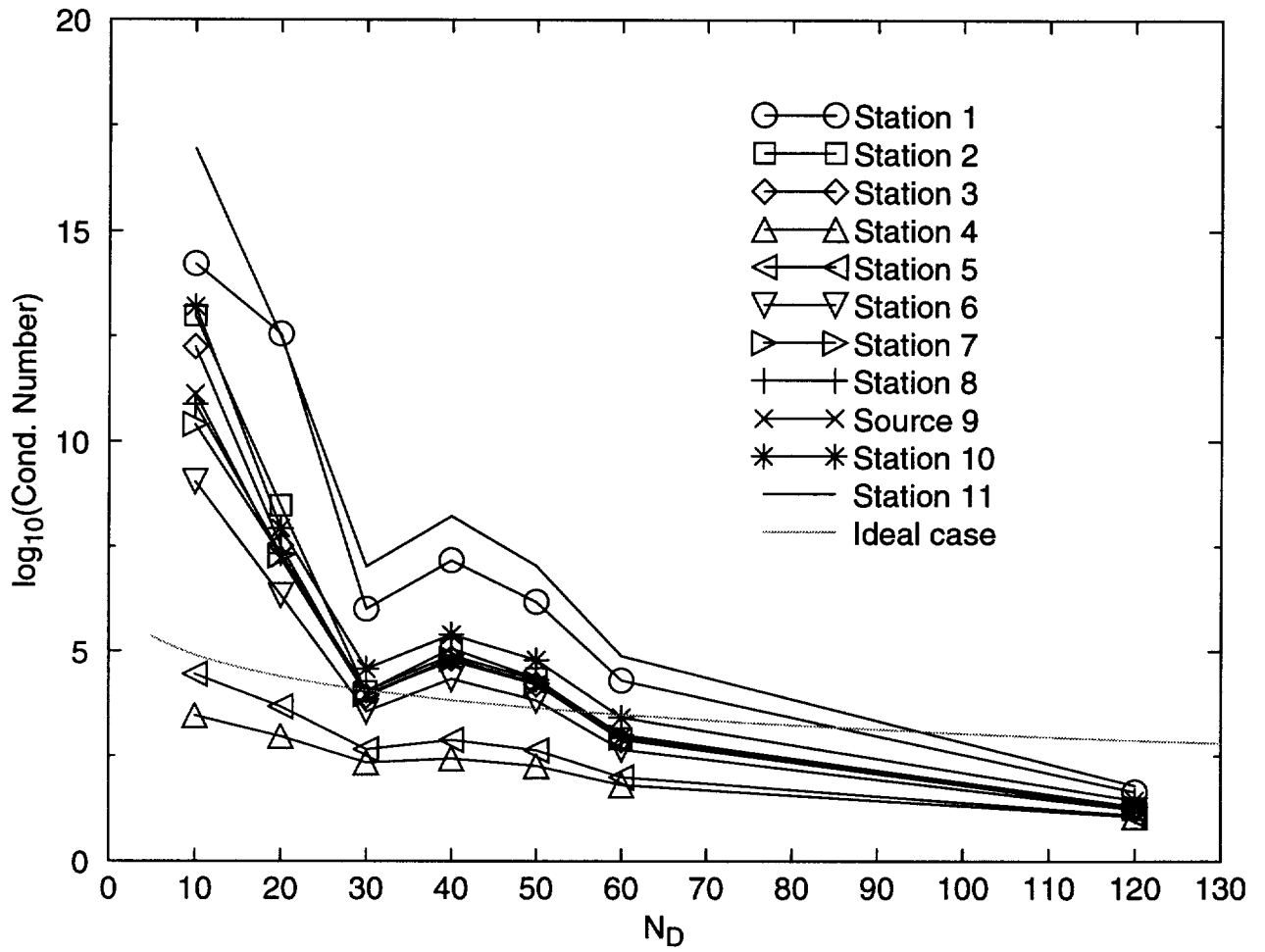


**Figure 3.5 Relationship between the condition number and the “dense-sampling” parameter. Note that the condition numbers are calculated for source 3 and stations 1-11.**

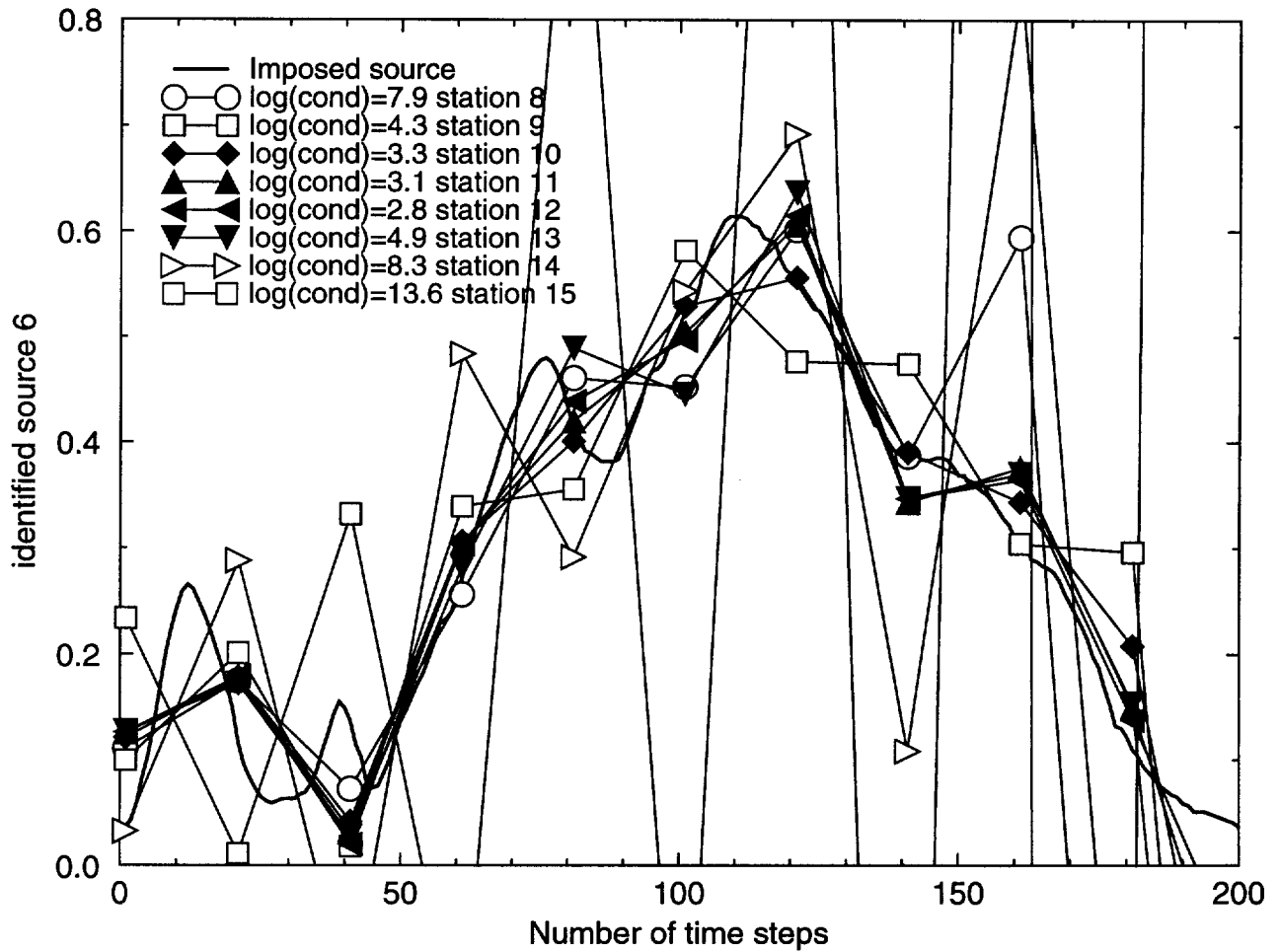


**Figure 3.6 Source 6 is identified by different stations with different condition numbers. Clearly, when condition numbers  $< 10^5$ , the station can precisely invert the source. When condition numbers  $> 10^7$ , the station can't obtain a stable inversion.**

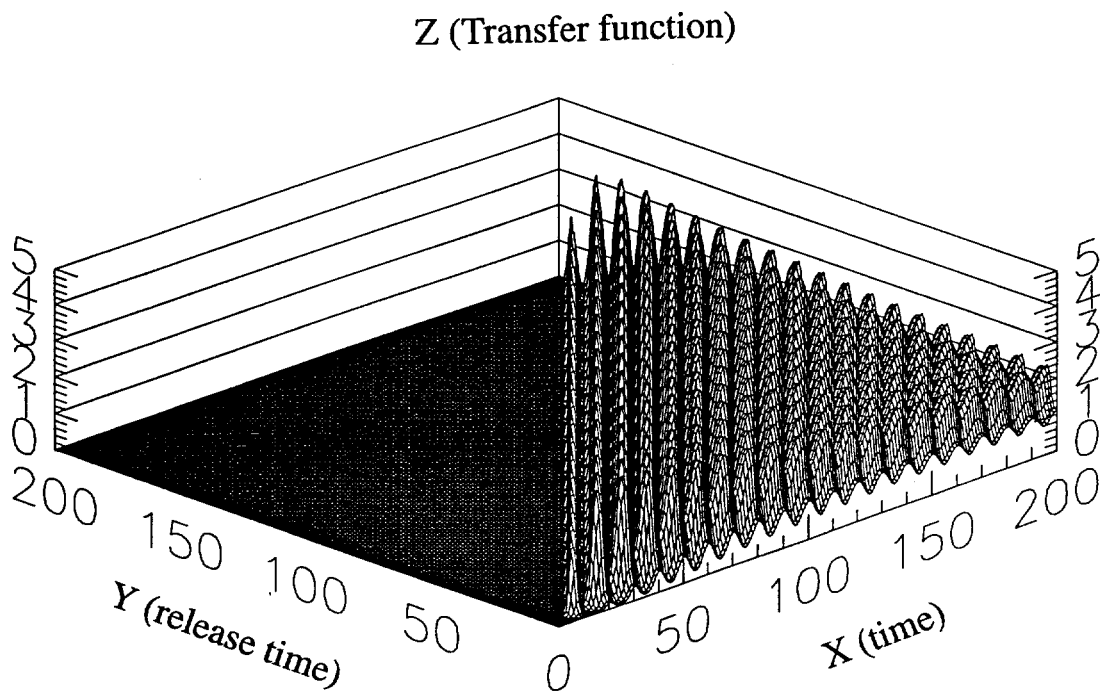


**Figure 3.7** Transfer function between source 6 and station 13. Note that the transfer function has a periodical pattern due to the moon-tide-advection and a decrease in time as a result of diffusion.

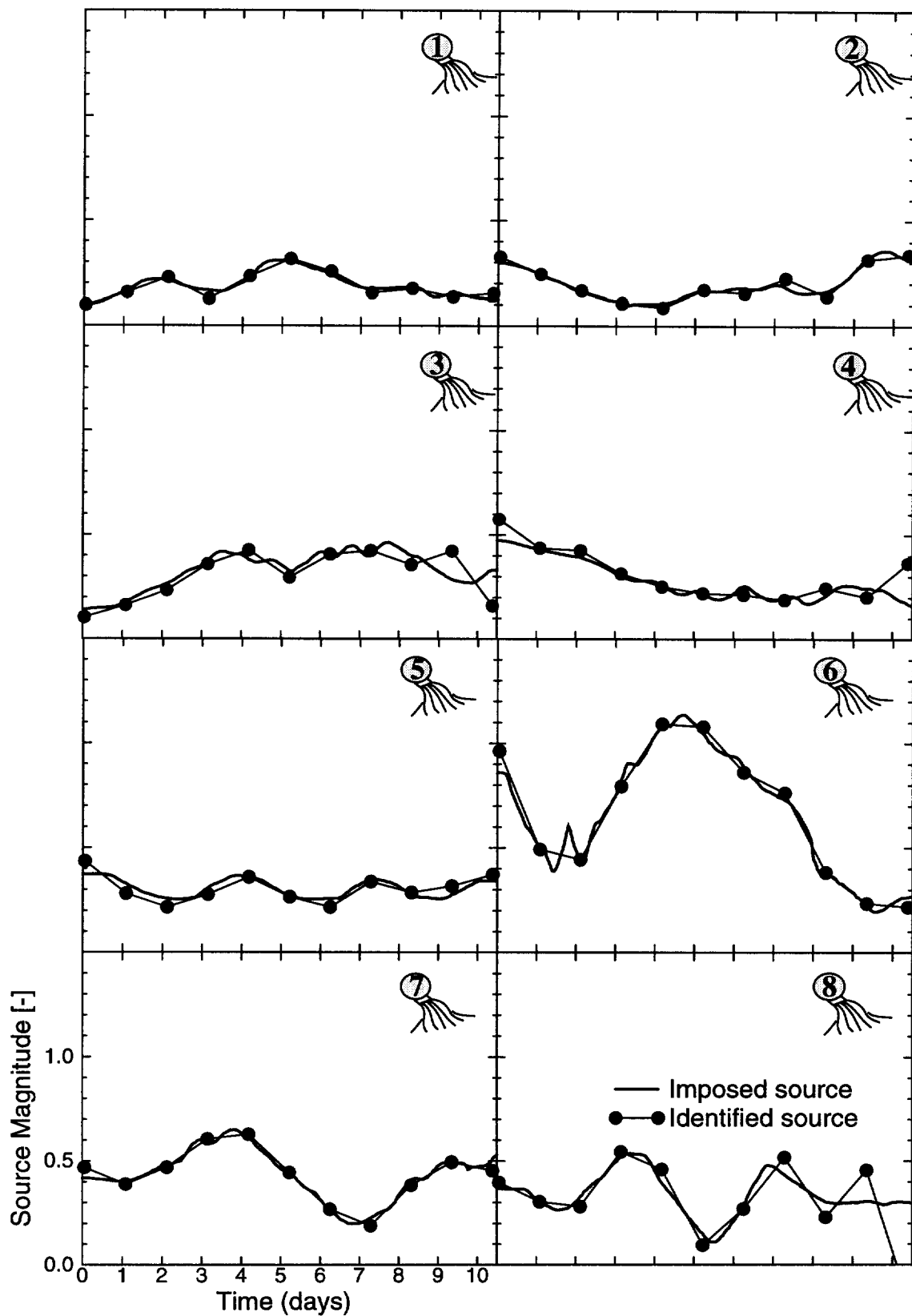


**Figure 3.8** The validation of the designed sampling network. The 8 sources are identified based on the designed sampling network.

18	INF	9.1						
17	INF	INF	INF	INF	INF	INF	14.7	4.0
16	INF	INF	INF	INF	INF	INF	9.4	<u>2.6</u>
15	INF	INF	INF	INF	INF	13.6	5.6	3.7
14	INF	INF	INF	INF	12.7	8.3	2.7	8.4
13	INF	INF	INF	14.4	8.7	<u>4.9</u>	<u>3.0</u>	13.4
12	INF	11.2	10.0	8.6	3.8	2.8	5.8	17.6
11	12.5	7.4	6.1	5.2	2.7	3.1	9.5	INF
10	12.6	5.8	4.5	3.1	2.4	3.3	12.0	INF
9	7.9	<u>3.3</u>	<u>2.6</u>	<u>2.5</u>	<u>3.1</u>	<u>4.3</u>	14.6	INF
8	7.2	2.5	2.2	2.4	3.3	7.9	19.0	INF
7	7.3	2.5	2.0	1.9	3.6	9.5	INF	INF
6	7.3	2.4	1.7	2.6	4.7	10.5	INF	INF
5	6.3	1.9	2.0	2.6	6.9	12.3	INF	INF
4	<u>3.7</u>	<u>2.5</u>	<u>4.2</u>	<u>5.2</u>	9.8	15.7	INF	INF
3	3.0	4.5	6.9	8.3	12.4	17.3	INF	INF
2	7.5	2.5	2.1	2.5	7.7	13.1	INF	INF
1	8.5	2.4	2.1	2.4	8.5	13.2	INF	INF
0								

**Table 3.1 Condition number table of the synthetic St. John's Landfill surface water environment. Note that the table has 8 sources and 18 stations and the condition number is in log scale. It indicates that the 8 sources can be identified by stations 4, 9, 13, and 16.**

### 3.6 References

- Andricevic, R. and E. A. Fofoula-Georgiou, Transfer function approach to sampling Network design for groundwater contamination. *Water Resour. Res.*, 27, 2759-2769, 1991.
- Carrera, J., E. Usunoff, and F. Szidarovsky, A method for optimal observation network design for groundwater management. *J. Hydrol.*, 73, 147-163, 1984.
- Christakos, J. and B. R. Killam, Sampling design for classifying contaminant level using annealing search algorithms, *Water Resour. Res.*, 29, 4063-4076, 1993.
- Christakos G. and R. A. Olea, Sampling design for spatially distributed hydrological and environmental process, *Advances in Water Resources*, 15, 219-237, 1992.
- Golub, H. G. and C. V. Loan, *Matrix Computation*, The John's Hopkins University Press, Baltimore, Maryland, 1983.
- Hsu, N. S. and W.W.-G. Yeh, Optimum experimental design for parameter identification in groundwater hydrology. *Water Resour. Res.*, 25, 1025-1040, 1989.
- Hsueh, Y. W. and R. Ragagopal, Modeling groundwater quality sampling decisions, *Ground Water Monitor. Rev.*, 121-134, 1988.
- Loaiciga, H.A., Groundwater monitoring network design, in *Proc. VII Intl. Conf. Computational Methods in Water Resources*, vol. 2, edited by M. A. Celia, L. A. Brebia, N. G. Gray, and G. F. Pinder, Computational Mechanics Publications/Elsevier, New York, 371-376, 1988.
- Massmann, J. and R. A. Freeze, Groundwater contamination from waste management sites, *Water Resour. Res.*, 23, 351-367, 1987a.
- Massmann, J. and R. A. Freeze, Groundwater contamination from waste management sites, *Water Resour. Res.*, 23, 368-380, 1987b.
- Meyer, P. D. and E. D. Brill, A method for locating wells in a groundwater monitoring network under conditions of uncertainty, *Water Resour. Res.*, 24, 1277-1282, 1988.
- Shahrokh R., Variance reduction analysis, *Water Resour. Res.*, 21(6), 837-846, 1985.
- Westerink, J.J., J. J. Connor. and K. D. Stolzenbach, A primitive pseudo water equation formulation for solving the harmonic shallow water equations. *Advances in Water Resources*, 10, 188-199, 1987

## CHAPTER 4

# **A method of estimating oceanic and riverine boundary conditions for hydrodynamic models using inverse modeling**

### **4.1 Abstract**

This research develops a method for estimating the water sources of a confined water environment relying on measured water elevations and hydrodynamic models. Water sources can be represented of either water elevation or flux boundary conditions. This chapter discusses the theoretical and practical issues critical for the water sources estimation method. Then, we demonstrate the robustness of the method regarding nonlinear inversion, sampling error reduction, simultaneous water elevation and flux boundary inversion, and sampling location selection. Later, the chapter applies the method to estimate the oceanic boundary of the Tejo estuary in Portugal, which has irregular bathymetry and land boundaries.

Key words: Inversion, singular value decomposition, boundary inversion

### **4.2 Introduction**

A major problem confronting environmental hydrologists, when modeling an environment, is the lack of accurate and complete water source information. Although arguably an accurate oceanic boundary can be obtained at least when tides are dominant, the same is not true for non-tidal water boundaries. Lakes and rivers, for example, are influenced by a number of different water sources, such as ground water exchange, evaporation and precipitation, up and down stream river flows, factory discharges, and sewage overflows. These source terms are either too difficult or too expensive to measure. As a result, their hydrodynamic simulations rely on trial-and-error bases. Clearly, the accuracy of hydrodynamic simulations is always hampered by the uncertainty of the water sources.

This chapter presents an innovative methodology for estimating water sources accurately. The method is demonstrated when we use it to solve the following persistent questions: (1) How can we know if the sampled water elevation data is sufficient to estimate unknown water sources? (2) How can we determine the spatial and temporal sampling pattern that can account for all unknown water sources? (3) How can we estimate water sources from the measured water elevation with the help of highly accurate water circulation models?

In answering the first question, we show the method's capability of determining if the available data is sufficient for estimating the water sources. In answering the second question, we demonstrate the method's ability to design a sampling network for improving the water source measurements. Obviously, the successful solutions of the three questions prove the robustness of the method developed in this research. Finally, in answering the first question, the water sources can be represented by both water elevation and water flux boundaries, the former corresponding to oceanic boundaries and the latter to riverine boundaries. The method is then required to invert different types of water sources simultaneously.

A literature review on the subject did not reveal any previous systematic approach to address these questions. An existing approach is the stochastic simulation method (Ginn and Cushman, 1990, Satish and Zhou, 1992), which is widely used in groundwater modeling. In this method, the boundary conditions (BCs) are represented as expectations, variances and covariances of random quantities. Obviously, their statistical representations of the boundary conditions cannot quantify the time history of the water source. Another approach is the frequency domain inversion methods (Bennett and McIntosh, 1982, McIntosh and Bennett, 1984, Nuñez, 1990), which estimate the water boundary of a tidal environment. All three of these methods calculate the amplitude and phase of the BCs by optimizing the boundary condition to match the model output with the measured water elevations. However, because they are frequency domain inversion methods, they do not address the non-periodic riverine BCs. In summary, neither approaches can solve the problem of a general water environment. It is apparent that a true time-domain inversion method is needed to estimate water sources completely and accurately.

This research develops a true time-domain non-linear inversion method for estimating the water sources of a water environment based on measured water elevations and

non-linear-time-domain water circulation models. Conceptually, the method extends the linear “dense-sampling” technique proposed in Chapter 2. By reducing the inversion sensitivity, we achieve a stable and meaningful inversion results even in the non-linear case. Additionally, the method utilizes the condition number of the inversion equations to represent the boundary’s identifiability of the water source. On the one hand, the method can determine if the available sampling data is capable of estimating water sources. On the other hand, it is able to determine the sampling locations in order to measure the water sources. In summary, the developed method can systematically guide water elevation measurement and utilize the sampled information to invert the water boundary conditions.

Section 4.3 reviews the water circulation model and defines the water elevation BC and water flux BC. Section 4.4 describes the formulation of the “dense-sampling” inversion. Section 4.5 diagnostically analyzes the method in a channel. Finally, section 4.6 applies the method to invert the oceanic boundary of the Tejo estuary (Portugal).

### 4.3 Statement of the problem

The following time-domain depth-integrated equations of mass and momentum conservation, subject to the incompressibility, Boussinesq, and hydrostatic pressure approximations, typically form the basis for shallow water hydrodynamic models (4.1), (4.2) and (4.3).

$$\frac{\partial \zeta}{\partial t} + \frac{\partial}{\partial x} UH + \frac{\partial}{\partial y} VH = 0 \quad (4.1)$$

$$\frac{\partial U}{\partial t} + U \frac{\partial U}{\partial x} + V \frac{\partial U}{\partial y} - fV = - \frac{\partial}{\partial x} \left[ \frac{p}{\rho_0} + g(\zeta - \alpha\eta) \right] + \frac{\tau_{sx}}{\rho_0 H} - \tau_* U \quad (4.2)$$

$$\frac{\partial V}{\partial t} + U \frac{\partial V}{\partial x} + V \frac{\partial V}{\partial y} + fU = - \frac{\partial}{\partial y} \left[ \frac{p}{\rho_0} + g(\zeta - \alpha\eta) \right] + \frac{\tau_{sy}}{\rho_0 H} - \tau_* V \quad (4.3)$$

where  $\zeta$  is the free surface elevation;  $U, V$  are depth-averaged horizontal velocities;  $H = \zeta + h$  is the total water depth;  $h$  is bathymetric depth relative to the geoid;  $f$  is the Coriolis parameter;  $p$  is atmospheric pressure at the free surface;  $g$  is acceleration due to gravity;  $\eta$  is Newtonian equilibrium tide potential;  $\alpha$  is the effective Earth elasticity factor;  $\rho_0$  is the reference density of water;  $\tau_{sx}, \tau_{sy}$  are applied free surface stress; the friction term  $\tau_* = n^2 g (U^2 + V^2)^{1/2} / h^{1/3} H$ ; and  $n$  is the Manning bottom friction factor.

The generalized wave-continuity equation (GWCE) is derived by combining a time-differentiated form of the continuity equation and a spatial differentiated form of the momentum equation, as expressed here:

$$\begin{aligned}
& \frac{\partial^2 \xi}{\partial t^2} + \tau_0 \frac{\partial \xi}{\partial t} + \frac{\partial}{\partial x} \left\{ \left( U \frac{\partial \xi}{\partial t} - UH \frac{\partial H}{\partial x} - VH \frac{\partial U}{\partial y} + fVH \right) \right. \\
& \quad \left. - H \frac{\partial}{\partial x} \left[ \frac{p}{\rho_0} + g(\xi - \alpha\eta) \right] + \frac{\tau_{sx}}{\rho_0} - (\tau_* - \tau_0)UH \right\} \\
& + \frac{\partial}{\partial y} \left\{ V \frac{\partial \xi}{\partial t} - UH \frac{\partial V}{\partial x} - VH \frac{\partial V}{\partial y} - fUH - H \frac{\partial}{\partial y} \left[ \frac{p}{\rho_0} + g(\xi - \alpha\eta) \right] \right. \\
& \quad \left. + \frac{\tau_{sy}}{\rho_0} - (\tau_* - \tau_0)VH \right\} = 0
\end{aligned} \tag{4.4}$$

Equation (4.4), rather than equation (4.1), is solved in conjunction with the momentum equations (4.2) and (4.3).

The boundaries include the rigid land boundary  $B_c$  and open water boundary  $B_o$ . The  $B_c$  is defined as

$$Flux \cdot n = 0 \tag{4.5}$$

where  $n$  is the outward unit normal at boundary nodes. The  $B_o$  can be defined as either water elevation BC (4.6) or flux BC (4.7).

$$\xi_{BC} = \zeta_t \tag{4.6}$$

$$Flux \cdot n = Flux_t \tag{4.7}$$

Contrary to predictive modeling, where we simulate  $\xi$ ,  $U$ , and  $V$  based on the bathymetry and BCs, equation (4.5), (4.6) and (4.7), inverse modeling inverts the BCs based on the system hydrodynamics, represented by equation (4.2) through (4.4), and measurable variables ( $\xi$ ,  $U$  and  $V$ ) at certain sampling locations. By comparing the known-unknown domain of the inverse modeling with the forward modeling, we can visualize the advantage of the inverse modeling. On the one hand, unknowns of inverse modeling are water sources, which are not easily measurable in reality, while unknowns of the forward modeling are water elevations and velocities at station fixed, which are comparatively much easier to measure. On the other hand, knowns of the inverse modeling are

measurable elevations, and knowns of the forward modeling are immensurable water boundaries. Obviously, the known-unknown domain of the inverse modeling reflects their relationship in reality, and the forward modeling does not. Therefore, the inverse modeling approach is more promising than the forward modeling approach in understanding the environment.

Inverse modeling, however, is more difficult than forward modeling. First of all, inverse modeling needs to correctly formulate the relationships among BCs, model simulations, and measurable variables ( $\xi$ ,  $U$  and  $V$ ). Secondly, the inverse formulation are generally highly sensitive, with small sampling errors prone to create large inversion errors. Finally, the detection of the high-sensitive inversion is very difficult to accomplish. Therefore, the development of the inverse modeling method is more challenge than that of the predictive method.

#### 4.4 Non-linear “dense-sampling” method

The method accomplishes the nonlinear inversion by iterating between linear-inversion (Chapter 2) and nonlinear simulations based on equations (4.2) - (4.4). Conceptually, surface water hydrodynamics yield the nonlinear transformation between BCs ( $\dot{S}$ ) and measured water elevation ( $\dot{C}$ ), through advection of momentum, finite amplitude, and bottom friction. Their relationships can be expressed by the non-linear function  $F$ .

$$\dot{C} = F(\dot{S}) \quad (4.8)$$

Unfortunately, nonlinear inversion has no general theory that provides a complete solution. In this research, we convert the nonlinear problem to a quasi-linear problem using the Taylor series expansion equation (4.9). In this equation,  $\dot{C}^*$  denotes the measured elevation, and  $\dot{C}^0$  represents a space closing to  $\dot{C}^*$ .

$$\dot{C}^* = \dot{C}^0 + \sum_{n=1}^{\infty} \frac{1}{n!} \times \frac{\partial^n F(\dot{S})}{\partial \dot{S}^n} \times \Delta \dot{S}^n \quad (4.9)$$

When  $n=1$ , the conceptual formula (4.9), after simple mathematical manipulation, can be modified to become the “Newton-Raphson” type iteration equation (4.10), where  $\frac{\partial F(\dot{S})}{\partial \dot{S}}$  is replaced by the transfer function and  $R$  indicates the iteration level.

$$\vec{C}^* = \vec{C}^R + \sum_{i=1}^{N_s} \left\{ \sum_{t=1}^{\frac{N_R-1}{N_D}} \left\{ \sum_{t_1=-N_D}^{N_D} \frac{N_D - |j_2|}{N_D} \times \omega_{i,j,t_x,t_0} \times \Delta \hat{S}_{j,t_1}^{R+1} \right\} \right\} \quad (4.10)$$

The nonlinear inversion involves steps 3 through 6 in Figure 4.1. The first linear inversion starts with a null vector space  $\vec{C}^0$  and generates  $\hat{S}^1$  (steps 1, 2, and 3). Based on the linearly inverted  $\hat{S}^1$ , step 4 simulates the water elevations  $\vec{C}^1$  responding to the  $\hat{S}^1$ . The next iteration estimates  $\hat{S}^2$  from  $\vec{C}^*$ ,  $\vec{C}^1$ , and  $\omega$ . Step 5 compares the  $\vec{C}^R$  with  $\vec{C}^*$ . If the root mean square difference is smaller than the sampling error,  $\hat{S}^R$  is the nonlinear inversion result. Otherwise, another iteration is conducted. The iteration terminates when the difference between  $\vec{C}^*$  and  $\vec{C}^R$  is below the sampling error elevation.

## 4.5 Numerical experiments

In this section, we examine the performance of the proposed method in a channel, which has two open boundaries and three sampling stations (Figure 4.2). The channel's boundaries include one elevation BC and one flux BC, so that we can demonstrate the method's ability to estimate elevation-and-flux boundaries simultaneously. Inside the channel, the water elevations are modeled by solving the shallow-water equations (Luettich et al. 1991) from the finite element grid, land boundary, and the boundary conditions. The method's performance is represented by the sampling location selection, non-linear-inversion, sampling error reduction, and simultaneous elevation-flux boundary inversion. In addition to the above performance evaluations, we further demonstrate the method's robustness by comparing its performance with the frequency-domain method (Nuñez, 1990) in solving frequency-domain problems. Finally, we demonstrate the method's capability of inverting a system with irregular bathymetry and irregular land boundaries by applying the method to estimate the oceanic boundary of the Tejo estuary.

### 4.5.1 Non-linear, noise-free, elevation-flux boundary inversion

In this integrity test, the left boundary is prescribed by an  $M_2$  elevation boundary and the right boundary is driven by a randomly generated flux boundary. In response to the two imposed water sources, the "measured elevation time histories" at the selected stations are simulated by solving the GWCE. As the nonlinear terms, such as advection, finite

amplitude, and bottom friction, are active, the “measured water elevation” is non-linearly associated with the water source magnitudes. The experiment doesn’t introduce any sampling errors, except the round-off errors. Therefore, the integrity test is a non-linear, noise-free, elevation-flux boundary inversion.

According to Figure 4.1, the first step of the inversion characterize the channel’s water circulation by calculating its transfer functions. The transfer function, by definition, is the measured water elevation at sampling stations in response to a unit boundary forcing. Theoretically, this unit forcing is a Dirac delta function. However, the infinite wave number of the Dirac delta function makes the numerical solution unstable. Therefore, this research approximates the delta function by the Gaussian function (4.11)

$$BC(t) = e^{-\frac{(t-t_0)^2}{2\sigma^2}} \quad (4.11)$$

In the equation,  $t$  represents the time;  $t_0$  is the central time of the Gauss distribution, and  $\sigma$  is the width of the Gauss distribution.

The transfer function of both boundaries to the three stations is illustrated in Figure 4.3. The parameters of the Gauss function are  $t_0 = 7200$  seconds,  $\Delta t = 400$  seconds, and  $\sigma = 7200$  seconds. Clearly, the transfer function represents the water circulation characteristics of the channel. First of all, the figure shows that the response magnitude and the response time of the unit forcing is determined by the station location. If the station is located closer to the boundary, the response magnitude becomes higher and the response time is shorter. This is the case for stations 1 and 3. On the contrary, station 2 is located far from both boundaries, and its response magnitude is twenty times smaller than those of station 1 and 3. So, in the inversion, station 2 will not provide as much information as stations 1 and 3. Secondly, the response shape of station 2 becomes more flat than those of stations 1 and 3. Again, this means that station 2 doesn’t provide as much information as stations 1 and 3 do. It is clear that the transfer functions characterize the hydrodynamics of the channel.

Because the transfer function characterizes the channel’s hydrodynamics, its condition number represents the water source’s identifiability (Chapter 3.) Previous research has shown that the condition number of the transfer function can determine the water source’s identifiability.

In Table 4.1, the small condition numbers ( $10^{8.3}$  and  $10^{8.17}$ ) show that when  $N_D=2$ , the BC 1 and 2 can only be identified by stations 1 and 3 individually. On the contrary, the large condition numbers ( $10^{52}$ , INF,  $10^{29}$ ) indicate that station 2 cannot estimate either boundary. In addition, the table also indicates that if we increase the  $N_D$  from 2 to 20, the above identifiability relationships don't change, as the  $10^{29}$ ,  $10^{71}$ , and INF are still large condition numbers. Note that even if using station 2 to estimate any of the two boundaries generates unstable results, the results are not unstable when we invert both boundaries by station 1, 2, and 3. Therefore, the table suggests that we can invert boundary 1 and 2 from measured elevations at stations 1, 2, and 3.

**Table 4.1 The condition numbers (log scale) of the transfer functions**

	$N_D=2$		$N_D=20$	
	BC <sub>1</sub>	BC <sub>2</sub>	BC <sub>1</sub>	BC <sub>2</sub>
Station 1	8.33	INF	2.42	71.22
Station 2	52.50	INF	29.92	INF
Station 3	INF	8.17	70.89	2.40

In the system measurement step, the water circulation model simulates the water elevations at the three sampling stations using the two imposed water boundaries (Figure 4.4). The figure illustrates that the response time of station 1 equals the response time of station 3 as a result of their relative locations to the adjacent boundaries. Also, the flux boundary at the second boundary makes the measured elevation at the third station vary more irregularly than that of the first station. Furthermore, the response time at station 2 is delayed compared with stations 1 and 3. This is because station 2 is located several times further from the boundary than both stations 1 and 3, and the wave travels longer before it reaches station 2. In the next step, the sampled elevations at three stations are used to invert both boundaries.

As shown in Figure 4.5, the third step inverts both the elevation boundary and the flux boundary from the transfer function and the measured water elevations. The figure clearly illustrates that the "dense-sampling" inversion method accurately inverts the imposed boundaries. Notice that the mismatch between the inverted boundary and the imposed boundary is quite obvious, both at the beginning and the end of the inverted

boundary. This is because the inverted boundary is estimated by the weighted summation of the unit-Gaussian forcings. Accordingly, a unbiased inverted data has the same number of the unit-Gaussian on both left and right sides. However, this is not true at both the beginning and the end of the inverted boundaries. Consequently, the inverted boundary conditions don't match well at the beginning and the end of the inversion.

Moreover, the experiment displays the converging speed of the non-linear inversion (Figure 4.6). In this test, we measure the agreement between the inverted boundary and the imposed boundary by the root mean square error.

$$RMS = \left[ \frac{1}{N} \sum_{k=1}^N \{ (\eta_k - \tilde{\eta}_k) - \left( \sum_{p=1}^N \frac{1}{N} (\eta_p - \tilde{\eta}_p) \right) \}^2 \right]^{\frac{1}{2}} \quad (4.12)$$

where  $\eta_k$  and  $\tilde{\eta}_k$  refer to observed and computed elevations, respectively, at the  $k$ th of  $N$  equally-spaced sampling times.

The figure shows that the linearly inverted BC has approximately 0.015 m error, which decreases to less than 0.01 m after two iterations, remaining approximately constant thereafter.

The experiment shows that the proposed method can simultaneously invert both types of boundary conditions (Figures 4.5 and 4.6). This accomplishment is determined by the way the transfer function is generated. For example, if we assign the unit-forcing at the boundary as the elevation Gaussian, the corresponding inversion result is the elevation boundary. Instead, if we impose the flux unit-forcing, the estimated boundary is the flux boundary.

Finally, it is worth pointing out that the proposed method does not invert the initial condition. This is due to the fact that the transfer function excludes the system response to the initial condition. Specifically, the "blind-window" of the transfer function between the unit-forcing-release-time and the system-response-time (Figure 4.3) eliminates the initial condition's signal. Therefore, the method can not invert the initial condition.

To sum up, the method integrity test suggests that the proposed method can achieve the non-linear inversion of simultaneous elevation and flux boundary condition, when no sampling error is present.

#### 4.5.2 Random and systematic error reduction

The inversion's success depends upon its ability to reduce sampling error (Xiang and Elsworth 1992). If the inversion method can not suppress the sampling error amplification, inversion becomes unstable. Along the way, we can measure the inversion's success by investigating its ability to reduce the effect of sampling errors.

This research developed the "dense-sampling" technique to reduce the sampling error amplification. The range of the dense-sampling parameter ( $N_D$ ) is determined by three factors: the BC's variation period ( $T_{BC}$ ), the sampling error magnitude, and the inverted boundary resolution. The first factor requires that there must be enough sampling data to represent the BC variations. In this experiment, the period of the elevation boundary is 12.4 hours. According to sampling theory as shown in equation (4.13), there must be at least two sampling data in each period. Consequently, the boundary variation period determines that  $N_D$  varies from 1 ( $\Delta t=0.11$  hour) to 25 ( $\Delta t=2.7$  hour).

$$1 \leq N_D \leq \frac{T_{BC}}{2\Delta t} \quad (4.13)$$

In addition, the second factor declares that  $N_D$  must be large enough to suppress the sampling error and round-off error amplification. This is demonstrated in the method integrity test, where inversion must use the "dense-sampling" scheme ( $N_D=2$ ) to suppress the round-off error. Furthermore, the third factor indicates that  $N_D$  should be as small as possible so as to obtain the smallest inversion resolution. Typically, the selection of  $N_D$  requires the balance among the three factors.

Both random and systematic error reductions are tested in the channel. The random errors are the artificially introduced 5%, 10%, and 20% relative random errors in the sampling data (Figure 4.4). The systematic error is introduced in the water elevation by simulating the St. John's Landfill environment using a wrong friction coefficient (true value=0.0225, value for systematic error simulation = 0.0322). The sampling error reduction is represented by the RMS error (Figure 4.7).

In the figure, the first iteration is the linear inversion. Linear inversion has a large RMS error, reflecting the non-linearity of the problem. As the iterations proceed, errors converge to smaller values. For example, the RMS of the elevation boundary converges from 0.02 to about 0.008 m, while the RMS of the flux boundary converges from 0.02 to about 0.009 m/s. Another interesting point is that the inverted RMS errors are not significantly related to the scale of the random error. For instance, the RMS errors do not diverge significantly, even though the random errors range from 5% to 20%. This is due to the fact that the average of the random sampling error is zero, and the magnitude of the inverted errors corresponds to the averaged random errors. Consequently, inversion RMS errors are not significantly interrelated with the random-error magnitude. Similarly, the method is also very efficient at suppressing systematic errors. This can be seen from the inversion with a 10% random sampling error and a 43% systematic error. Indeed, the inverted RMS errors are very similar to those of the random errors. After six iterations, the nonlinear inversion converges to the imposed boundaries. In summary, the diagnostic analysis demonstrates the capacity of the developed method to deal with both non-linear inversions and sampling error reductions.

### **4.5.3 Comparison between the proposed time-domain method and the frequency-domain (ITM) method**

This section demonstrates the robustness of the developed time-domain inversion method by comparing its performance with the frequency-domain inversion method (Nuñez, 1990) in solving frequency-domain problems. Naturally, the time-domain problem stems from the riverine boundary, where the boundary of water-flux is controlled by both natural and human-controlled processes. The frequency-domain problem comes from the oceanic boundary, where the water elevation is highly periodic. The objective of this experiment is to show that the developed time-domain method can efficiently solve the frequency-domain inversion problem.

We compare the time-domain inversion method with the frequency-domain inversion method in the channel (Figure 4.2), where the left boundary is activated with a  $M_2$  boundary, and its corresponding water elevation is measured at station 1. In the experiment, we first employ the frequency-domain method to estimate the amplitude and phase of the boundary elevation from the amplitude and the phase of the measured water elevation. Later, we apply the developed time-domain inversion method to estimate the bound-

ary elevation history from the measured water elevation history. Finally, we evaluate the performance of the two methods by comparing the inverted boundary (Figure 4.8, Figure 4.9 and Figure 4.12) and the inverted elevation at station 1 (Figure 4.10 and Figure 4.11).

The experimental results suggest that the developed time-domain method solves the frequency-domain problem as effectively as the frequency-domain method. First of all, Figure 4.8 and 4.9 indicate that both methods can accomplish the non-linear inversion. Specifically, the inverted boundary elevations by both the frequency-domain method and time-domain methods converge to the imposed values after 4 iterations. Additionally, Figures 4.10 and 4.11 illustrate that the inverted elevations from both methods also converge to the measured water elevations after four iterations. Both figures reveal that the inversion converges to the synthetic reality. Notice that the time-domain inversion generates an irregular shape at iterations 1, 2, and 3. This is due to the fact that the first iteration is a linear inversion, and the non-linearity between the boundary condition and measured water elevation results in larger inversion error. After four nonlinear iterations, the nonlinear errors are minimized and the inversion converges to the imposed boundary.

Moreover, Figure 4.12 compares the inversion's converging speed of both methods. From the figure, we can see that the inversion errors for both methods (relative RMS) decrease from 0.8% to 0.1% after four nonlinear iterations. This RMS reduction indicates that both methods converge with the same speed. It is worth pointing out that the time-domain method has larger normalized RMS errors than those of the frequency-domain method. Our explanation is that the frequency-domain method utilizes amplitude, phase, and frequency to represent the water-elevation, while the time-domain method uses central Gaussian location, Gaussian width, and Gaussian magnitude to describe the water elevation. Because the time-domain method has larger errors in representing the tidal signal than the frequency-domain method, the time-domain method has larger inversion errors than those of the frequency-domain method, at the same inversion level. In conclusion, the experiment suggests that the developed time-domain inversion method performs similarly to the frequency-domain method in solving the frequency-domain problem.

## **4.6 Oceanic boundary inversion of the Tejo estuary**

After ensuring the method's basic integrity, we use it to estimate water sources of the Tejo Estuary in Portugal. Because the Tejo estuary has irregular land boundaries and

bathymetry (Figure 4.13), this application further explores the method's integrity in a new situation. This estuary area ranges from the XF Xira river to the open ocean boundary. Because its hydrodynamics is dominantly controlled by the oceanic boundary, this inversion only focuses on the estimation of the oceanic BC.

We use five stations (Cascais, Pedroucos, Lisboa, Cacilhas, and Trafaria) to invert the oceanic BC. By applying the developed method, we successfully invert the oceanic boundary, as shown in Figure 4.14. The comparisons between the measured water elevations and the simulated water elevations are shown in Figure 4.15. Again this application verifies that the developed method can effectively estimate the boundary condition, even if the bathymetry and the land boundary are extremely irregular. First of all, the successful inversion again demonstrates that the frequency-domain problem can be solved by the developed time-domain method. Secondly, the irregular land boundary and bathymetry do not degrade the method performance. In fact, the application proves that the land boundary and bathymetry do not effect the method's integrity.

Thirdly, the RMS spatial distribution shows that small inversion errors happen at stations close to the ocean boundary (Cascais and Trafaria). In contrast, large inversion errors occur at stations located farther away from the oceanic boundary (Pedroucos, Lisboa, and Cacilhas). Our explanation is that the Cascai and Trafaria stations have a better bathymetry and land boundary than the Pedroucos, Lisboa, and Cacilhas stations. Therefore, the former stations have smaller RMS errors than the latter stations. Finally, the successful inversion validates, to a certain extent, the accuracy of the grid and the circulation model. Given the fact that the inversion RMS error at each station is the same as that of the frequency-domain inversion (Figure 4.15), we can see that the time-domain and frequency-domain models have the same capability of representing a tidal dominant system. Notice that because the above inversion does not account for the riverine boundary, its successful inversion further justifies the assumption that the exclusion of the Tejo riverine boundary does not yield a noticeable error in its hydrodynamic simulation.

## 4.7 Summary and Conclusions

In this chapter, we described, analyzed and applied the water source non-linear inversion method. The analysis and the application concludes that the method is capable of accomplishing nonlinear inversion, suppressing the sampling error, simultaneously esti-

mating both the elevation and flux boundaries, and solving the frequency-domain problem. In summary, this research developed a scientifically-sound and practical methodology for estimating the water sources of a general water environment.

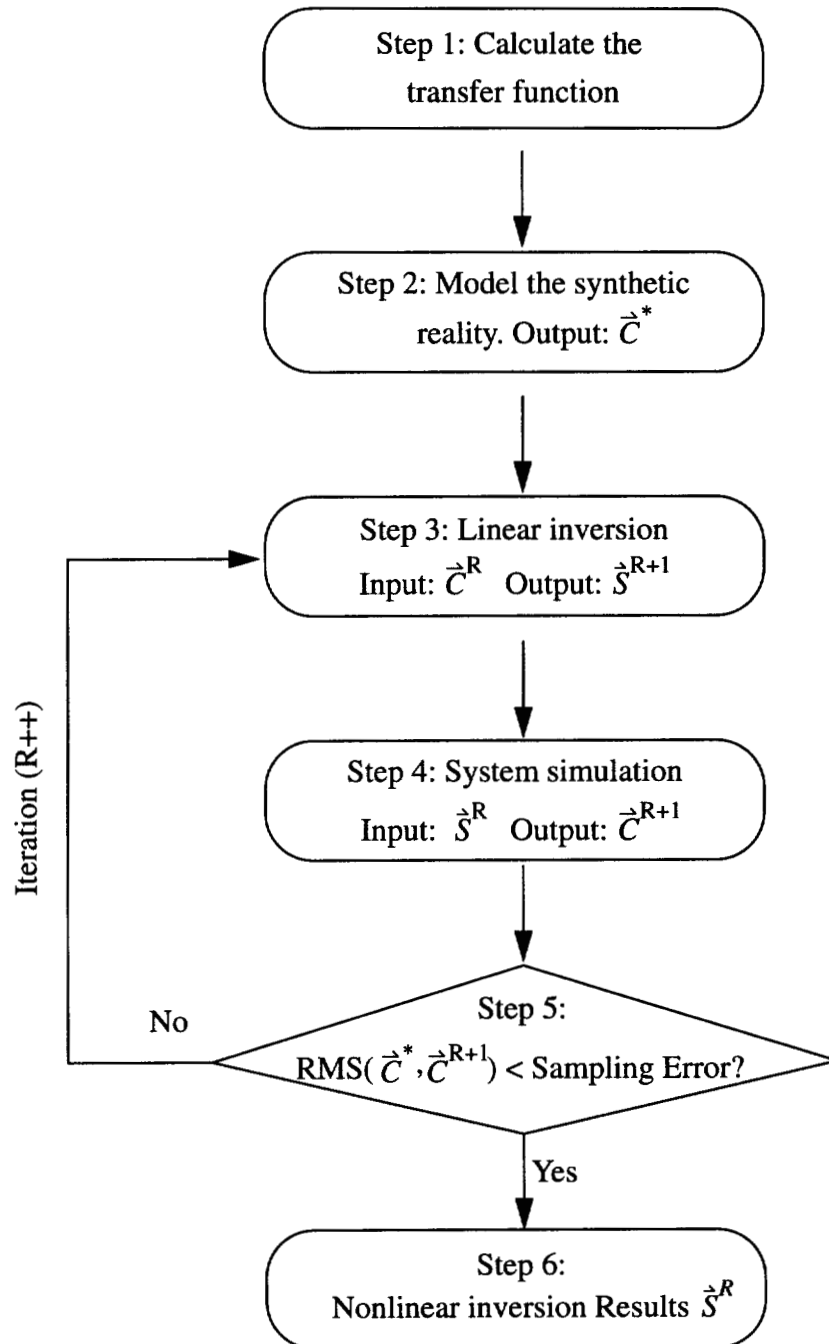


**Figure 4.1** General steps for the non-linear estimation of water sources.

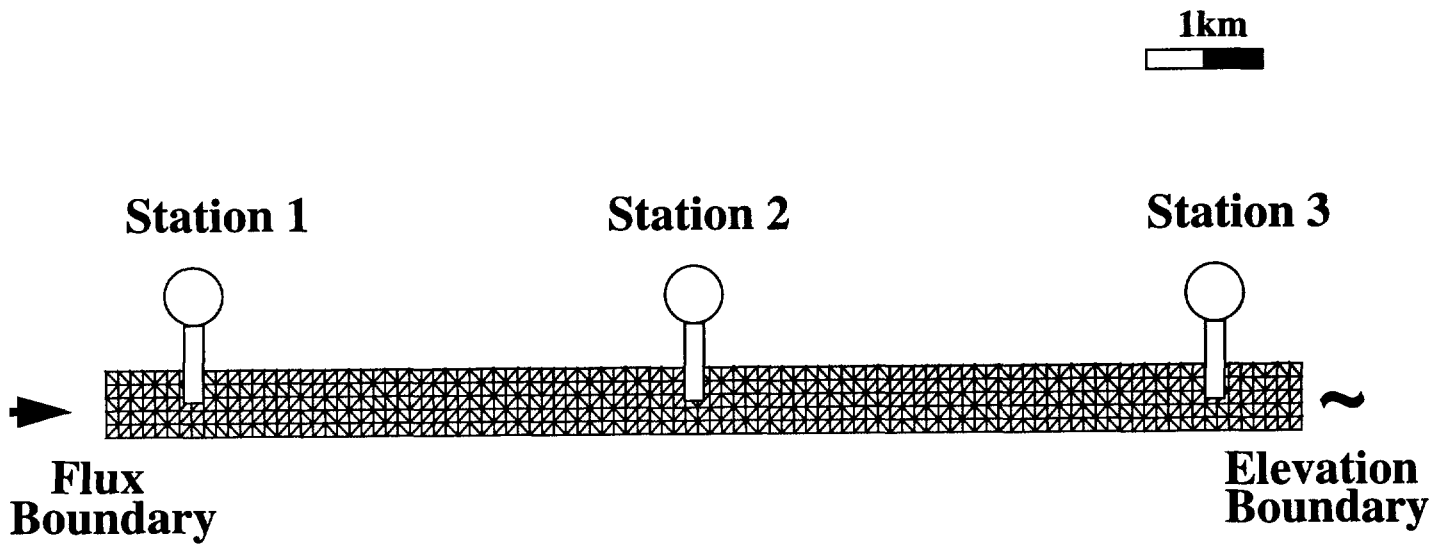


**Figure 4.2** The finite element grid of the channel case. Notice that the problem includes one elevation boundary, one flux boundary, and three sampling stations.

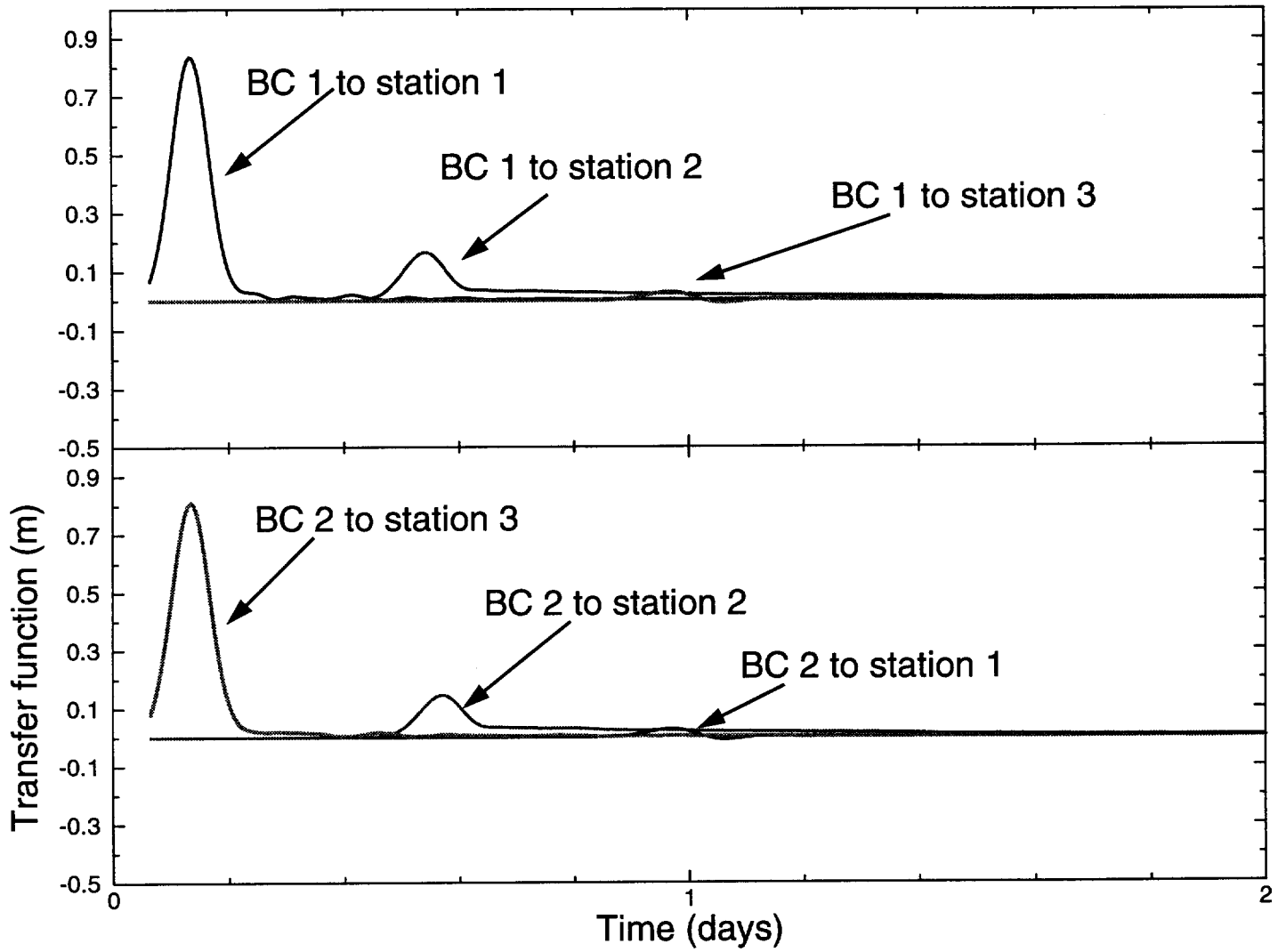


**Figure 4.3** The transfer functions of the channel, with two open boundaries and three sampling stations.

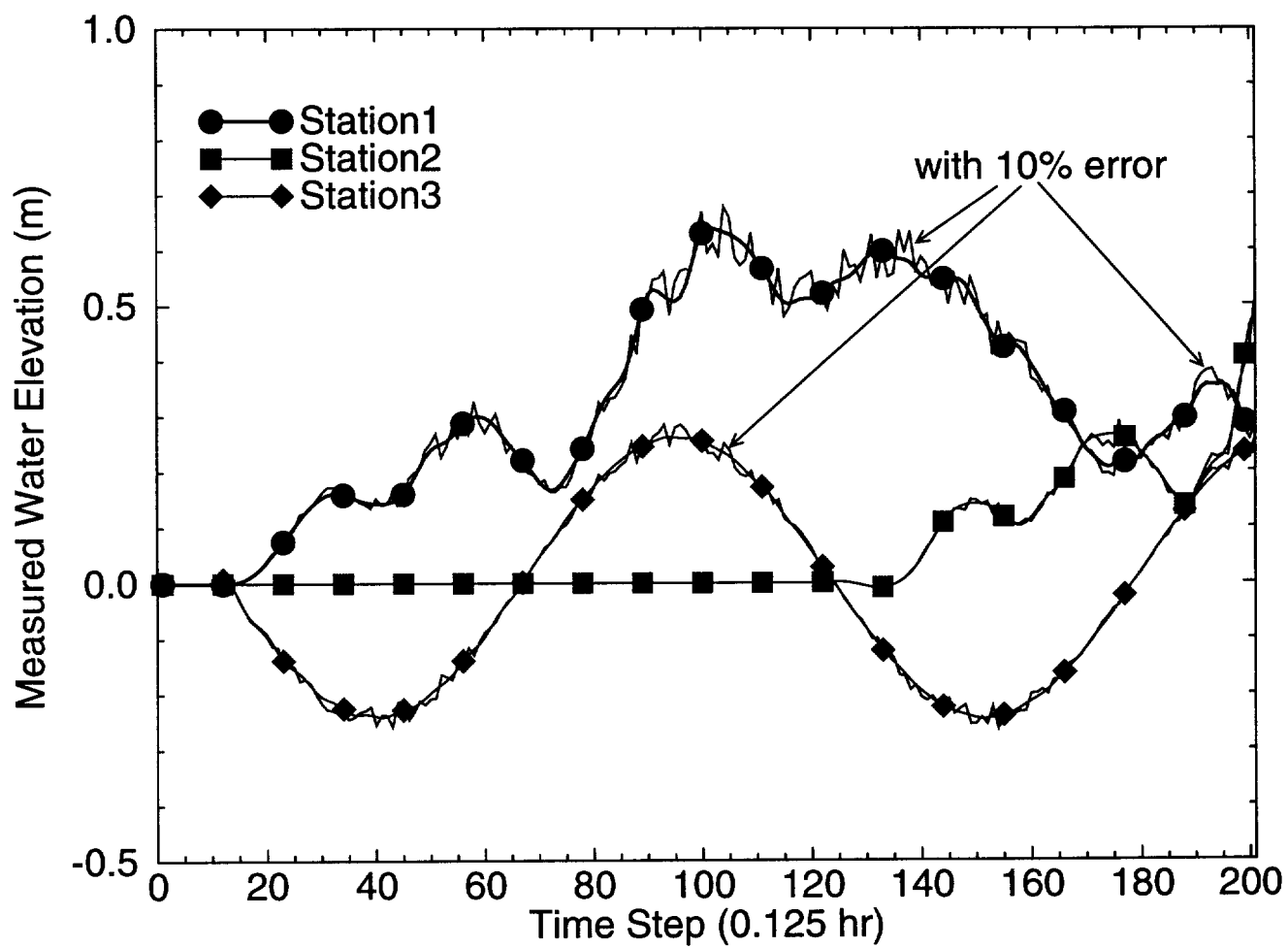


**Figure 4.4** Measured water elevations at three stations (original and with 10% relative error).

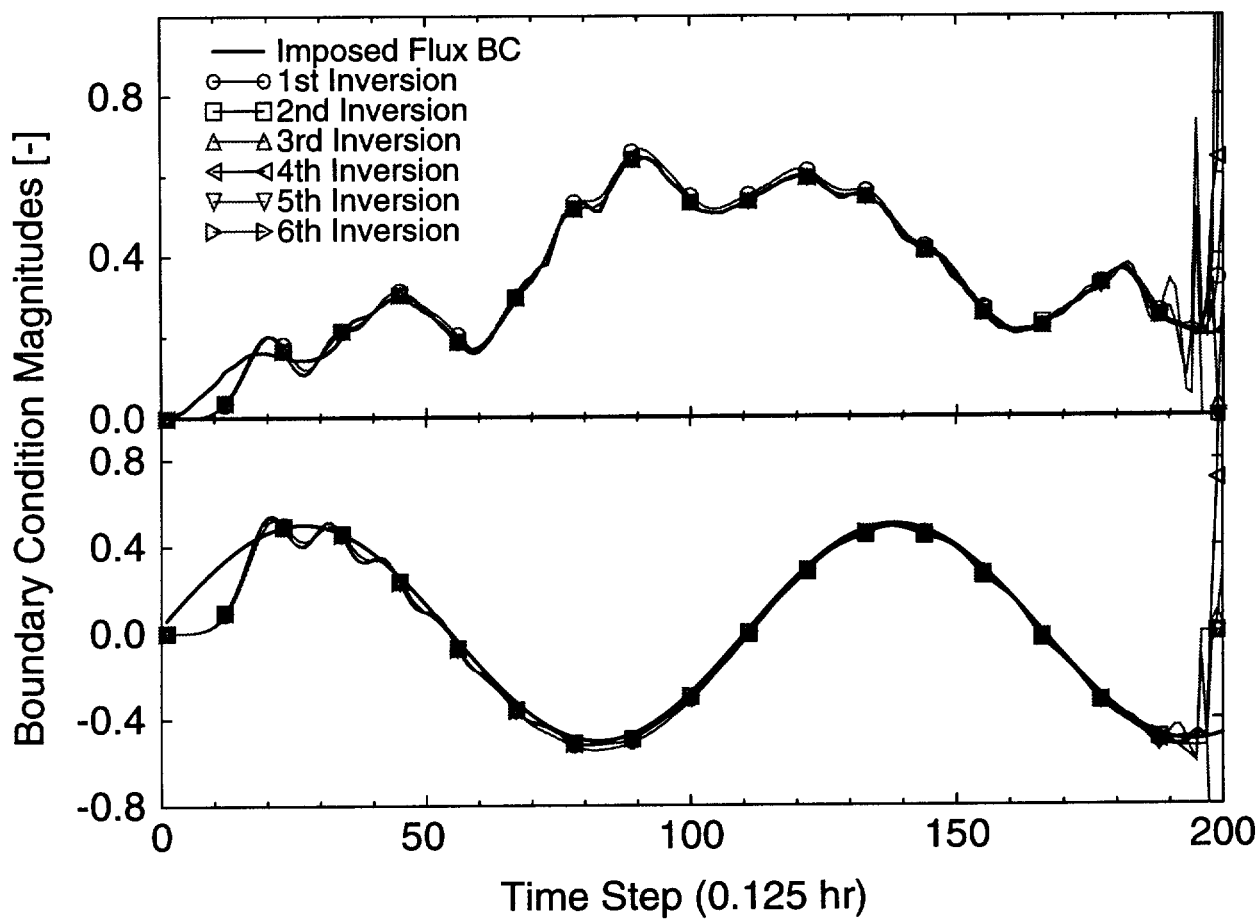


**Figure 4.5** Nonlinear noise-free inversion of both water elevation and flow boundary conditions from sampled elevation at three stations (channel case)

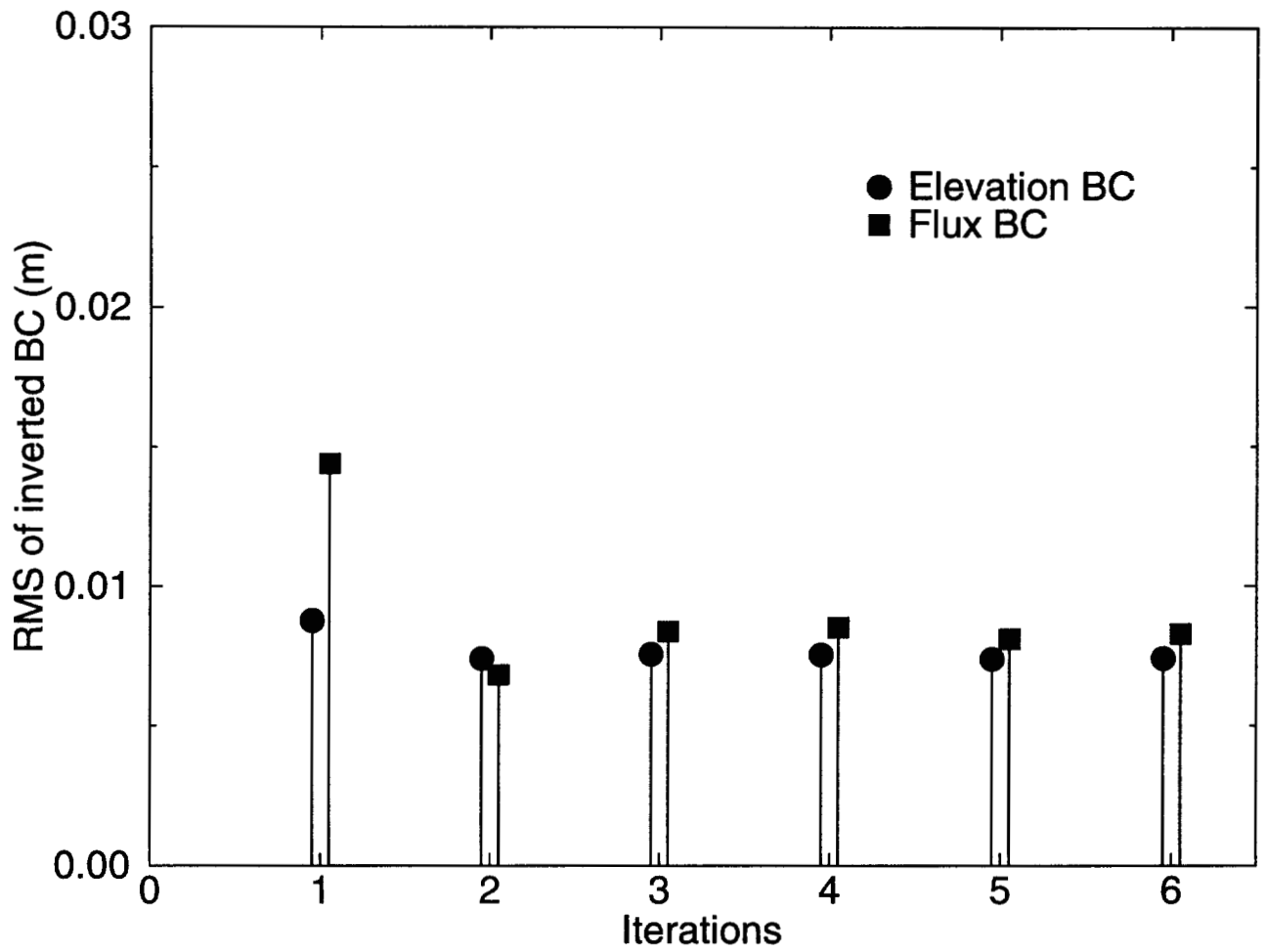


**Figure 4.6** The root mean square errors of noise-free nonlinear inversion, where there are one water elevation boundary, one flux boundary, and three sampling stations.

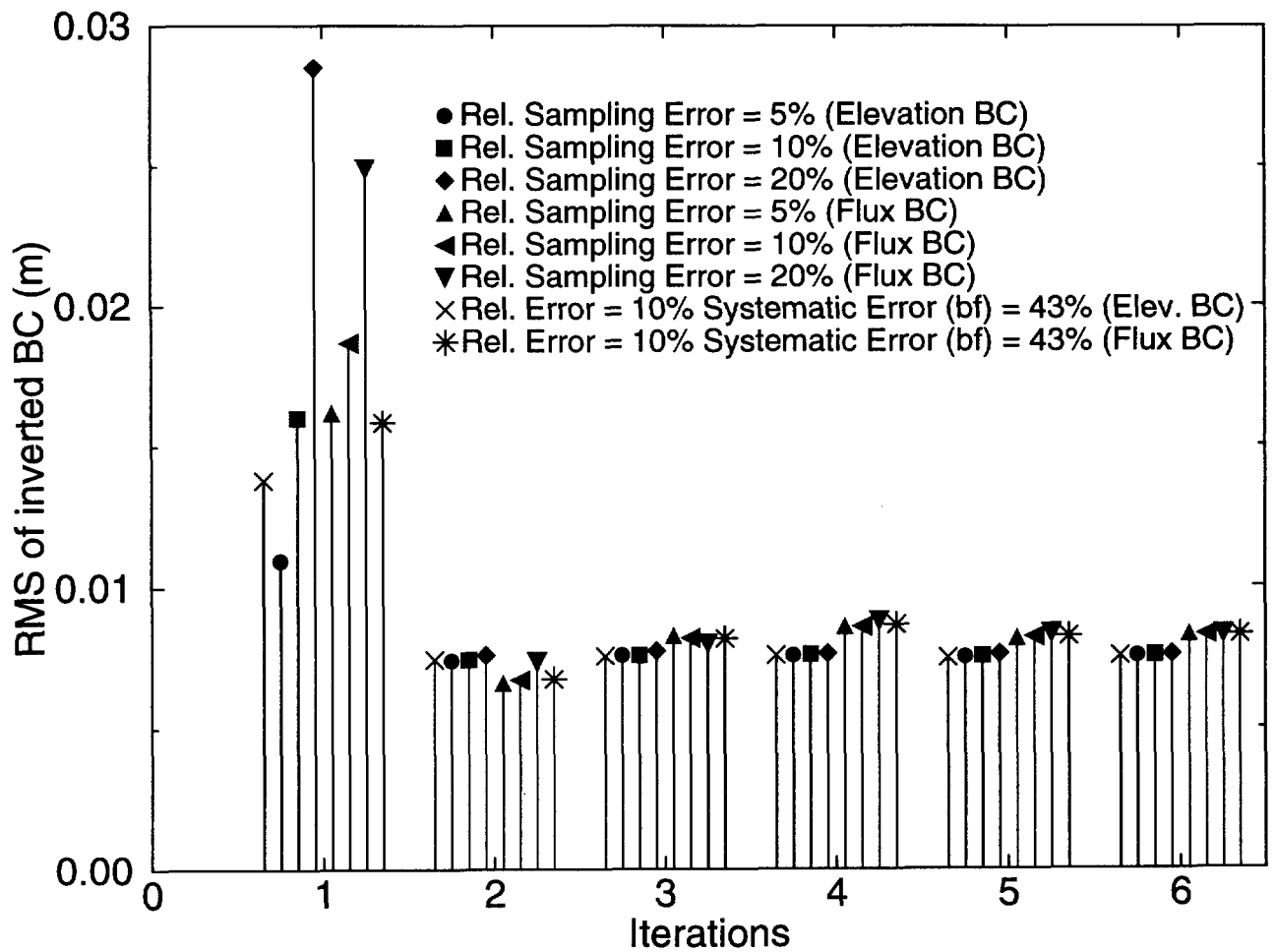


**Figure 4.7** The root mean square error of the estimated water elevation and flux boundary conditions of each iteration. Note that non-linear inversions demonstrate both the sampling error reduction and simultaneous elevation and flux boundary inversion.

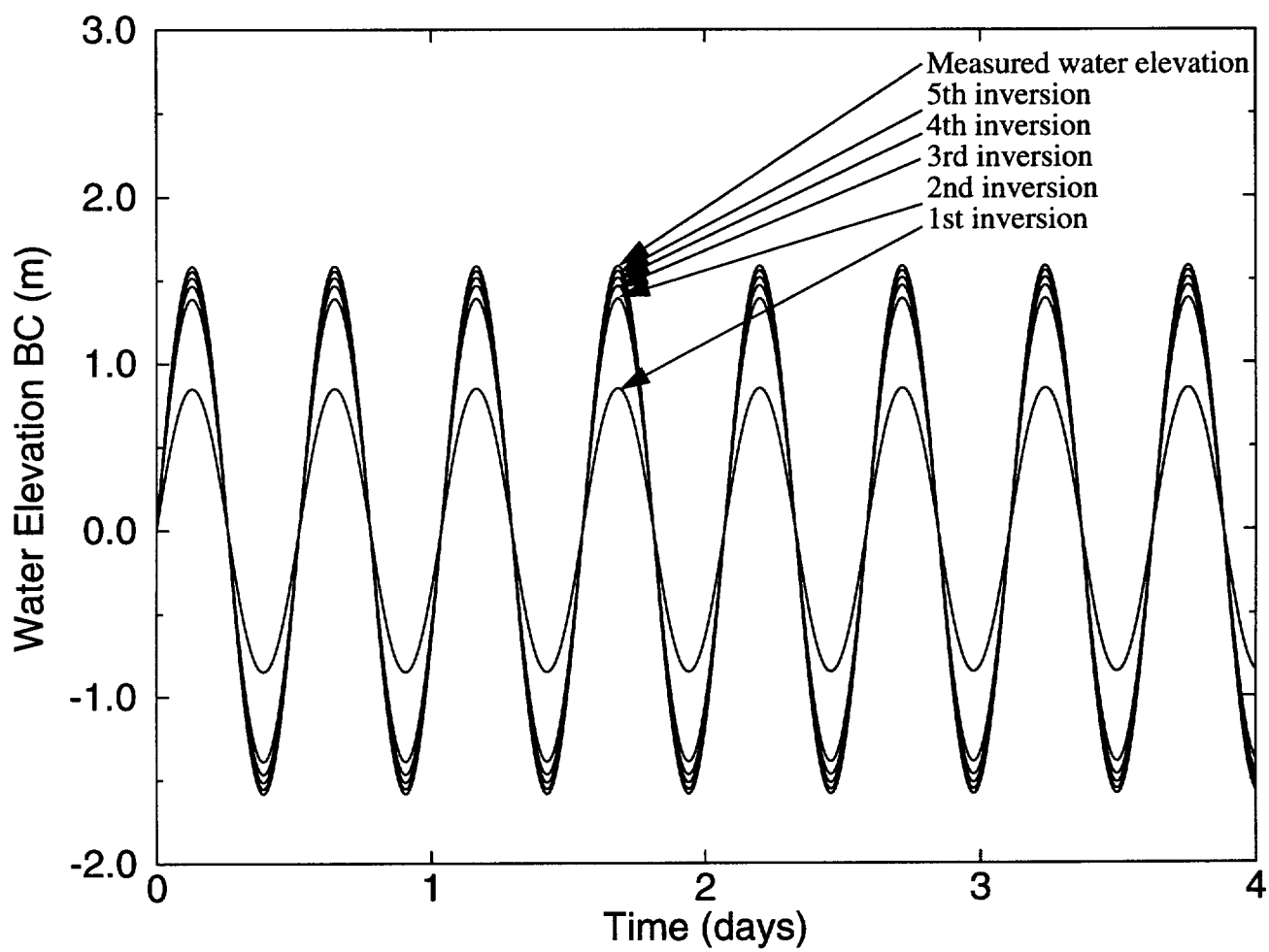


**Figure 4.8 Comparison between the inverted boundary elevation and the imposed boundary elevation by the frequency-domain method.**

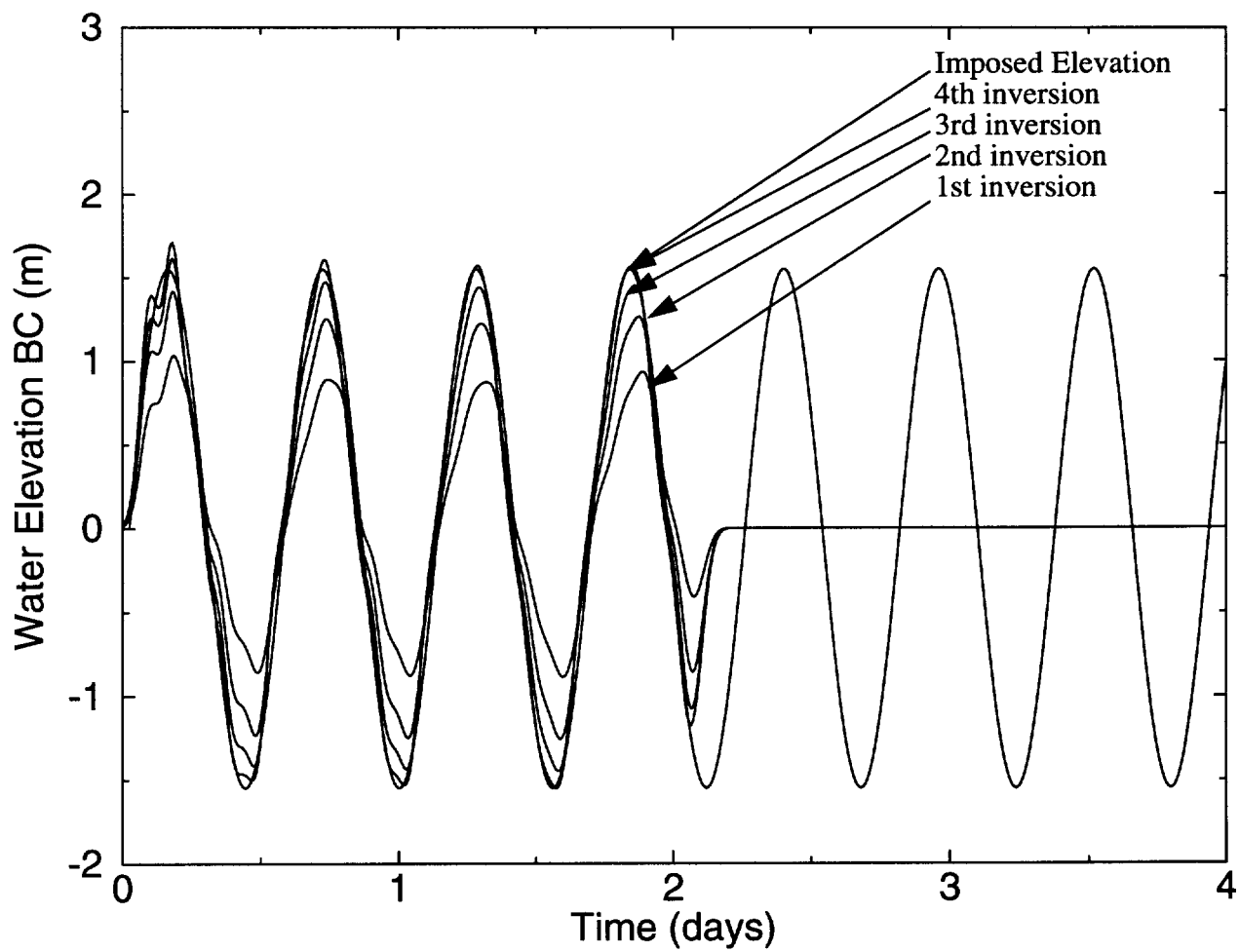


**Figure 4.9 Comparison between the inverted elevation boundary and the imposed boundary elevation by the time-domain inversion.**

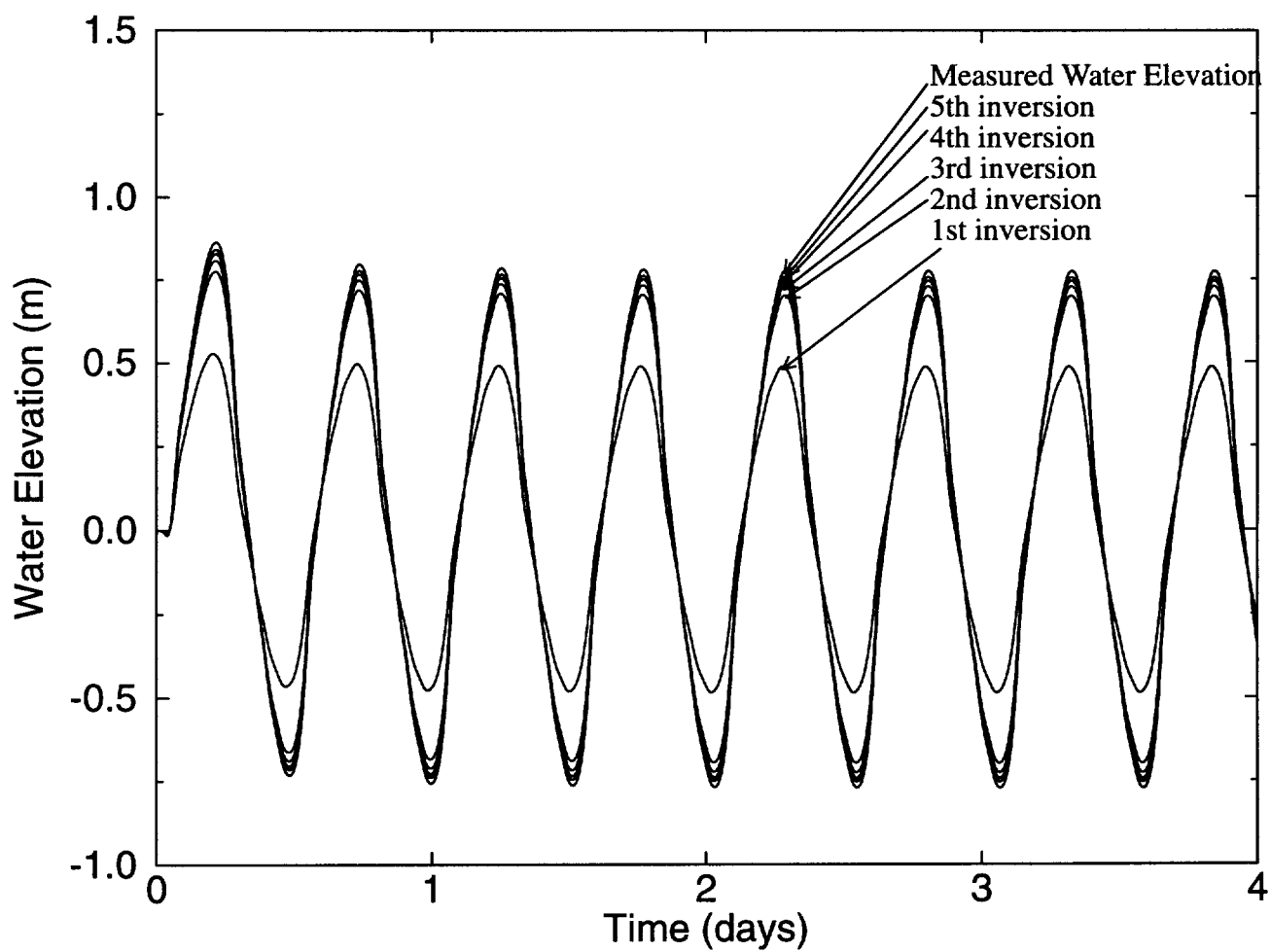


**Figure 4.10 Comparison between inverted water elevations and the measured water elevations for the frequency domain inversion.**

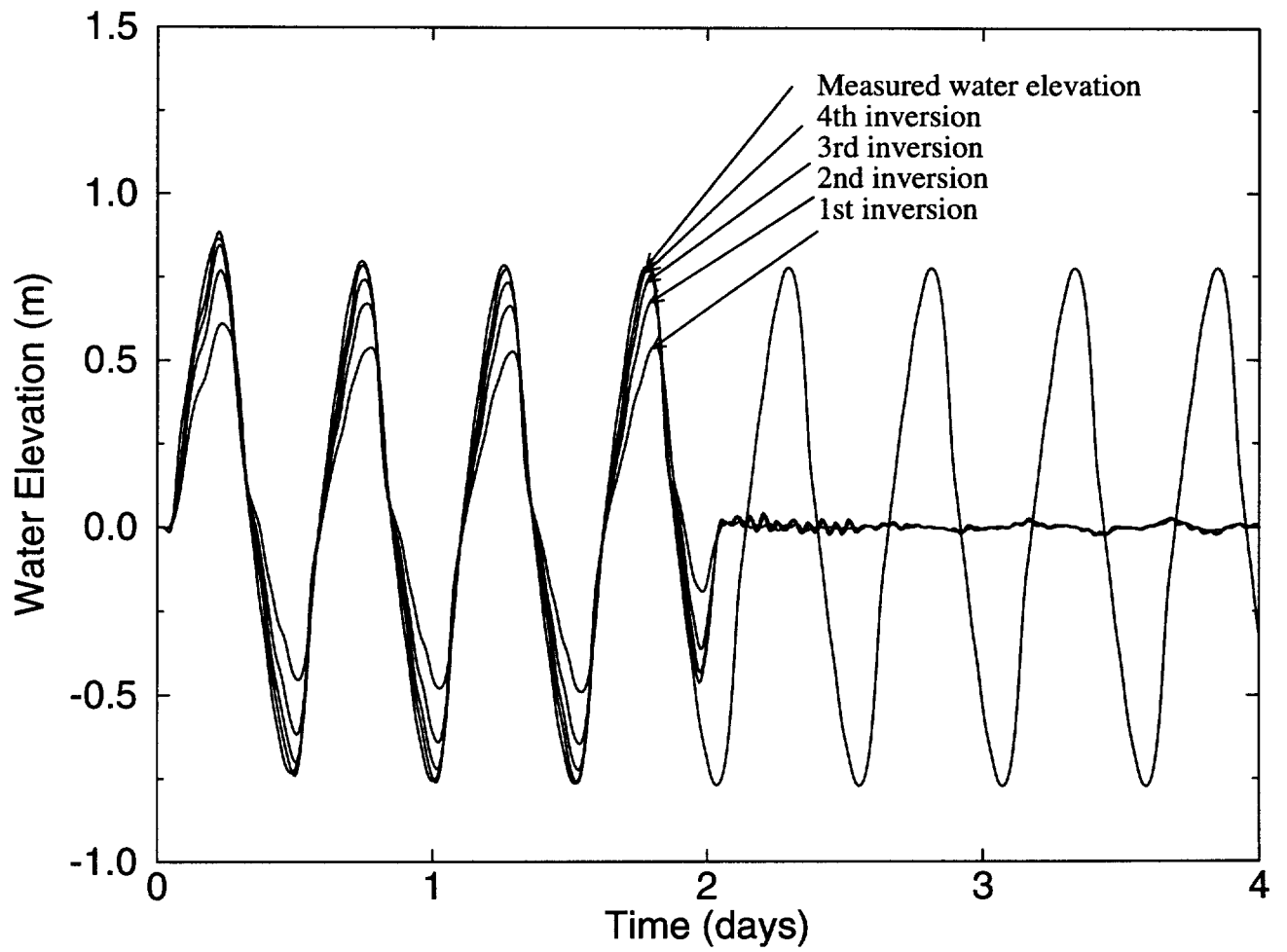


**Figure 4.11 Comparison between the inverted water elevation and the sampled water elevation for the time domain inversion**

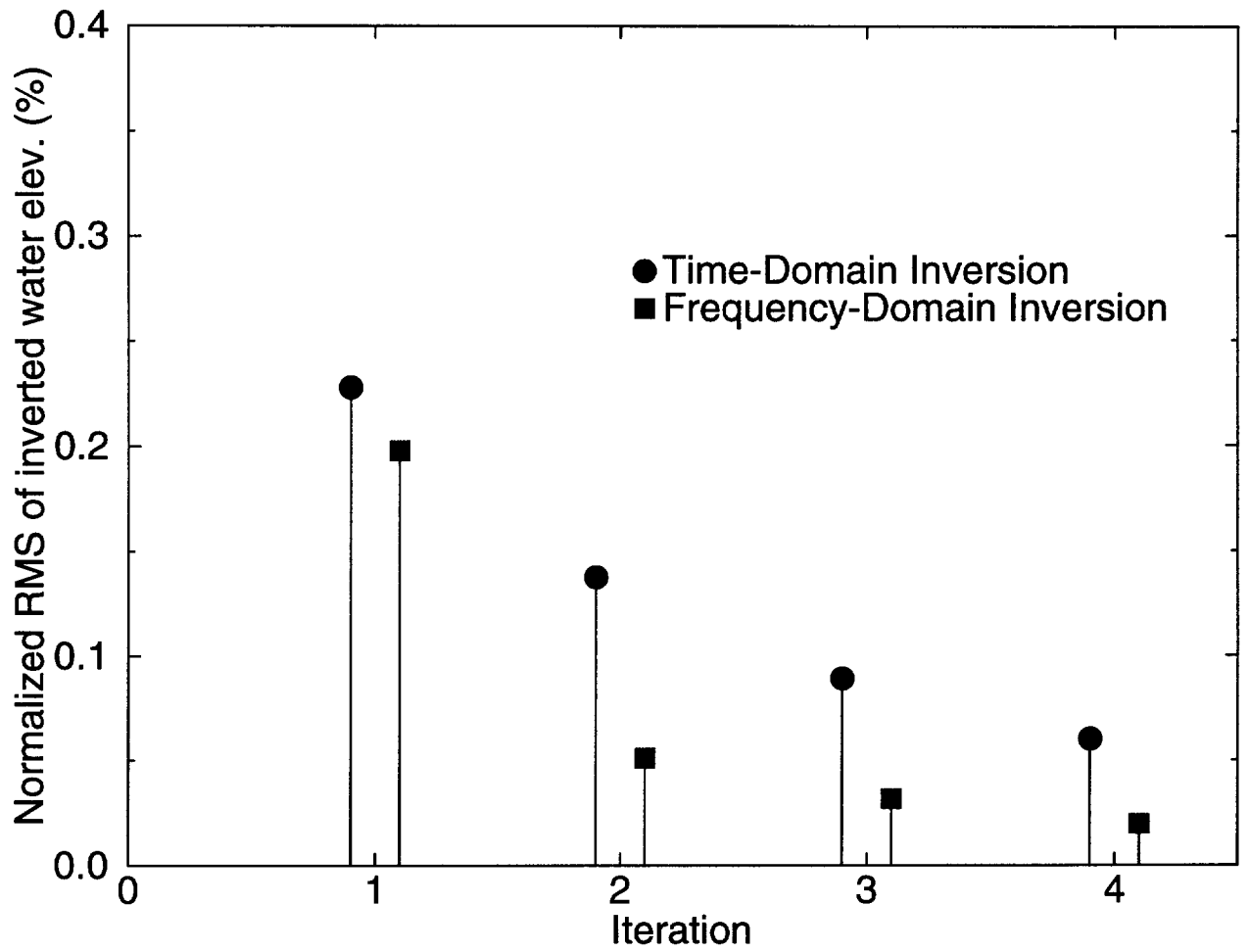


**Figure 4.12 Comparison of the converging speed between the frequency-domain inversion and the time-domain inversion**

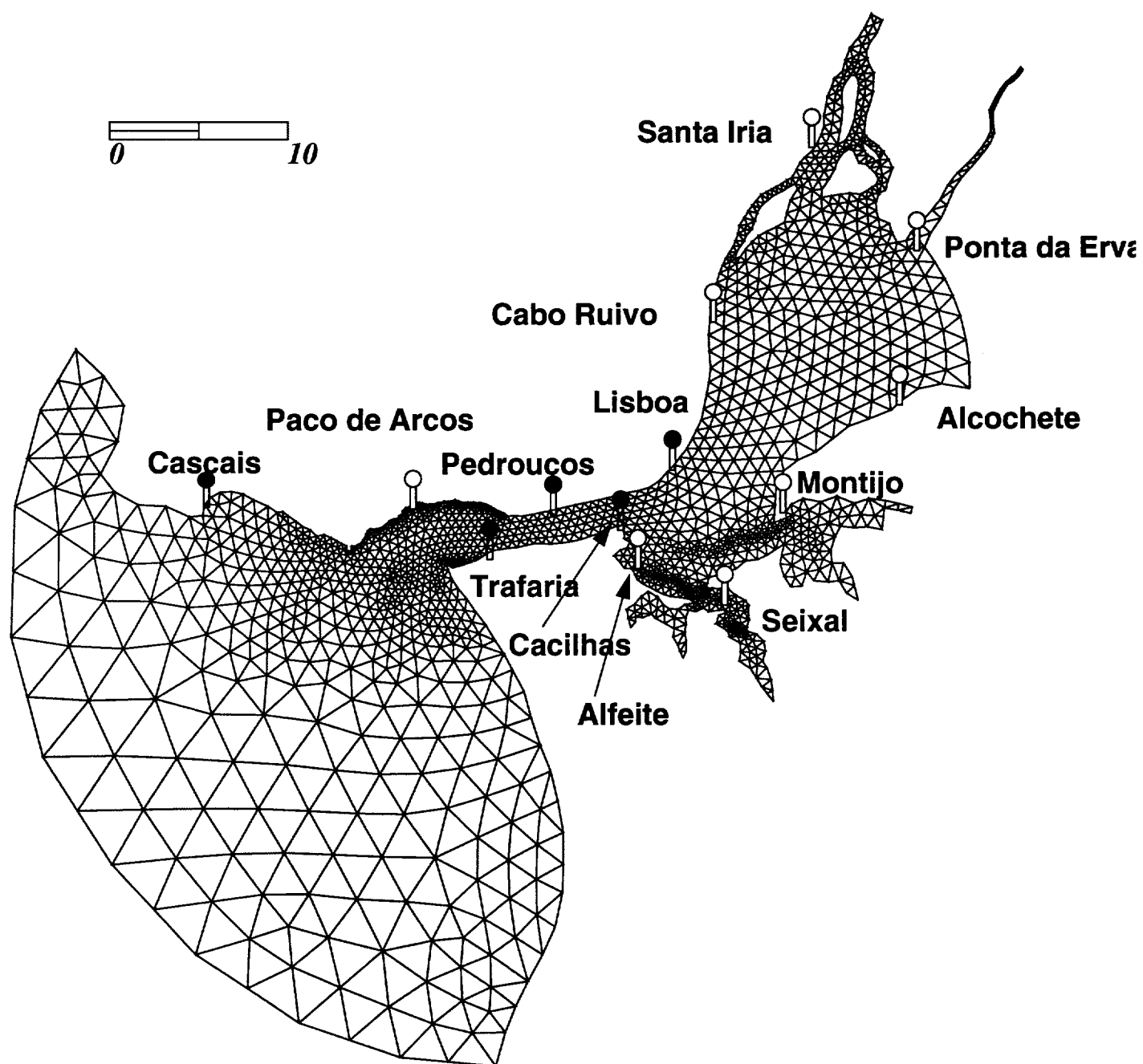


**Figure 4.13** Diagram of the Tejo's finite element grid and the tidal station locations. Note that the Tejo application utilizes the 5 stations (Cascais, Pedrouços, Lisboa, Cacilhas, and Trafaria) to invert the oceanic boundary condition.

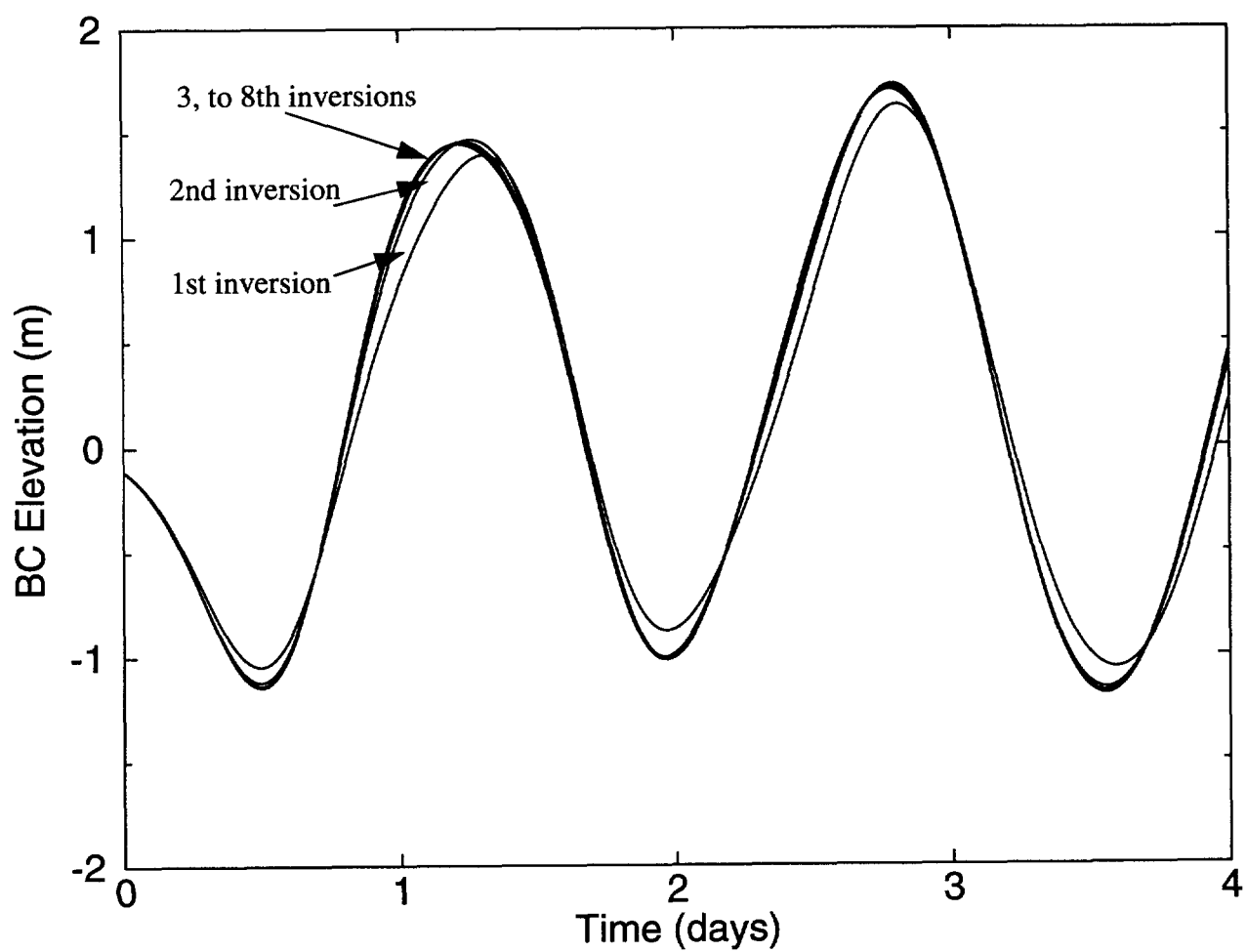


**Figure 4.14** Estimated Tejo oceanic boundary condition based on the measured water elevations at Cascais, Pedroucos, Lisboa, Cacilhas, and Trafaria stations using the developed “dense-sampling” inversion method.

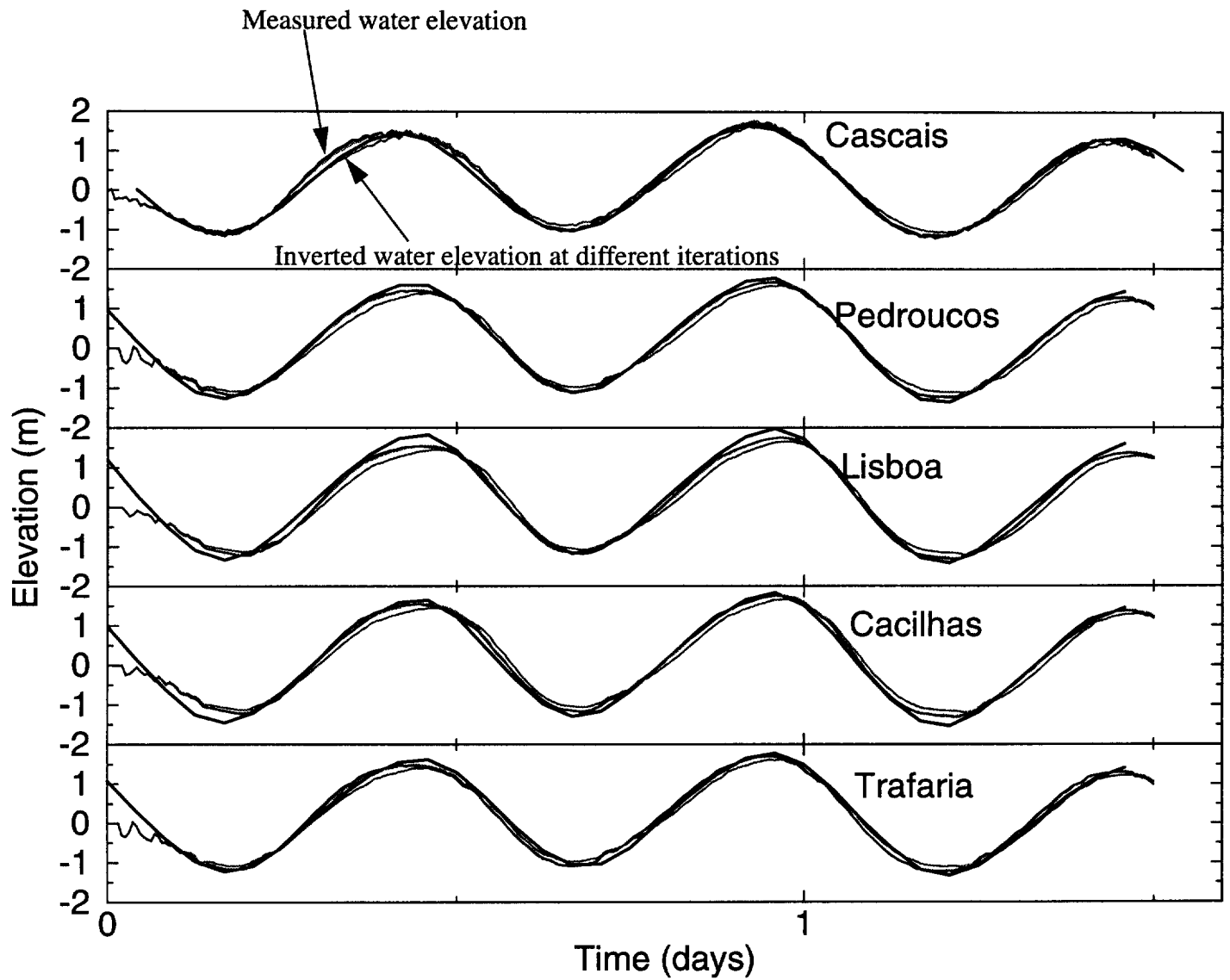


**Figure 4.15** Comparisons of the measured water elevations of Tejo estuary with the simulated elevations based on the inverted boundary conditions.

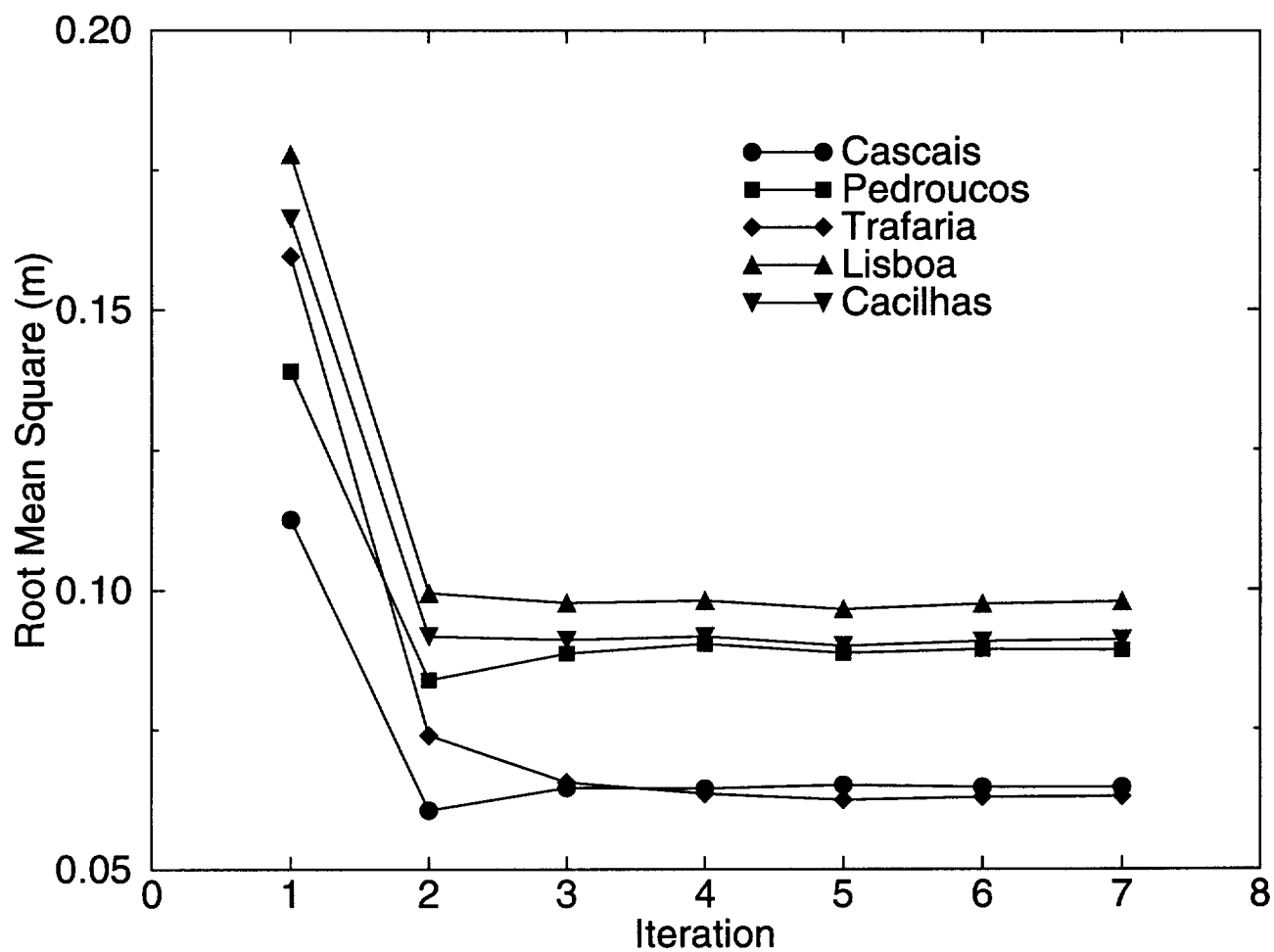


**Figure 4.16** Comparisons of the measured water elevation with the inverted water elevation by the root-mean-square errors.

## 4.8 References

- Bennett, A. F. and P. C. McIntosh, Open ocean modeling as an inverse problem, *Journal of Physical Oceanography*, 12, 1005-1018, 1982.
- Ginn, T. R. and J. H. Cushman, Inverse methods for subsurface flow: A critical review of stochastic techniques, *Stochastic Hydrology and Hydraulics*, 4, 1-26, 1990.
- Luetlich, R. A., J. J. Westerink, and N. W. Scheffner, *ADCIRC: An Advanced Three-dimensional Circulation Model for Shelves, Coasts and Estuaries*, Coast. Engr. Res. Ctr., U.S. Army Engrs. Wtrways. Experiment Station, Vicksburg, Miss, 1991.
- McIntosh, P. C. and A.F. Bennett, Open ocean modeling as an inverse problem, *J. of Physical Oceanography*, 14(3), 601-614, 1984.
- Núñez, R. H., *Prediction of tidal propagation and circulation in Chilean inland seas using a frequency domain model*, M. Sc. dissertation, Oregon State University, Corvallis, OR, 1990.
- Satish, M. G. and J. Zhou, Stochastic approach for groundwater flow in a semiconfined aquifer subject to random boundary conditions, *Advances in Water Resources*, 15, 329-339, 1992.
- Xiang, J. and D. Elsworth, Parameter identification of non-steady groundwater flow systems, *Advances in Water Resources*, 15, 259-269, 1992.

# CHAPTER 5

## Summary and conclusions

This thesis proposes the “dense-sampling” inverse modeling method to address critical issues in analyzing time-variant, linear and nonlinear, environmental system. The applications of this method to analyze the surface water environment establishes practical methodologies for estimating pollutant source time-series, designing a sampling network for monitoring pollutant sources, and calculating water sources. The diagnostic analysis of these methodologies allows us to summarize their scientific contributions, their theoretical and practical limitations, and to suggest future research.

### 5.1 Scientific Contributions

The research develops the “dense-sampling” concept to formulate the relationship between the measurable variables (such as contaminant concentration and water elevation) and the environmental sources (like pollutant source and water source). This innovated formula successfully reduces the high inversion sensitive so that the formula can achieve a highly-resolved temporal-inversion. The research also defines the source identifiability index as the condition number, a numerical variable generated during the inversion. As a result, the research finds a new technique to both evaluate and design a sampling network for monitoring an environmental system. These scientific contributions are exemplified by the following four practical applications.

The first application of the “dense-sampling” inverse modeling theory calculates the pollutant source time-series from the transport model and the measured tracer concentration. This has significant scientific value, because we have not found any published research claiming to have solve the problem. The second application applies the source identifiability index, the condition number, to designs a sampling network for monitoring pollutant sources. The application shows that the discovered source identifiability index is the theoretical basis for systematically designing a sampling network for monitoring environmental system. Similar to the first application, we have not found any mathematics-based sampling network design method. Therefore, the application has scientific values. The third application estimates the water sources of a confined surface water environment.

The research developed a successful nonlinear time-domain inversion method, that can estimate different types of water sources. Again, we have not found any published research that can solve the problem. Obviously, the application is scientifically significant. The fourth application (Myers et al. 1993) quantifies the tsunami bottom deformation from the run-up data and the tsunami wave data. This application illustrates that the “dense-sampling” inverse modeling theory is scientifically sound such that it can be applied to solve different environmental problems.

The above scientific contribution of this Ph.D research indicates that the “dense-sampling” formula can address fundamental issues in understanding a linear/nonlinear environmental system by predicting the unknown’s identifiability and estimating the identifiable unknowns.

## **5.2 Theoretical and practical limitations**

“Dense-sampling” inverse modeling has both theoretical and practical limitations. First of all, the method’s inability to invert the spatial variation is still a major limitation. Indeed, we must know the spatial variations of the identified pollutant sources and water sources in order to estimate their temporal variation. The difficulties of solving the spatial inversion are both theoretical and practical. Theoretically, the spatial inversion generally is not unique, which means the inversion has more than one solution. This non-unique problem does not have a mature theoretical solution. Practically, the extension of the method for spatio-temporal inversion requires unrealistically intensive sampling. In the usual sense, the application of the “dense-sampling” concept to carry out spatial-temporal inversion requires the “dense-sampling” parameter to be several hundreds, which is estimated based on the “dense-sampling” parameter of temporal inversion. Clearly, it is unrealistic to estimate one spatial unknown from several hundreds measurements. Therefore, the solution of the spatial inversion will be a major step towards real-world inversion.

The developed theory also has several practical limitations. The pollutant source characterization method requires a time-series sampler for monitoring the pollutant tracer. However, it is difficult to find a sampler, that can work consistently in a real environment for a long period of time. Even though there are several substitutions, like temperature, conductivity, DO, turbidity, and BOD/COD etc., the problem is that it is difficult to find the relationship between these measurable variables and the inverted contaminant. Obvi-

ously, the developed theory is limited by the sampling technology. The other practical limitation is computational. Specifically, the simulation time for analyzing an environmental system generally exceeds their natural time. For instance, by simplifying the hydrodynamics of the synthetic St. John's Landfill environment, the time of hydraulic characterization decreases from about 80 days to around 10 days, which is still longer than its natural time. Clearly, the theory needs a fast computer. Moreover, the storage capacity is a potential problem. On the one hand, the file size of the transfer function increases exponentially with the number of sampling data. On the other hand, the number of transfer function files is the product of the station number and the source number. Consequently, the disk-usage of a field application can easily reach the storage limit. However, with the fast development of storage technology, this limitation is not critical.

### **5.3 Directions for future research**

Follow-up research is needed on the issue of spatial variation of the source. Our preliminary research shows that the non-uniqueness becomes more dominant in the spatial inversion than in the temporal inversion. The difficulties of spatial inversion are how to represent source spatial variation and how to estimate large number of unknowns. Evidently, spatial inversion must solve both the error amplification and the non-uniqueness.

The simultaneous parameter-and-source estimation also needs to be further investigation. As discussed in Chapter 1, model parameter estimation and model source inversion share the same theoretical limitations. Therefore, the solution of the source characterization implies the solution of the parameter estimation, and simultaneously parameter-source inversion. The difficulties are how to represent the model parameters as the "model input" and how to formulate the non-linear relationship between the parameter-magnitude and measured variables.

A third follow-up research subject is the development of the automatic sampling network design method. Right now, we still can not automatically design a sampling network design for a environmental sampling based on the model and the source spatial distribution. However, the theory is the guide for the automatic sampling network design. One fundamental theme is to find the universal identifiable criterion for source identifiability. Searching for this general criterion can be accomplished by the theoretical analysis of the "dense-sampling" inverse modeling theory. Its difficulty is that the research requires

a broad knowledge of modeling theories, numerical techniques, and optimization methods.

Finally, the theory demands more accurate and computational efficient numerical models. Even though the developed theory can not automatically optimize model parameters and model source/sink terms, it can identify an incorrect model by generating an unstable inversion. In addition to accuracy, computational efficiency will play a major role in the field application. Therefore, the development of advanced environmental models and the “dense-sampling” inverse modeling theory are mutually beneficial.

## 5.4 References

Myers, E.P., A.M. Baptista, and Y. Wang, Non-linear Inversion Waveforms: Diagnostic Analysis for the 1992 Nicaragua and 1993 Hokkaido Tsunamis, *AGU 1993 Fall Meeting*, Dec. 6-10, 1993, San Francisco, CA, 1993

## VITA

The author was born on the 1st of July, 1963, in Beijing, P. R. China. In 1986, he finished his B. S. from the Chemistry Department, Nankai University, P. R. China. In 1989, he completed his M. S. in Environmental Chemistry, at the Department of Environmental Science, Nankai University, P. R. C. The author came to the United States in 1990 to pursue the Ph.D. degree in environmental science and engineering at Oregon Graduate Institute of Science & Technology, where his research focused on how to use sophisticated environmental models to understand fundamental issues in environmental and coastal systems. Currently, the author is working at Automatic Data Processing, Portland, Oregon, as a software engineer.